Spastic paraplegia related loss of Kinesin-1 function causes developmental defects and synapse degeneration in a *Drosophila* model.

Dissertation

zur Erlangung des Grades eines

Doktors der Naturwissenschaften

der Mathematisch-Naturwissenschaftlichen Fakultät

und

der Medizinischen Fakultät

der Eberhard-Karls-Universität Tübingen

vorgelegt

von

Carola Dorothee Schneider

aus Sigmaringen

September 2015

Tag der mündlichen Prüfung:	18. Januar 2016
Dekan der Math.-Nat. Fakultät:	Prof. Dr. W. Rosenstiel
Dekan der Medizinischen Fakultät:	Prof. Dr. I. B. Autenrieth
1. Berichterstatter:	Prof. Dr. Thomas Gasser
2. Berichterstatter:	PD Dr. Bernard Moussian
Prüfungskommission:	Prof. Dr. Thomas Gasser
	Prof. Dr. Philipp Kahle
	PD Dr. Bernard Moussian
	Prof. Dr. Ludger Schöls

Ich erkläre, dass ich die zur Promotion eingereichte Arbeit mit dem Titel:

“Spastic paraplegia related loss of Kinesin-1 function causes developmental defects and synapse degeneration in a *Drosophila* model.”

selbstständig verfasst, nur die angegebenen Quellen und Hilfsmittel benutzt und wörtlich oder inhaltlich übernommene Stellen als solche gekennzeichnet habe. Ich versichere an Eides statt, dass diese Angaben wahr sind und dass ich nichts verschwiegen habe. Mir ist bekannt, dass die falsche Abgabe einer Versicherung an Eides statt mit Freiheitsstrafe bis zu drei Jahren oder mit Geldstrafe bestraft wird.

Tübingen, den 19. Januar 2016

Unterschrift

TABLE OF CONTENTS

ABBREVIATIONS

AA	Amino Acid
AD	Autosomal Dominant
ADP	Adenosine DiPhosphate
ALS	Amyotrophic Lateral Sclerosis
AMPA	α-Amino-3-hydroxy-5-Methyl-4-isoxazolePropionic Acid
APPL	β-Amyloid Precurser Protein-Like
AR	Autosomal Recessive
ATP	Adenosine TriPhosphate
AZ	Active Zone
Brp	Bruchpilot
Ca^{2+}	Calcium
CAST	Cytomatrix of the active zone Associated STructural protein
CMT	Morbus Charcot-Marie-Tooth
Dlg	Discs large
DNA	Deoxyribonucleic acid
DSHB	Developmental Studies Hybridoma Bank
EM	Electron Microscopy
EtOH	Ethanol
FasII	Fasciclin II
FRET	Fluorescence Resonance Energy Transfer
GFP	Green Fluorescent Protein
GluR	Glutamate Receptor
HRP	Horseradish peroxidase
HSP	Hereditary Spastic Paraplegia
JIP	Jun N-terminal kinase interacting protein
KAc	potassium acetate
khc	kinesin heavy chain
klc	kinesin light chain
KO	Knock Out
MAP	Microtubules Associated Protein
MT	MicroTubule

NaCl	sodium chloride
NGS	Normal Goat Serum
NMDA	N-Methyl-D-Aspartat
NMJ	NeuroMuscular Junction
PBS	Phosphate Buffered Saline
PBST	Phosphate Buffered Saline Triton
PSD	PostSynaptic Density
RNA	RiboNucleic Acid
RRP	Readily Releasable Pool
SNARE	Soluble N-ethylmaleimide-sensitive-factor Attachment REceptor
SOD	SuperOxide Dismutase
SPG	Spastic Paraplegia Gene
SSR	SubSynaptic Reticulum
SV	Synaptic Vesicle
UAS	Upstream Activating Sequence
VGlut	Vesicular glutamate

LIST OF FIGURES

LIST OF TABLES

SUMMARY

Autosomal dominant mutations in the gene coding for the neuronal Kinesin-1 isoform KIF5A cause spastic paraplegia type 10 (SPG10). The mechanism behind Kinesin-1 mutation leading to slow progressing spasticity and weakness of the lower limbs of patients is not clear and there is no causative treatment. One of the point mutations in KIF5A is Khc^{N256S}. *In vitro* studies show that Khc^{N256S} acts dominant negative over wild type Khc [Ebbing et al. 2008]. Mouse and zebrafish animal models with loss of Khc function hint at predominantly neurodevelopmental defects [Hurd and Saxton 1996; Xia et al. 2003; Karle et al. 2012; Nakajima et al. 2012; Campbell et al. 2014]. In contrast human SPG10 is clinically classified as a neurodegenerative disorder. The fly model used in this study is characterized by low-level ectopic overexpression of the *Drosophila melanogaster* orthologue of *KIF5A* (kinesin heavy chain, *khc*) bearing the SPG10 point mutation (khc^{N262S}). As Khc^{N262S} acts in a dominant negative manner, overexpression of mutant Khc resembles more closely the situation in heterozygous SPG10 patients. Using this milder affected model the parallel occurrence of neurodevelopmental defects and neurodegeneration could be shown for the first time. Larvae expressing khc^{N262S} build less new synapses in a given time window than controls. In addition to this neurodevelopmental defect, neuromuscular junctions (NMJs) of khc^{N262S} expressing larvae show overgrowth including enhanced transport of active zone (AZ) precursor vesicles that also lead to increased Brp intensity, a marker for AZs, at the NMJ. But in parallel neurodegenerative signs such as accumulation of neuronal membranes inside boutons and disorganized microtubule (MT) cytoskeleton are detectable. In larvae expressing khc^{N262S}, the impaired axonal transport of mitochondria leads to a reduced number of mitochondria at the NMJ. This could explain the behavioral defects, characteristic

for fly models of axonal transport deficits [Hurd and Saxton 1996; Gindhart et al. 1998; Martin et al. 1999; Bowman et al. 2000]. These results show in greater detail the progression of paralysis in the posterior part of larvae because the chronology of emerging pathological characteristics of a *Drosophila* model of SPG10 could be described. To further study the way of degeneration in a model of loss of functional Khc, NMJs of *khc*$^{-/-}$ larvae were analyzed. They grow much slower than controls and die before pupation. NMJs are characterized by smaller size compared to controls and show frequent occurrence of accumulated neuronal membranes in NMJs as well as in axons. Cargos like Brp or synaptic vesicle marker VGlut accumulated in- and outside of axonal swellings and were diminished at the NMJ. The NMJ was especially marked by fragmentation of neuronal membranes and MTs. These did not retract from the terminal bouton as described for classical neuronal retraction [Eaton et al. 2002], but dispersed in central regions of the NMJ, separating parts of the NMJ from the innervating axon. Therefore, they show a disassembly of the NMJ, which is different from classical neuronal retraction and resembles more a Wallerian-like deconstruction of neuron-muscle innervation.

1 INTRODUCTION

1.1 Hereditary spastic paraplegia

Hereditary spastic paraplegias (HSPs) are a group of heterogeneous neurological disorders with an estimated prevalence of 3-9/100 000 [Blackstone et al. 2011].

1.1.1 Clinical symptoms

HSPs are clinically classified as pure or complex [Harding 1983]. Symptoms of pure HSPs are confined to the pyramidal track leading to weakness and spasticity of lower extremities, bladder disturbances and to a lesser extent sensory impairments [Harding 1983; Fink 2003; Martin et al. 2012]. Patients with a complex form of HSP might suffer from additional neurological defects such as optic neuropathy, retinopathy, deafness, ataxia, ichthyosis, dementia, mental retardation and epilepsy [Blackstone et al. 2011].

The onset of HSP is mild and from early childhood to late adulthood [Salinas et al. 2008]. It is characterized by the development of leg stiffness, because of a dramatically increased tone in the legs, but a relative maintenance of power, which is different to other causes of spastic paraplegias like multiple sclerosis and spinal cord injury [Harding 1981; Salinas et al. 2008].

1.1.2 HSP treatment

To date there is no causative treatment of any subtype of HSP [Fink 2013; Lo Giudice et al. 2014]. Only the symptoms can be treated with different drugs for muscle relaxation [Fink 2013; Lo Giudice et al. 2014] or injections of botulinum toxin (A or B) in selected areas [Geva-Dayan et al. 2010] to reduce spasticity. For long-time treatment surgically implanted

pumps are also in use [Motta and Antonello 2014]. Regular physical therapy can improve walking speed and also maintains or increases the physical strength in lower extremities [Zhang et al. 2014]. As many patients of HSP are dragging toes, foot orthotics and a special nerve stimulation that is synchronized with the gait phase can meliorate the phenotype [Fink 2013].

1.1.3 Genetic background and pathophysiology of HSP

To date more than 70 HSP loci (spastic paraplegia gene, SPG1-72 [Finsterer et al. 2012; Fink 2013; Novarino et al. 2014]) have been identified for which autosomal dominant, autosomal recessive and X-linked modes of inheritance have been described.

Table 1: Selected mutant proteins in HSP

SPG	Heredity	Involved Protein	Protein Function	Reference
SPG3a	AD	Atlastin-1	ER morphogenesis	[Zhao et al. 2001]
SPG4 (SPAST)	AD	Spastin	cytoskeletal remodeling	[Hazan et al. 1999]
SPG6	AR	NIPA1	endosomal trafficking	[Rainier et al. 2003]
SPG7	AD	Paraplegin	mitochondrial protease	[Casari et al. 1998]
SPG10	AD	KIF5A	fast axonal transport	[Reid et al. 2002; Schüle et al. 2008]
SPG11	AR	Spatacsin	motor neuron development, lysosome formation	[Stevanin et al. 2007; Chang et al. 2014]
SPG13	AD	heat shock protein 60	mitochondrial chaperone	[Hansen et al. 2002]

SPG	Heredity	Involved Protein	Protein Function	Reference
SPG15	AR	Spastizin	motor neuron development, lysosome formation	[Hanein et al. 2008; Chang et al. 2014]
SPG20 Troyer Syndrome	AR	Spartin	endosomal trafficking, regulates mitochondrial calcium homeostasis, localizes near ER	[Patel et al. 2002; Joshi and Bakowska 2011]
SPG21	AR	Maspartin	endosomal trafficking, cellular transport, axonal branching	[Simpson et al. 2003]
SPG30	AR	KIF1A	intracellular anterograde transport of dense core vesicles	[Klebe et al. 2006]
SPG31	AD	REEP1	mitochondrial chaperone-like	[Zuchner et al. 2006]
SPG55	AR	C12orf65/ C12ORF65	peptide chain termination in the mitochondrial translation machinery	[Shimazaki et al. 2012]

AD: autosomal dominant heredity, AR: autosomal recessive heredity. References show first mentioning authors. Table is modified from [Salinas et al. 2008; Blackstone et al. 2011]

Studies of different genes that are involved in HSP show, that distal parts of neurons are predominantly affected showing a “dying back” mechanism when axonal transport of macromolecules, organelles or other cargo is impaired [Crosby and Proukakis 2002;

Soderblom and Blackstone 2006; Salinas et al. 2008]. It is likely the unique morphology of spinal cord axons which can be up to one meter in humans, that leads to their apparent dependence on membrane trafficking, cytoskeletal organization and microtubule (MT) based transport (Figure 1). The mechanisms could be “cell autonomous” and lead to degeneration only in the affected neurons, but also “non-cell autonomous” where structure degenerates on which the axon relies on [Fink 2013]. SPG2 (proteolipid protein) and SPG42 (Connexin 47) are encoding proteins that are primarily expressed in oligodendroglia and not in neurons [Fink 2013], but proteins, that are implicated in axonal transport like SPG10 and SPG30 rise evidence for primary pathology of axons, rather than glia.

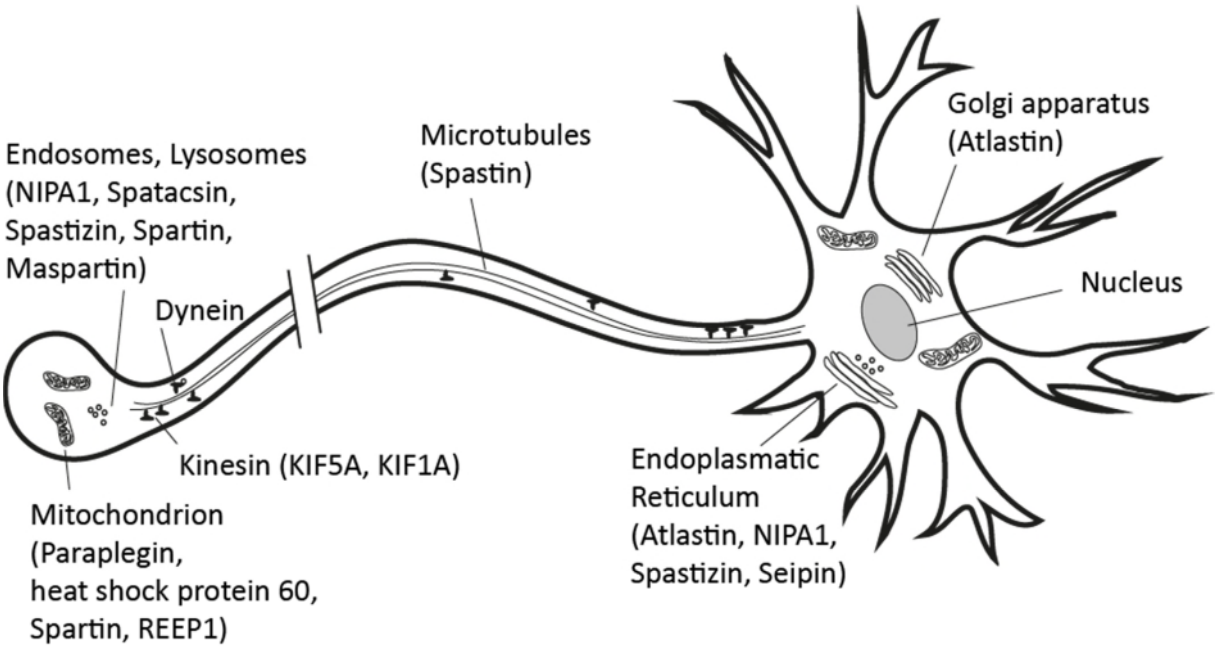

Figure 1: Potential pathogenic pathways of HSP proteins in a schematic neuron

The schema shows sites of possible pathogenic interventions of mutant HSP proteins in a neuron. Mitochondria are affected by mutations in Paraplegin, Spartin and REEP1. KIF5A and KIF1A mediate anterograde transport. Endosomal trafficking (NIPA1, Spartin, Maspartin) and lysosome formation (Spastizin, Spatacsin) can also be implicated in HSP pathology. The cytoskeleton can be affected by Spastin mutations. The endoplasmic reticulum can be influenced by mutations in Atlastin, NIPA1 and Spastizin. Image is modified from [Salinas et al. 2008].

Most of the HSP-related proteins are implicated in mitochondrial function and axonal transport (compare Table 1). Therefore, these predominant targets of HSP pathology will be explained in detail below.

1.2 Molecular railways and motor proteins

In neurons the complexity of motor proteins is higher than in most other cell types, which likely reflects the special importance of specific intracellular transport in these cells because of their high polarization [Silverman et al. 2010]. The transport of cargo with motor proteins is adenosine triphosphate (ATP) dependent and unidirectional. Kinesins are the motor proteins for anterograde, Dynein for retrograde direction. With hydrolyzing ATP, they undergo conformational changes and thereby walk continuously along their tracks. MTs, actin filaments and intermediate filaments form the cytoskeleton of neurons and contribute to their morphology and function. However, axonal transport depends mainly on MTs. They are important for long distance axonal transport, whereas actin maintains the movement near the plasma membrane at the presynapse.

1.2.1 Microtubules

MTs are formed out of polarized tubulin polymers with fast-growing plus ends and more stable minus ends. In the axon, parallel MTs form a unipolar array with plus ends orientated towards the neuromuscular junction (NMJ) and minus ends towards the cell body [Burton and Paige 1981; Stepanova et al. 2003]. In dendrites, MT arrays are often of mixed polarity [Baas et al. 1989; Kwan et al. 2008; Kleele et al. 2014]. MT associated proteins (MAPs) bind along the length of axonal and dendritic MTs and are responsible for polymerization and stabilization of MTs [Maday et al. 2014]. MAPs also link MTs with other components of the cytoskeleton. At the *Drosophila* NMJ presynaptic MTs are associated with

Futsch, a MAP1B homologue [Hummel et al. 2000; Roos et al. 2000]. Futsch molecules can be observed as a single filamentous bundle that traverses the center of each NMJ branch [Ashley et al. 2005].

The various cargos that are transported along MTs move in a saltatory fashion with periods of rapid movements, pauses and directional switches [Wang et al. 2000; Lovas and Wang 2013].

1.2.2 Actin

Actin filaments (F-actin) are polarized polymers that function as tracks for the large family of myosin proteins [Fletcher and Mullins 2010]. The continuous assembly and disassembly of F-actin is mediated by local activity of signaling systems [Parent 2004]. F-actin localizes beneath the plasma membrane of the pre- and postsynapse (Figure 2, [Hirokawa et al. 2010]). In the postsynapse it is associated with postsynaptic receptors [Ruiz-Canada et al. 2004; Dobbins et al. 2006]. Presynaptic actin based myosin transport is important for the delivery of synaptic vesicle (SV) precursors to the terminals (Figure 2, [Bridgman 1999]). F-actin is also implicated in the refilling of the readily releasable vesicle pool of vesicles [Doussau and Augustine 2000; Cingolani and Goda 2008]. Inhibited actin dynamics leads to altered NMJ morphology and disrupted synaptic endocytosis [Zhao et al. 2013].

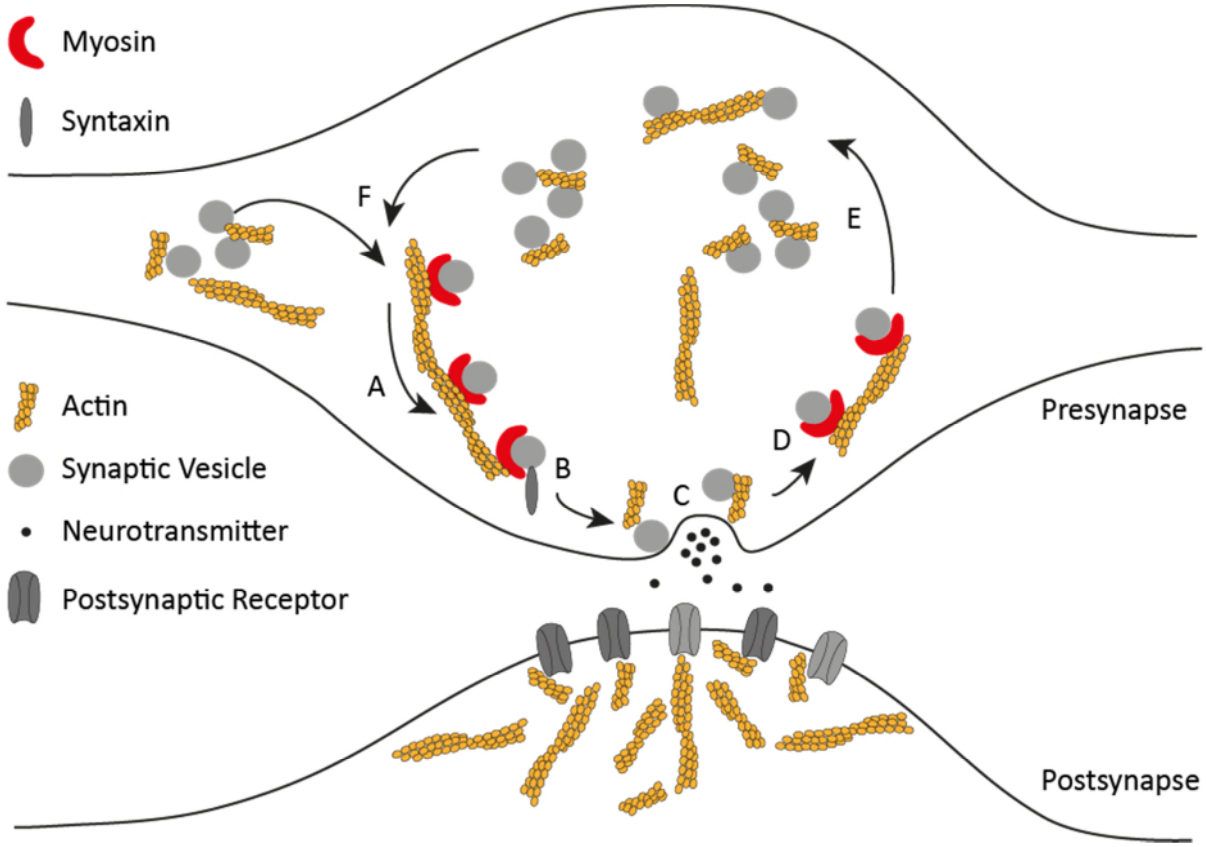

Figure 2: Functions of myosin and actin at the presynapse

(A) SVs are transported to the AZ via F-actin (yellow) by myosin (red), which then binds to Syntaxin. (B) Vesicle priming for the entry into the readily releasable pool. (C) Vesicle fusion with the AZ membrane. (D) Myosin transports recycled vesicles to the center of the bouton. Vesicles exit (E) or re-enter (F) the presynaptic terminal. At the postsynapse actin is important for proper receptor clustering. Image is modified from [Cingolani and Goda 2008].

1.2.3 Dynein

Dynein-1 is the major motor protein of organelle dynamics in the retrograde direction [Paschal and Vallee 1987]. It consists of two heavy chains, three intermediate chains and four light chains [Paschal and Vallee 1987]. Most of its function in the cell requires the dynein activator Dynactin [Gill et al. 1991]. The p150Glued subunit of Dynactin drives transport initiation from the distal axon [Lloyd et al. 2012; Moughamian and Holzbaur 2012]. Dynein transports neurotrophin-signaling endosomes [Ibanez 2007], mitochondria [Hollenbeck and Saxton 2005], injury-generated signals [Perlson et al. 2005] and RNA-associated proteins [van Niekerk et al. 2007]. Interestingly, the opposing motor proteins

Kinesin-1 and Dynein can be interdependent. Kinesin-1 mutations can inhibit transport in both directions, whereas mutant Dynein only inhibits the retrograde direction [Pilling et al. 2006; Füger et al. 2012]. This might be explained by the anterograde transport of Dynein and Dynactin by Kinesin-1 [Yamada et al. 2010].

1.2.4 Kinesins

The human genome encodes for more than 45 proteins that contain a domain homologous to the kinesin motor domain and are members of the kinesin superfamily. 38 of them are expressed in the brain [Miki et al. 2001]. Kinesins are grouped into 14 subfamilies (Kinesin-1 – Kinesin-14, Table 2). Kinesin-1, Kinesin-2 and Kinesin-3 contribute to axonal transport [Maday et al. 2014].

Table 2: Kinesin superfamily members and their functions

Family	Functions
Kinesin-1	vesicle, organelle and mRNA transport
Kinesin-2	vesicle, melanosome and intra-flagellar transport
Kinesin-3	vesicle transport
Kinesin-4	chromosome positioning, organelle transport
Kinesin-5	spindle pole separation and spindle bipolarity
Kinesin-6	central spindle assembly and cytokinesis
Kinesin-7	kinetochore–MT attachment and chromosome congression
Kinesin-8	chromosome congression
Kinesin-9	glia and flagella (?)
Kinesin-10	chromosome positioning
Kinesin-11	signal transduction

Family	Functions
Kinesin-12	spindle pole organization
Kinesin-13	kinetochore–MT error correction and chromosome segregation
Kinesin-14	spindle pole organization and cargo transport

Table is modified from [Miki et al. 2005; Verhey and Hammond 2009].

1.2.5 Kinesin-1

Kinesin-1, also called conventional kinesin, is the founding member of the kinesin superfamily [Vale et al. 1985]. It transports cargo like vesicles, organelles, proteins and RNA particles. In *Drosophila* oocytes, Kinesin-1 is also required for establishing the anterior-posterior axis with transporting a complex containing *oskar* mRNA and the associated protein Staufen to the posterior pole [Brendza et al. 2000]. Kinesin-1 contributes to the fast axonal transport on MTs in the anterograde direction with velocities from 0.5µm/s to 1µm/s [Hirokawa et al. 2010]. Its movement is ATP dependent [Hua et al. 1997; Rice et al. 1999].

Domain structure of Kinesin-1

Kinesin-1 consists of a dimer of kinesin heavy chains (Khcs) that are encoded by the three mammalian genes *KIF5A*, *KIF5C* (neuron specific) and *KIF5B* (ubiquitously expressed), which differ in their coiled-coil domain [Aizawa et al. 1992; Kanai et al. 2000].

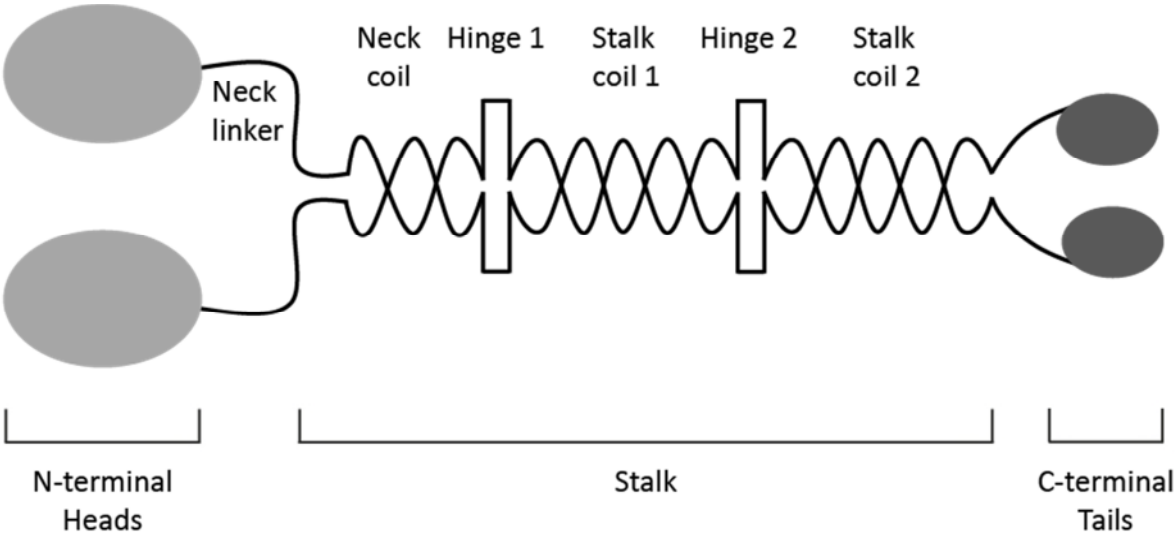

Figure 3: Subunit composition of Kinesin-1

Kinesin-1 consists of three subunits: First: the N-terminal heads (light grey), which are connected to the stalk domain via the neck linkers. The heads contain the motor domain including ATP hydrolysis and MT binding sites. Second: the coiled-coil stalk domain (black line), where dimerization of the Khcs takes place. This unit contains two hinges. Hinge 2 allows kinking of the stalk during autoinhibition, hinge 1 probably enables movements of the stalk during the conformational changes of the heads while walking. The C-terminal tail (dark grey) is the third subunit. It is responsible for cargo recognition and binding. It is also involved in autoinhibition of the motor protein. Image is modified from [Verhey et al. 2011].

Each Khc contains an N-terminal motor domain, a coiled-coil stalk and a C-terminal globular tail domain (Figure 3, [Hirokawa et al. 1989; Scholey et al. 1989]). Both Khc monomers bind with their C-terminal tails to cargo or cargo adaptors and with their N-terminal heads to MTs. Dimerization of two Khc monomers to form a Kinesin-1 dimer takes place at the coiled-coil stalk domain (Figure 3). Two hinges interrupt this domain. Hinge 1 is probably important for providing a larger range of motion for the neck linkers and the N-terminal heads during walking [Hunt and Howard 1993; Gutierrez-Medina et al. 2009]. Hinge 2 plays a role in autoinhibition of Kinesin-1 (see below).

Cargo binding of Kinesin-1

Most cargo is transported by multiple transport proteins. *In vitro* assays showed increasing velocity for increasing number of motor proteins [Gagliano et al. 2010]. However,

in vivo experiments with varying the expression of *kinesin-1* in *Drosophila* eggs claimed the opposite [Shubeita et al. 2008]. The resulting force is also not increasing with the numbers of motor proteins [Furuta et al. 2013].

In half of all Khc molecules in a cell, the C-terminal domain is bound to Klc [Gyoeva et al. 2004], the rest binds to other cargo adaptors or directly to the cargo (reviewed by [Lovas and Wang 2013]). Cargos of Khc in mammals are for example neurofilaments [Xia et al. 2003], GAP-43 and Synapsin in cultured hippocampal neurons [Ferreira et al. 1992].

Transport of RNA granules [Brendza et al. 2000; Kanai et al. 2004; Ling et al. 2004], cytoplasmic streaming [Palacios and St Johnston 2002] and MT-MT sliding [Straube et al. 2006; Jolly et al. 2010] does not require Klc as an adaptor for cargo binding to Khc. For mitochondrial transport a complex of Khc with the two adaptor proteins Milton and Miro is required [Glater et al. 2006].

Khc also carries soluble N-ethylmaleimide-sensitive factor attachment protein receptor (SNARE) proteins [Hirokawa and Noda 2008] and synaptosomal-associated protein 25 (SNAP25), which both directly bind to Khc [Diefenbach et al. 2002] and Syntaxin, which binds Khc via Syntabulin [Su et al. 2004]. Direct binding to Khc was also shown for DISC1 [Taya et al. 2007], and JIP family proteins [Bowman et al. 2000; Kelkar et al. 2000; Verhey et al. 2001]. In dendrites KIF5 transports α-amino-3-hydroxy-5-methyl-4-isoxazolepropionic acid (AMPA) receptors [Kim and Lisman 2001; Setou et al. 2002], mRNA [Severt et al. 1999] and members of the mRNA/Protein complex [Ohashi et al. 2002; Kanai et al. 2004]. The binding of cargo also seems to determine the destination of the motor protein [Setou et al. 2002].

Autoinhibition of Kinesin-1

Kinesin-1 is the best studied motor protein for autoinhibition. Active Kinesin-1 exists in an extended conformation, whereas inactive cytoplasmic Kinesin-1 is folded [Cai et al. 2007]. Thereby hinge 2 in the coiled-coil stalk domain is important for the inactivation of Kinesin-1 [Coy et al. 1999; Kirchner et al. 1999]. Through kinking the stalk domain at hinge 2 the C-terminal tail domain of Khc can bind to the N-terminal motor domain, which then leads to inactivity [Friedman and Vale 1999; Kaan et al. 2011]. The tail domain blocks intrinsic and MT stimulated release of adenosine diphosphate (ADP) from the nucleotide binding site [Coy et al. 1999; Hackney and Stock 2000, 2008; Wong et al. 2009]. During inactivation the two head domains are separated from each other [Cai et al. 2007]. Kinesin light chain (Klc) can also inhibit the MT binding of Khc [Verhey et al. 1998]. The reactivation is dependent on cargo binding [Hirokawa and Noda 2008], e.g. the binding of JNK-interacting protein 1 (JIP1) and fasciculation and elongation protein ζ (FEZ1) to the Khc tail domain [Blasius et al. 2007]. By reactivation the two motor domains are again pushed closer together for proper MT interaction [Cai et al. 2007].

Models of Kinesin-1 movement

The movement itself seems to follow an asymmetric hand-over-hand mechanism with alternating steps causing the Kinesin-1 to limp [Asbury et al. 2003].

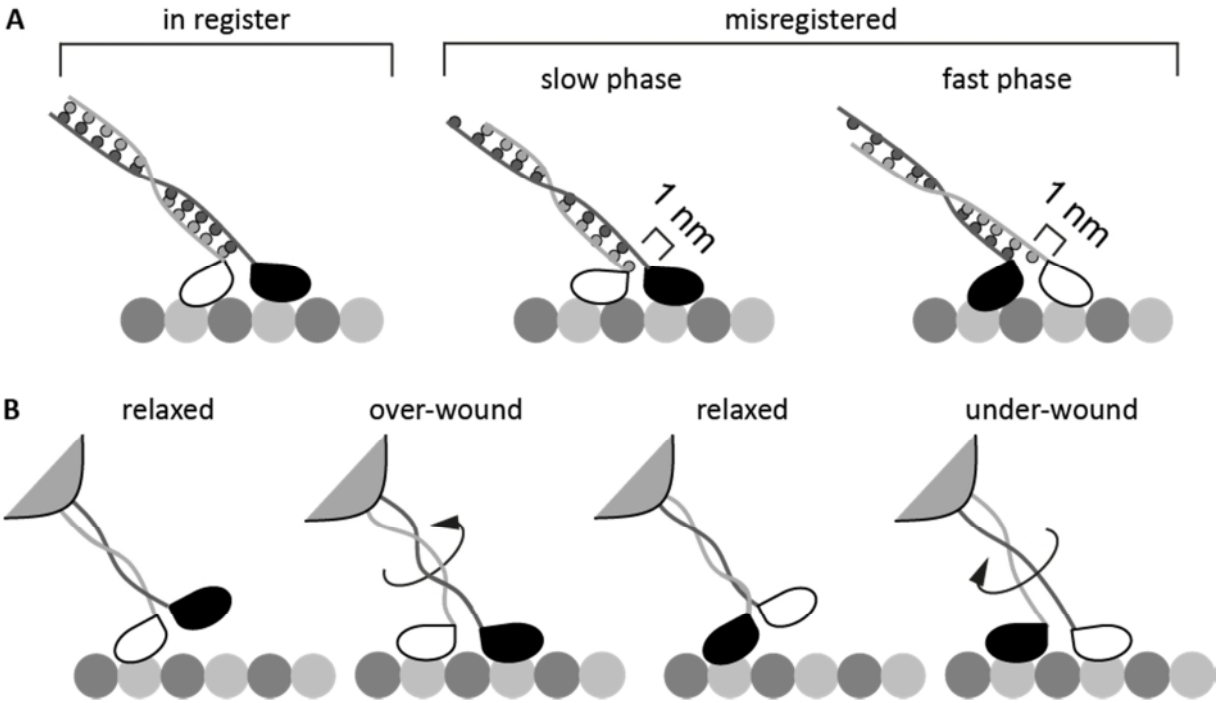

Figure 4: Asymmetric hand-over-hand walking mechanism of Kinesin-1

Models explaining the limping nature of kinesin walk. MTs are shown as light and dark grey beads; Kinesin-1 motor proteins are shown in black and white. **(A)** The misregistration model: left panel shows a model where the dimerization happened in register. Right panel shows a model where the dimerization happened with a shift in register, leading to a length difference in the tails of one heptad (~1 nm). **(B)** The winding model: Along with stepping forward of the black head the coiled-coil stalk domain gets over-wound relative to the relaxed state. With stepping forward of the white head the coiled-coil domain gets under-wound. This leads to asymmetric torsional force in the two heads. Figure is modified from [Asbury et al. 2003].

One possible cause for the limping is a possible misregistration by one heptad repeat, which would shift the globular heads and increase the length of one neck linker compared to the other (Figure 4A [Asbury et al. 2003]). Thereby, the distance of the heads to the MT is different, leading to altered velocity of MT binding of both heads. Another possible cause is that the coiled-coil stalk domain has an asymmetric torsional compliance because of its chirality (Figure 4B, [Bryant et al. 2003]). This would lead to over- or under-wound positions of the coiled-coil stalk domain [Asbury et al. 2003]. A forward step of the first head provokes the coiled-coil stalk to get over-wound relative to the relaxed state. The step of the next head leads to an under-wound condition of the coiled-coil stalk. Thereby asymmetric torsional forces arise from the stalk.

Influence of MT configuration and MAPs on kinesin movement

Posttranslational modifications of MTs and MAPs can possibly alter the binding affinity of Kinesin-1 [Hammond et al. 2010]. Acetylated or detyrosinated MTs show different transport events in cells. Increased tubulin acetylation navigated Kinesin-1 motor proteins to axons [Reed et al. 2006; Konishi and Setou 2009] and leaded to higher transport rates in a model of Huntington's disease [Dompierre et al. 2007]. MAPs like tau regulate the stability of the MT network and can interact with motor proteins on MTs ([Seitz et al. 2002; Mandelkow et al. 2004], reviewed in [Marx et al. 2006]).

Kinesin-1 walking on MTs by ATP hydrolysis

The interplay between MT binding, ATP binding and hydrolysis drives the motor activity of Kinesin-1 [Gigant et al. 2013]. With cryo-electron microscopy (cryo-EM) reconstructions a description of the three states of the motor domain of Kinesin-1 could be described: KIF5A bound to an αβ-tubulin dimer (1) with no nucleotide bound, (2) with a non-hydrolysable ATP analogue and (3) an ATP hydrolysis transition state mimic [Atherton et al. 2014; Shang et al. 2014]. During all nucleotide states the contact to the tubulin dimers is maintained from at least one of the two heads (Figure 5). The coordination of both heads is thought to be realized through a gating mechanism in which the different positions of the neck linkers of the rear and the leading head lead to different docking states [Shang et al. 2014].

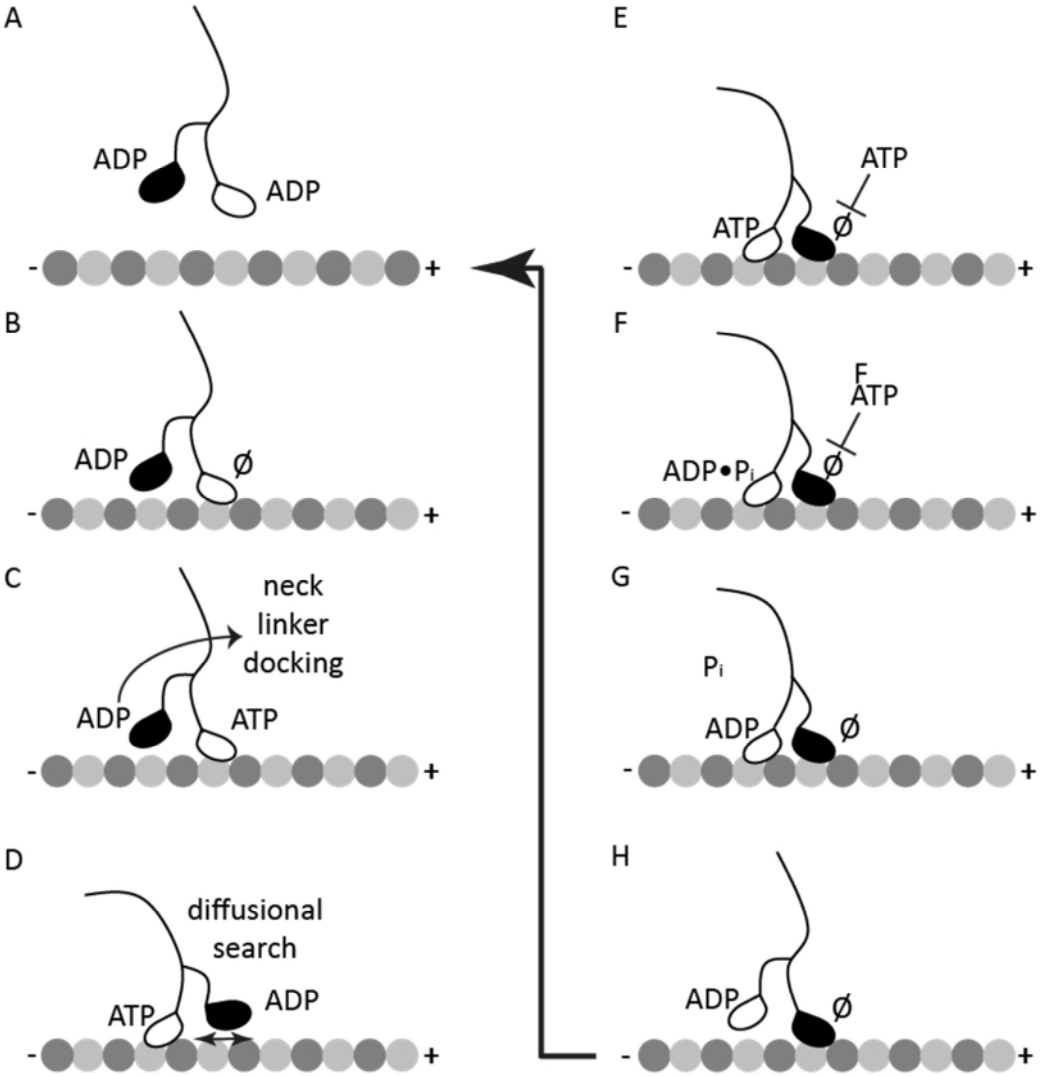

Figure 5: Sequential steps of Kinesin-1 walking

Kinesin-1 walks in an asymmetric hand-over-hand mechanism [Asbury et al. 2003]. Each head takes steps of 16 nm [Yildiz et al. 2004]. MTs are shown as light and dark grey beads, Kinesin-1 motor proteins are shown in black and white. **(A)** Free Kinesin-1 motor proteins bind ADP. **(B)** By activation, the first head (white) binds a MT and releases its nucleotide. **(C)** After ATP binding to the first head, conformational change pulls the new leading head (black) in front of the bound head**. (D)** Eventually diffusion plays also a role in new positioning of the leading head. **(E)** After ADP release of the leading head, head-head communication prevents new ATP binding in the leading head. **(F, G, H)** γ-phosphate release in the rear head (white) leads to its detachment from the MT. A new ATP hydrolysis cycle can start (step **(B)**). Figure is modified from [Valentine and Gilbert 2007].

Free cytosolic Kinesin-1 motor proteins bind ADP in their nucleotide cleft [Hackney 1994]. The release of ADP, when the Kinesin-1 binds to MTs, is the rate limiting step [Hackney 1988]. The first head bound is then the leading head, which can bind ATP [Hackney 1994; Ma and Taylor 1997]. This ATP binding results in a neck linker movement towards the

plus end of the MT [Rice et al. 1999; Gigant et al. 2013]. As this mechanical step covers only ~2.7nm of the whole 8nm step, diffusion might also play a role [Valentine and Gilbert 2007; Kawaguchi 2008]. The second head also releases its ADP when bound to MTs in front of the first head. To ensure sequential stepping of the two motor domains, the binding of new ATP to the leading head must be coordinated with the hydrolysis of ATP in the rear head [Valentine and Gilbert 2007]. Potential ways of head-head communication are proposed from Mori and colleagues and Alonso and colleagues (reviewed by [Gennerich and Vale 2009]). Mori et al. proposed that the detached (rear) head locates near the bound (leading) head which creates a closed “polymer gate”. Thereby, MT binding is abolished [Alonso et al. 2007]. The gate can be opened by ATP binding to the leading head. With an open polymer gate, the rear head can bind to MTs in front of the former leading head [Alonso et al. 2007]. Fluorescence resonance energy transfer analysis of Mori and colleagues show, however, that the detached head is positioned behind the attached head [Mori et al. 2007]. ATP hydrolysis only occurs in leading heads [Guydosh and Block 2006]. Thereby, the conformation of the neck linker at the free head could prevent the head from MT binding and ADP from disassociation [Mori et al. 2007]. This rear head gating mechanism is supported by Uemura and Ishiwata who showed that ADP affinity increases with forward tension of the neck linker [Uemura and Ishiwata 2003].

Biochemical structure of Kinesin-1

Kinesin-1 function is dependent on ATPase activity because it enables the movement on MTs [Hirose et al. 1995]. In turn MT binding accelerates the rate limiting step of ADP release [Ma and Taylor 1997; Yun et al. 2001]. Binding and hydrolyzing ATP leads to conformational changes in Kinesin-1 motor proteins [Hirose et al. 1995] that results in

sequential steps of ~8nm [Schnitzer and Block 1997], the exact distance between two αβ-tubulin subunits [Svoboda et al. 1993].

The motor domain of Kinesin-1 is located in the C-terminal heads of the protein, which also contains the MT binding motives. A description of the head domain in closer detail is shown in Figure 6.

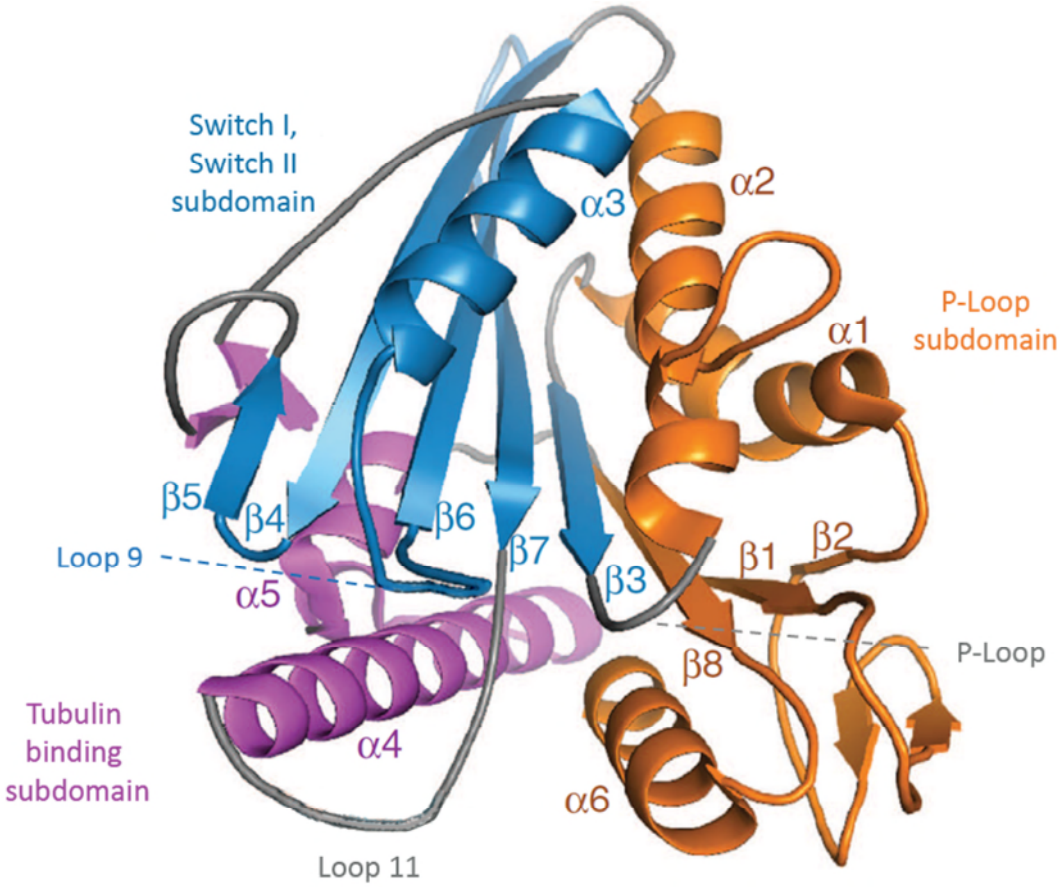

Figure 6: Subdomains important for conformational changes in Kinesin-1

The motor domains are built out of several α-helices, loops and β-sheets. The three domains that can be distinguished, are shown in different colors: the P-loop subdomain in orange, the tubulin binding domain in purple, which is connected to the switch domain (blue) by loop 11 (grey). Figure is modified from [Atherton et al. 2014; Cao et al. 2014].

Structurally Kinesin-1 shows high similarity to myosins [Kull et al. 1996]. They both bind nucleotides in a well conserved P-loop [Hirokawa and Noda 2008]. The P-loop connects β-sheet 3 to helix-α2 (Figure 6, [Atherton et al. 2014; Cao et al. 2014]).

Analogous to G proteins loop 9 undergoes the major conformational change during the ATPase cycle [Hirokawa and Noda 2008; Atherton et al. 2014]. This conformational change leads to a change in the nucleotide binding site of the protein [Sablin et al. 1996]. It contains switch I and connects helix-α3 to β-sheet 6.

Loop 11 (contains switch II) that connects strand-β7 to helix-α4, is part of the MT binding surface together with Loop 12 and helix-α5 [Hirokawa and Noda 2008; Atherton et al. 2014]. Loop 11 and helix-α4 are thought to mediate the communication between the nucleotide and the MT binding site [Sablin et al. 1996; Song and Endow 1998]. The binding of Khc to MTs is thought to trigger helix-α4 to recruit the adjacent ~10 amino acids of loop 11 into an extended helix [Djagaeva et al. 2012].

The coupling of conformational changes to the ATP hydrolysis cycle

The ADP bound state is characterized by an association of loop 11 and the N-terminal part of helix-α4 to MTs. By the subsequent amino acid shift from loop 11 to helix-α4, loop 11 is shortened and switch II is shifted [Djagaeva et al. 2012]. Thereby binding of MTs to loop 11 triggers the ADP release and facilitates the exchange of ADP for ATP [Woehlke et al. 1997; Ebbing et al. 2008; Uchimura et al. 2010; Atherton et al. 2014]. The binding to MTs causes a distortion of the nucleotide binding site by rotations of the switches I and II and the P-loop [Cao et al. 2014]. By releasing ADP the conformation of loop 11 and helix-α4 gets stabilized [Atherton et al. 2014]. Loop 9 changes conformation during ADP release and extends around the nucleotide binding site [Atherton et al. 2014; Shang et al. 2014]. Due to additional contacts the conformations of loop 9 and loop 11-helix-α4 complex are likely further stabilized through the extended conformation of loop 9 [Woehlke et al. 1997; Ebbing et al. 2008; Uchimura et al. 2010; Atherton et al. 2014]. Thereby a nucleotide free motor protein is

strongly bound to MTs [Nakata and Hirokawa 1995]. ADP release also seems to prime the motor domain for the next ATP binding [Atherton et al. 2014]. The binding of ATP itself does not lead to major conformational changes in the motor domain, but it is critical for a pincer-like spatial approach of loop 9 and 11 (contain switches I and II) [Atherton et al. 2014]. This again leads to strong additional contacts between them and the N-terminal of helix-α4 and the P-loop [Atherton et al. 2014]. Thereby the switch regions are thought to "sense" the presence or absence of γ-phosphate [Kull and Endow 2013]. During ATP binding, the nucleotide cleft undergoes a clamshell distortion [Shang et al. 2014]. This in turn causes the large movement of the neck linker, which is necessary for determining the direction of movement and new neck linker docking [Rice et al. 1999]. The direction of neck linker movement towards the MT plus end also seems to be determined by hydrogen bonds and hydrophobic interactions that exist between the neck linker and the core of the motor domain [Gigant et al. 2013]. The force needed for detaching the motor protein from MTs in the minus direction is much higher (140%) than the force needed towards the plus direction [Uemura et al. 2002]. The mechanical amplification, needed for neck linger docking, results out of β-sheet tilting and multiple rearrangements across the domain, but mostly in helix-α6 [Atherton et al. 2014]. Thereby the direction of movement as well as the head-head tension is ensured which is necessary for proper amplification. With neck linker docking the hydrolysis of ATP takes place [Atherton et al. 2014].

MT binding stimulates the release of ADP and seems to prepare the catalytic site for ATP hydrolysis as the conformation of the active site is very close to that during catalysis [Atherton et al. 2014]. Consistently ATP hydrolysis is increased by a multiple when the motor domain is bound to MTs [Ma and Taylor 1997].

The MT binding complex can form two conformations: In the “up” conformation helix-α4 fits into the intra-dimer groove between α- and β-tubulin and loop 11 moves toward the MTs and thus contributes to the strong binding state [Hirokawa and Noda 2008]. In the second (“down”) conformation helix-α4 is located between helices-α5 and -α6 and loop 11 is bended towards helix-α4. Consequently the binding to MTs is weak [Hirokawa and Noda 2008].

1.3 Mitochondria

One known cargo of Kinesin-1 is mitochondria [Glater et al. 2006]. As most ATP in the brain is produced by mitochondria [Lin et al. 2010; Hall et al. 2012], their distribution is essential for proper function of neurons. In humans the nervous system consumes a high fraction of the resting energy production. The brain represents only 2% of the body weight, but uses 20% of the overall O_2 consumption [Mink et al. 1981].

1.3.1 ATP consumption at synapses

In the brain the major consumers of energy are electrical signaling processes (Figure 7, [Harris et al. 2012]). Chemical synapses are connecting neurons with each other and build a huge neuronal network. The signal transduction occurs via the coupling of electric signal that arrives at the presynapse. There the signal gets translated into the release of chemical messengers (neurotransmitters) that are released into the synaptic cleft. In the membrane of the postsynaptic side these messengers bind to ligand gated receptors. Either the receptor directly opens a chemical channel causing ions to enter the postsynaptic cell [Pollard et al. 2007]. Thereby, the membrane potential is changed and a postsynaptic potential is initiated. The other possibility is that the activated receptor leads to production of chemical messengers inside the postsynapse [Pollard et al. 2007].

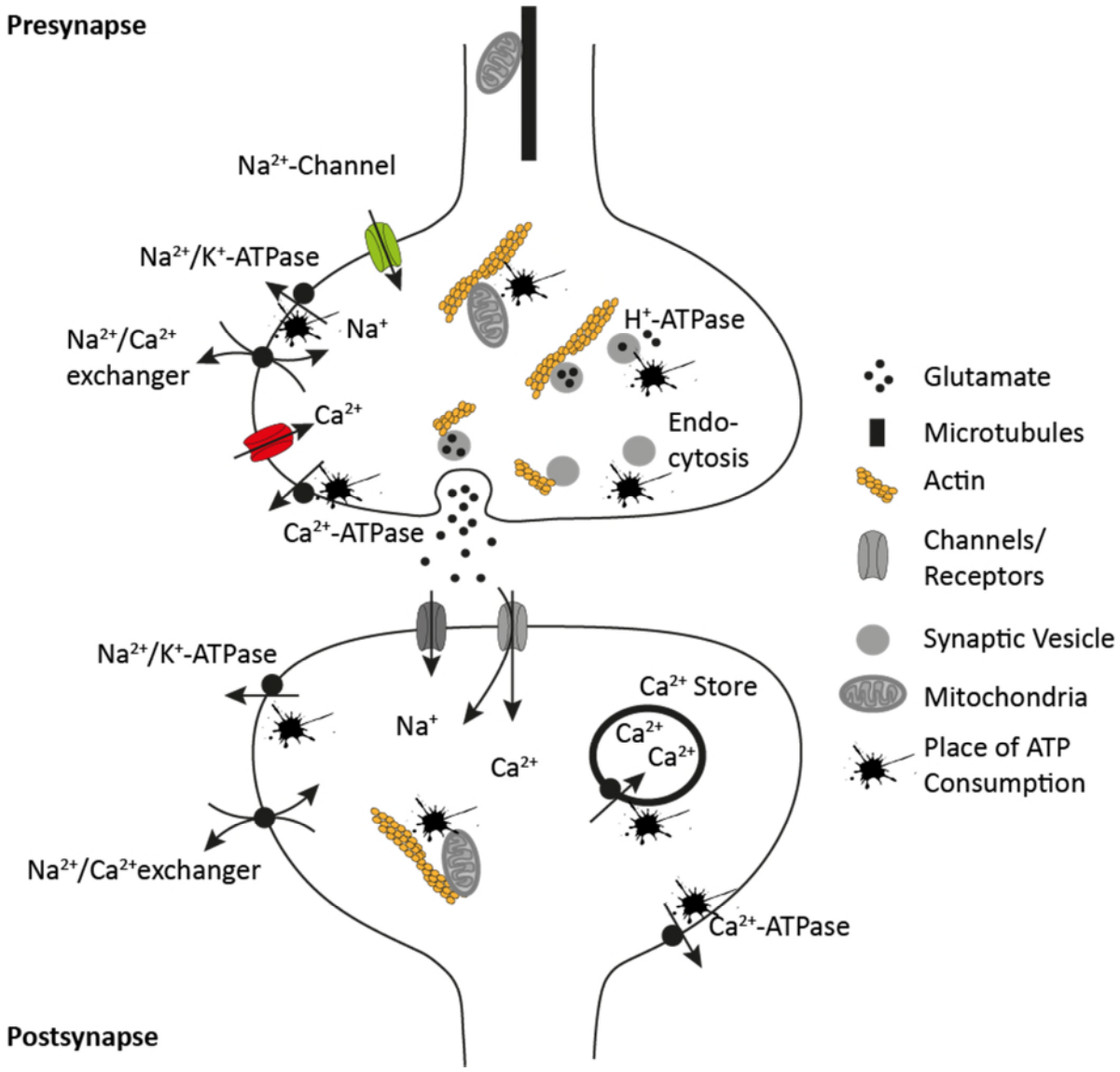

Figure 7: Sites of ATP consumption at synapses

Signaling mechanisms consume high ranges of ATP at synapses. The sodium pump ejects Na^+ ions and powers calcium removal by Na^+/Ca^{2+} exchange. The Ca^{2+}-ATPase and H^+-ATPase (for vesicle transmitter uptake) and also motor proteins (kinesins, dyneins and myosins) consume ATP. Figure is modified from [Harris et al. 2012].

Due to a massive shift in ion distribution during the signal transduction, ion pumps need to maintain the concentration of Na^+ (sodium), K^+ (potassium) and Ca^{2+} (calcium). Carriers in the presynapse and adjacent supporting cells transport the neurotransmitters from the synaptic cleft back to the presynapse and thereby terminate the transmission [Pollard et al. 2007]. In the presynapse, the load and unload of neurotransmitters into SVs

and the transporters of vesicles from the different vesicle pools are also energy consumers [Verstreken et al. 2005]. As all these processes are active transports and they all consume ATP.

1.3.2 Homeostatic function of mitochondria

In the adult brain ATP is produced mostly from mitochondria, the rest coming from glycolysis [Lin et al. 2010; Hall et al. 2012]. Consistently mitochondria are preferentially located at the pre- and postsynapse, where ATP is consumed [Chang et al. 2006]. With ATP consumption, the ratio of (ADP/ATP) will rise. By the law of mass action, this will increase ATP production by oxidative phosphorylation [Chance and Williams 1955]. Additionally, there is another stimulus for ATP production during synaptic activity from rising intracellular calcium concentrations because of neurotransmitter release presynaptically and from cation channel N-methyl-D-aspartate (NMDA) receptors or AMPA receptors postsynaptically [Gellerich et al. 2009; Gellerich et al. 2010; Chouhan et al. 2012]. Therefore, mitochondria are essential for neuronal function and survival [Nicholls and Budd 2000].

Additionally to their energy production, mitochondria have an enormous capacity to sequester calcium transients from action potentials [Werth and Thayer 1994]. During signal transduction in chemical synapsis calcium concentration is an essential chemical messenger [Katz and Miledi 1970]. The arriving action potential triggers voltage gated calcium channels to open. Due to a concentration gradient between intra- and extracellular calcium concentrations, the opening of calcium channels lead to calcium influx into the presynapse. The increase of intracellular calcium, in turn, leads to neurotransmitter release into the synaptic cleft. Thereby chemical synapses are highly dependent on tightly regulated calcium homeostasis (reviewed in [Frank 2014]). Mitochondria regulate cytosolic calcium during normal transmission, but also during synaptic depression high calcium sequestration is

necessary for recovery [David and Barrett 2003]. Especially during and after tetanic stimulation mitochondria buffer calcium and release it after stimulation to maintain residual calcium levels [Tang and Zucker 1997].

Drosophila larvae with an axonal transport defect of mitochondria have been shown to be unable to maintain vesicle release during prolonged stimulation [Guo et al. 2005]. The lack of mitochondria at the synapse also leads to a defect in cycling of reserve pool vesicles [Verstreken et al. 2005]. Furthermore, damaged mitochondria not only lead to altered ATP production and impaired calcium buffering, but also release apoptotic cell death signals (for review see [Green and Van Houten 2011]). Consequently, regulated mitochondrial transport is essential for functional cellular homeostasis.

1.3.3 Mitochondrial dynamics

Mitochondria are highly mobile organelles that form dynamic networks [Westermann 2012]. They are often located at sites of high energy demand like nodes of Ranvier, the axon initial segments and presynaptic sides [Hollenbeck and Saxton 2005]. Mitochondria are thought to be mainly synthesized in the cell body [Hollenbeck and Saxton 2005]. But frequent cycles of fission and fusion of mitochondria can also maintain their proper function outside the cell body [Westermann 2012]. Partly damaged mitochondria can be rescued by fission with healthy mitochondria [Detmer and Chan 2007]. The importance of these fission and fusion events became clear by the discovery of various diseases (e.g. Charcot-Marie-Tooth disease type 2A, CMT2A [Zuchner et al. 2004], optic atrophy [Olichon et al. 2006]) that originate in the dysfunction of these processes and by the connection to apoptosis and mitophagy [van der Bliek et al. 2013]. Nevertheless, newly synthesized mitochondria need to be transported long distances, especially in neurons. Long distance transport of mitochondria is mainly driven by Kinesin-1 in the anterograde direction and Dynein in the

retrograde direction [Pilling et al. 2006; Karle et al. 2012; Sheng and Cai 2012; Campbell et al. 2014]. Kinesin-3 can transport mitochondria in tissue culture cells [Nangaku et al. 1994], but not in *Drosophila* [Barkus et al. 2008]. The binding of mitochondria to Kinesin-1 is Klc independent, but is mediated by the two adaptor proteins Miro and Milton. The C-terminal of Khc directly binds to Milton, which is associated to Miro. Miro is anchored to the outer mitochondrial membrane [Glater et al. 2006]. The movement of mitochondria is not uniform. It shows frequent pausing and halting at stationary residence sites between stable run periods [Chada and Hollenbeck 2004; Miller and Sheetz 2004]. Although energy for axonal vesicle transport seems to be provided from glycolysis, transport of mitochondria is not dependent on glycolysis [Zala et al. 2013]. Therefore, fast axonal transport is not totally blocked by perturbing glycolysis, but it gets decreased [Zala et al. 2013].

1.3.4 Regulation of mitochondrial transport

Synaptic activity is far from constant and ATP production needs to be matched to this demand. The organelles representing the major energy source are mitochondria. Therefore, their transport needs to be tightly regulated. What exactly controls anterograde or retrograde movement of mitochondria or their stationary periods is not entirely clear. One hypothesis is that all types of motor proteins could be attached to the mitochondrion, but differentially silenced and activated [Saxton and Hollenbeck 2012]. The other hypothesis says that the rapid change in stop and start movement of mitochondria could arise from complete release of motor proteins during pauses and new binding of motor proteins when movement starts again. It is also possible that both types of regulation co-exist [Saxton and Hollenbeck 2012].

Mironov and colleagues reported that the local ratio of ADP to ATP influences the movement of mitochondria near sites of synaptic activity [Mironov 2007]. In cardiac

myoblasts mitochondrial mobility can be controlled by the level of cytoplasmic calcium concentrations [Yi et al. 2004]. Local changes in intracellular calcium concentrations also regulate indirect the attachment of mitochondria to their tracks [Brough et al. 2005; Wang and Schwarz 2009].

The mechanism by which mitochondrial movement is regulated by calcium concentrations is probably at the level of motor protein function and through detachment from the tracks (Figure 8).

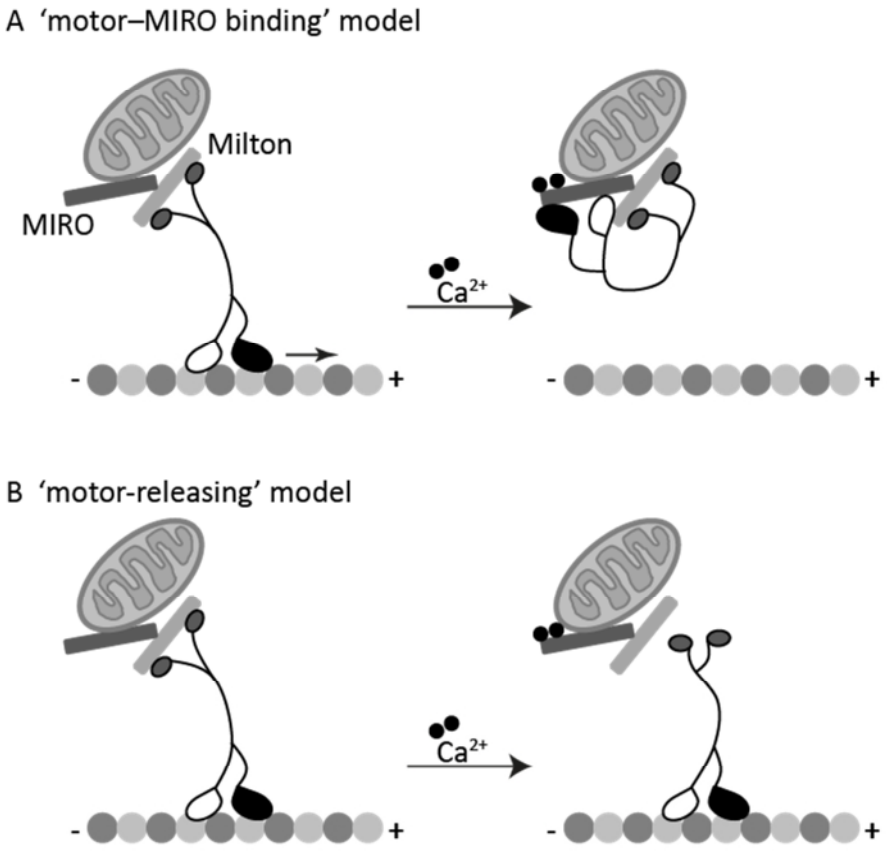

Figure 8: Two models for calcium dependent regulation of mitochondrial movement on MTs

MTs are shown as light and dark grey beads, Kinesin-1 motor proteins are shown in black and white. **(A)** In the "motor-Miro binding" model calcium binds to the EF hands of Miro and leads to the binding of the Khc motor domain to Miro instead of MTs. **(B)** In the "motor-releasing" model calcium induces separation of Khc from the Miro-Milton-mitochondria complex. Image is modified from [Sheng and Cai 2012].

There are two proposed models of the role of Miro in the calcium-mediated regulation of mitochondrial mobility (Figure 8). As Miro has two calcium binding sites (EF-hand motifs), it is able to regulate mitochondrial mobility in response to calcium signaling pathways. In the absence of calcium Kinesin-1 transports mitochondria via the Miro/Milton complex. In the 'motor-Miro binding' model calcium binds to the EF-hands of Miro [Wang and Schwarz 2009]. Thereby the Khc motor domain detaches from MTs and binds at Miro instead of MTs. In the 'motor-releasing' model [Macaskill et al. 2009], calcium binding to Miro leads to a release of Khc from Miro-bound mitochondria. Additionally, mitochondrial mobility can also be influenced by Miro dependent calcium influx in the mitochondrial matrix [Chang et al. 2011].

1.4 SPG10

This study focuses on the consequences of the expression of mutant Khc (Khc^{N262S}, $Khc^{-/-}$) in *Drosophila* larvae. Khc^{N262S} in *Drosophila* corresponds to Khc^{N256S} in the human genome, which represents one specific mutation in the HSP subtype SPG10. The SPG10 locus is on chromosome 12q13 and the affected gene codes for KIF5A [Reid et al. 1999; Reid et al. 2002], one of the three human Khcs. Non-functional Kinesin-1 inevitably leads to defects in axonal transport.

1.4.1 Mutations in the HSP locus SPG10

In the HSP locus SPG10, which contains the KIF5A gene, 20 different mutations were found in patients of HSP (Figure 9, [Reid et al. 2002; Fichera et al. 2004; Lo Giudice et al. 2006; Schüle et al. 2008; Tessa et al. 2008; Goizet et al. 2009; Crimella et al. 2011; Musumeci et al. 2011]. SPG10 accounts for approximately 3% of autosomal dominant HSPs in European families [Schüle et al. 2008] and causes pure and complex forms of HSP [Reid et al. 2002;

Goizet et al. 2009; Kawaguchi 2013]. The onset varies from early childhood to the third decade of life [Schüle et al. 2008].

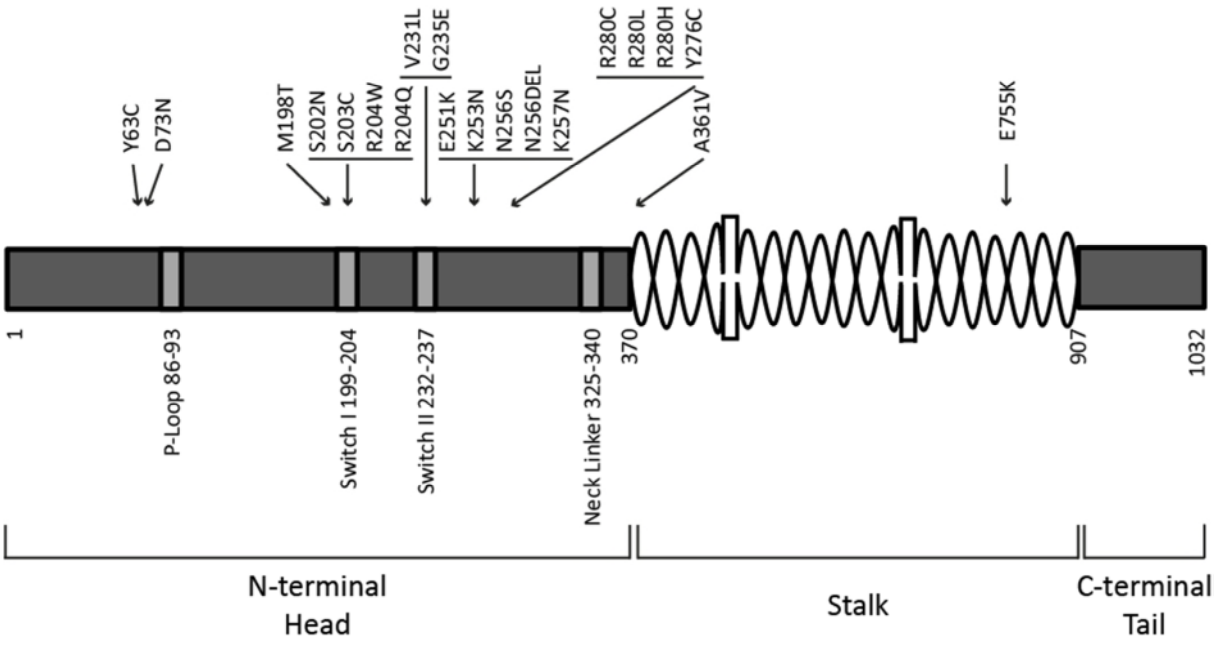

Figure 9: Domain structure of KIF5A and locations of SPG10 mutations

Most HSP mutations, identified in Kinesin-1, are located near to switch I or switch II cluster. Exceptions are located in the coiled-coil domain (E755K, [Crimella et al. 2011]) at the neck of the motor domain (A361V, [Goldstein 2001; Lo Giudice et al. 2006]) and near the P-loop (Y63C, D73N, [Schüle et al. 2008; Goizet et al. 2009]). Image is modified from [Kawaguchi 2013].

1.4.2 Possible consequences of SPG10 mutations

Mutations in *khc* might subsequently have numerous consequences on its function dependent on the affected residues. Mutations in loop 11 (amino acids 233-257) can lead to changed binding affinity on MTs, but also affect the coupling of MT binding and ATP hydrolysis.

The SPG10 mutation N256S was found by Reid and colleagues. The amino acid exchange at position 256 from asparagine (N) to serine (S) is caused by a point mutation at nucleotide 767. The wild type adenine is replaced by a guanine in the mutant gene [Reid et al. 2002]. In comparison to asparagine serine lucks one amino-residue and has thereby a

smaller molecular mass, but both are polar amino acids. The position N256 belongs to the ~10 amino acids of loop 11 that can be recruited by helix-α4 during MT binding conformational changes of Kinesin-1 [Djagaeva et al. 2012]. Consequently, an involvement in the coupling of MT binding and ATP hydrolyses cycle of the mutation is very likely.

In *Saccharomyces cerevisae* a mutation in the homologues amino acid position of Khc^{256} in KAR3 (N650K), a minus-end-directed motor protein of the mitotic spindle, was isolated [Hoyt et al. 1993]. This mutation showed dominance over the wild type, but did not gain a new activity compared to the wild type protein and thereby was suggested to act in a dominant-negative manner [Hoyt et al. 1993; Reid et al. 2002]. A more recent study showed that the mutant KAR3 could tightly bind MTs independent from nucleotide binding [Song and Endow 1998]. ATP binding and hydrolysis was not affected, whereas the coupling of nucleotide binding site and MT stimulation was disturbed [Song and Endow 1998]. This probably led to an inhibition of movement. An *in vitro* study of the SPG10 mutation Khc^{N256S} showed that MT and cargo binding was not affected, but sliding velocity and ATP hydrolysis rate were strongly reduced [Ebbing et al. 2008]. In summary the Khc^{N256S} mutation probably leads to normal cargo binding, but reduced ATP hydrolysis rates and thereby reduced transport velocities.

1.5 Defects of axonal transport in other neurodegenerative diseases

An increasing number of motor neuron diseases is linked to disrupted axonal transport [De Vos et al. 2008; Ikenaka et al. 2012]. Mitochondrial dysfunction or altered mitochondrial dynamics are also a common hallmark of many neurodegenerative disorders

(for review see [Chang and Reynolds 2006; Chen and Chan 2009; Schon and Przedborski 2011; Sheng and Cai 2012]).

Length dependent axonal neuropathy of peripheral neurons is a common feature of HSPs and CMT [Baloh et al. 2007]. CMT is the most common hereditary neuropathy and is characterized by weakness and atrophy of distal muscle and mild sensory loss. CMT2 has also been associated to mutations in SPG10 loci KIF5A [Crimella et al. 2011]. The close relation between CMT2 and HSP was also indicated in a study of Liu and colleagues. They describe two SPG10 mutations in patients with clinical symptoms of CMT2 [Liu et al. 2014]. CMT2A is also associated with several mutations in the mitochondrial fusion protein Mitofusin2 [Zuchner et al. 2004], which is needed for axonal transport of mitochondria as it interacts with mammalian Miro and Milton proteins [Misko et al. 2010]. Consequently, transgenic mouse models of CMT2A show disrupted axonal transport of mitochondria [Baloh et al. 2007; Cartoni et al. 2010]. Thereby, common pathological mechanisms for both CMT and HSP are conceivable.

The degeneration of motor neurons in cortex, bulbus and spine is characteristic for amyotrophic lateral sclerosis (ALS), which is the most common adult-onset motor neuron disease. EM analysis revealed swellings in motor axons of patients with ALS that contained vesicles, lysosomes, mitochondria and intermediate filaments [Sasaki et al. 1990; Corbo and Hays 1992]. Earliest symptoms may be lower extremity spastic weakness that is very similar to symptoms of HSP [Okada et al. 1995]. 20% of familial cases of ALS are caused by gain of function mutations in superoxide dismutase (SOD1). Then motor neurons degenerate first at the NMJ [Frey et al. 2000; Fischer et al. 2004]. Mice expressing mutant SOD1 show reduced anterograde and retrograde transport of mitochondria in motor neurons [De Vos et al. 2007], as well as impaired fusion and a reduced mitochondrial potential [Magrane et al.

2012]. Bosco et al. perfused misfolded SOD1 into squid plasm and inhibited fast axonal transport [Bosco et al. 2010]. Hence, impaired axonal transport might be a common pathological feature of ALS and HSPs.

Studies of neurotoxin-induced Parkinsonism have shown increased Dynein-mediated retrograde and decreased kinesin-mediated anterograde transport of vesicles [Morfini et al. 2007]. These transport impairments were accompanied by a loss of synaptic membranous organelles in presynaptic terminals and are therefore likely responsible for the altered synaptic function and the primary cause of the dying back pathology of Parkinson's disease [Morfini et al. 2007]. Parkinson's disease is characterized by the degeneration of dopaminergic neurons in substantia nigra, which causes rigidity, shaking and gait disturbance.

1.6 *Drosophila* as a model organism

Since more than a century, *Drosophila melanogaster* has been used as a model organism. Big advantages of the fruit fly are for example their short life cycle (Figure 10) and the large number of individuals that can be easily generated.

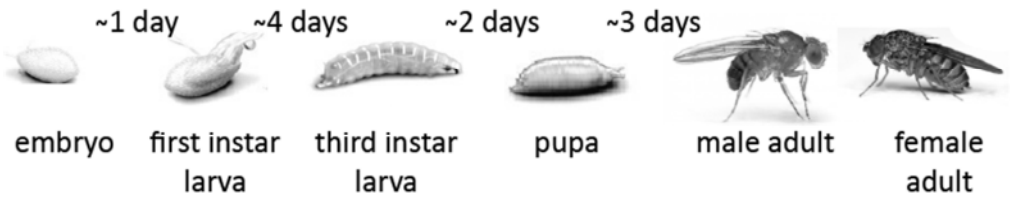

Figure 10: The *Drosophila* life cycle

The whole generation time of a *Drosophila melanogaster* fly takes about 10 days at 25°C. About 24h of embryogenesis after egg laying result in the hatching of a first instar larva that starts to feed. Once again 24h later, second instar larvae hatches. The next molt generates the third instar larva that persists two to three days. The prepupal stage crawls out of the food and attaches to a dry surface. After five days of metamorphoses the adult fly ecloses. After a few hours it becomes fertile. An adult fly can then live around four weeks.

A further characteristic is the unparalleled wealth of tools that have been generated (for review see [Frank et al. 2013]). For fundamental questions in synapse biology *Drosophila* serves well as a model for neuroscientists. Synaptic proteins of *Drosophila* are at the amino acid level about 70% similar to their mammalian counterparts. Almost every mammalian protein has a *Drosophila* orthologue [Littleton 2000; Littleton and Ganetzky 2000; Lloyd et al. 2000]. The NMJ as well as the innervating motor neuron is positioned near the muscle layer beyond the transparent body wall of *Drosophila* larvae. Thereby, they are easily accessible in filleted preparations, as well as by *in vivo* imaging [Füger et al. 2007]. These advantages have led to some of the first *in vivo* measurements of synaptic trafficking rates ever obtained in a model organism. It is a matter of cause that *in vivo* studies have great advantages to cultured systems because of the intact cellular and developmental context.

In many neurodegenerative diseases *Drosophila* serves as a model organism. Expression of α-synuclein leads to Lewy body like accumulations in the brain and flies show motor dysfunction by climbing defects [Feany and Bender 2000]. The common pathway of Pink1 and Parkin has also been found in *Drosophila* [Clark et al. 2006; Park et al. 2006; Yang et al. 2006]. As a model for Alzheimer's disease *Drosophila* has shown that overexpression of human wild type or mutant Tau leads to age-dependent axonal transport defects, neurodegeneration and death (for review see [Prüßing et al. 2013]). Therefore, the possibility of modeling fundamental aspects of human degenerative diseases in a simple model organism like the fly contains many advantages.

1.6.1 The *Drosophila* neuromuscular junction

The larval *Drosophila* neuromuscular system contains 32 motor neurons in each abdominal hemisegment that are innervating the 30 body wall muscles [Landgraf et al. 1997]. As they are organized in a stereotypical way, they are individually specified and easily to re-identify in single larvae [Johansen et al. 1989; Collins and DiAntonio 2007]. Each muscle in the fly is a single syncytial fiber that is innervated by up to three motor neurons [Bate and Broadie 1995]. These motor neurons end up in a NMJ, which connects the neuron to the muscle surface.

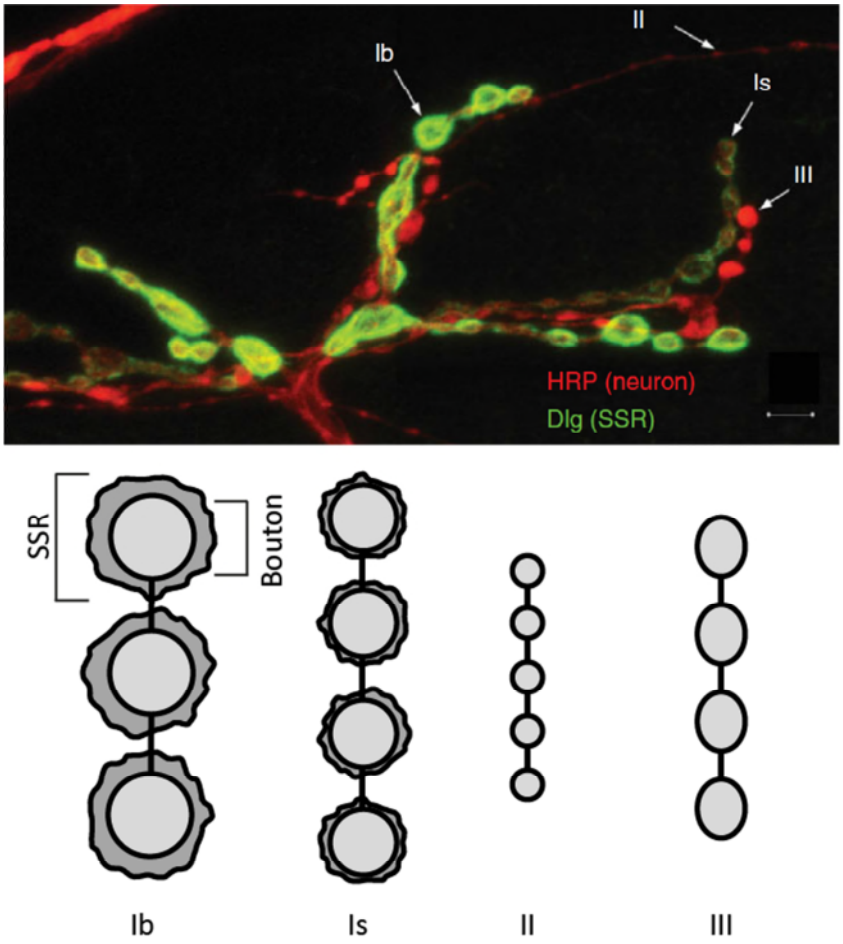

Figure 11: Different bouton types and their structure

Neuronal membranes were stained for horseradish peroxidase (HRP, red), subsynaptic reticulum (SSR) was stained by an antibody against discs-large (Dlg, green). Different types of boutons on a muscle 12 are indicated by arrows. Type Ib and Is boutons are both glutamatergic, but differ in size, morphology and the amount of SSR that surrounds them. Type II and type III boutons do not stain for Dlg and use peptides among others as neurotransmitters [Menon et al. 2013]. Scale bar 5µm. Image is modified from [Menon et al. 2013].

Each NMJ consists of about 20-50 boutons that are classified in three types: Type I is glutamatergic and is subdivided in Ib (large) and Is (small). Type II and type III boutons use primarily peptides for neurotransmission (Figure 11, [Menon et al. 2013]).

Each bouton consists of about 5-20 individual presynaptic release sites, also called active zones (AZs). The AZ is composed of a number of proteins that provide a scaffold for the vesicle docking procedure. Here, transmitter vesicles cluster and fuse with the synaptic membrane (chemical synapse, [Couteaux and Pecot-Dechavassine 1970]). In the larval NMJ ionotropic glutamate receptors are positioned at the postsynaptic side of the AZ to sense the released transmitters. The homology to AMPA-glutamate receptors in the mammalian brain makes the larval neuromuscular system a good model for vertebrate glutamatergic synapses [Collins and DiAntonio 2007].

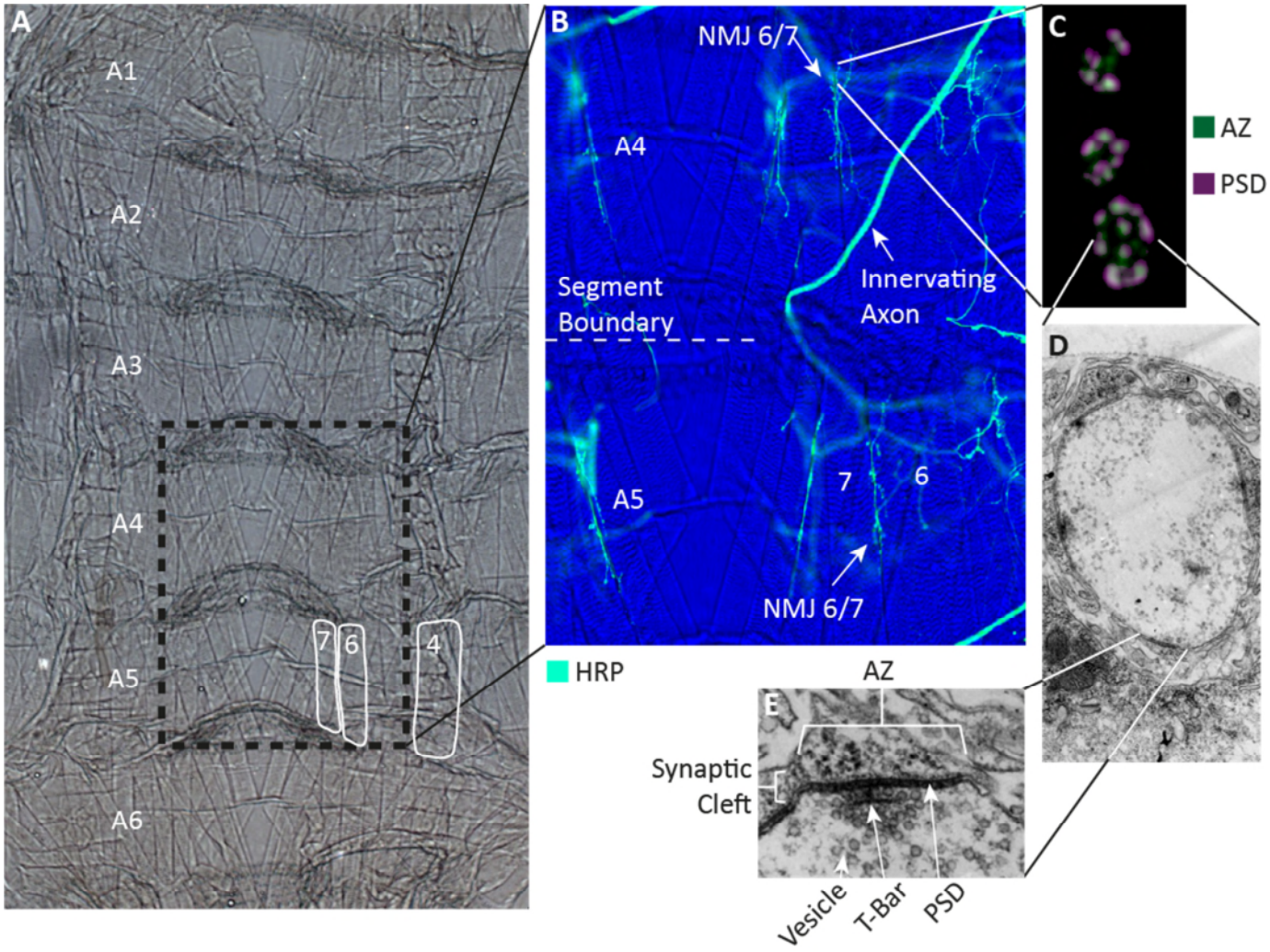

Figure 12: Organization of the NMJ

(A) Abdominal body wall muscles of *Drosophila* larvae are organized in overall eight segments that are almost equally constructed. **(B)** Magnification of segments A4 and A5 of a dissected and fixed L3 larva. Neuronal membranes are stained for HRP (cyan). Bright light image is shown in blue. The innervating axon spreads to its allocated body wall muscles from the medial axis. **(C)** Boutons of NMJ 6/7 are magnified and stained for Bruchpilot (Brp), an AZ protein and with glutamate receptor IIC to visualize postsynaptic densities (PSDs) **(D)** EM image shows one bouton with several dark spots at the surface that indicate PSDs. **(E)** Magnification of (D) shows the structural architecture of an AZ. The synaptic cleft spans the AZ and separates the pre- and postsynapse. Synaptic vesicles are arranged around the T-bar. EM images were kindly provided by J. Kern.

The presynapse

The presynaptic compartment of the NMJ is located at the neuronal part of the synaptic cleft (Figure 12). It consists of various proteins that localize near to the AZ. SVs store neurotransmitters. They exist in different populations depending on how they participate in synaptic transmission: the readily releasable pool, the recycling pool and the reserve pool [Rizzoli and Betz 2005]. The readily releasable pool (1-2% of the total vesicle pool) can directly fuse to the presynaptic membrane upon action potential arrival. On high frequent stimulation the reserve pool (80% of the total vesicle pool) provides neurotransmitter, when the readily releasable pool is empty. The recycling pool (~20% of the total vesicle pool) maintains exo- and endocytosis at moderate stimulation and can be continuously refilled by the endocytotic machinery (for review see [Rizzoli and Betz 2005; Denker and Rizzoli 2010]). The plasma membrane at the presynapse contains several proteins that enable signal transduction. Voltage-gated calcium channels are needed for action potential-driven calcium influx that triggers SV fusion [Kawasaki et al. 2004]. This vesicle fusion is mediated by the SNARE complex [Sudhof 2004]. The core SNARE complex consists of Synaptobrevin, Syntaxin, SNAP-25 and Synaptotagmin. Synaptobrevin anchors the vesicles to the SNARE complex, Syntaxin and SNAP-25 are located to the presynaptic membrane [Sollner et al. 1993]. Synaptotagmin is located in the membrane of the vesicles and serves as a calcium sensor [Mackler et al. 2002]. It was also shown to influence Bruchpilot (Brp) organization at AZs [Paul et al. 2015]. Brp is the *Drosophila* homologue to the mammalian ELKS/CAST/ERC protein and organizes the assembly of AZ cytomatrices, known as T-bars, in *Drosophila* [Wagh et al. 2006]. It also influences the size of the readily releasable pool of SVs [Matkovic et al. 2013]. T-bars are electron dense structures at the presynapse where calcium channels

cluster and the fusion of SVs takes place [Kittel et al. 2006]. Besides Brp, RIM-binding protein is a major component of the T-bar [Liu et al. 2011].

Adhesion molecules like integrins [Chavis and Westbrook 2001] and cadherins [Cifuentes-Diaz et al. 1994; Fannon and Colman 1996] also provide a proper apposition of pre- and postsynaptic structures.

The postsynapse

The specialized zone that opposes the presynaptic AZ on the postsynapse is ultrastructurally characterized by an electron dense structure and therefore called postsynaptic density (PSD). In this region adhesion molecules that associate with their presynaptic counterparts and glutamate receptors (GluRs) are enriched. GluRs are heterotetrameric complexes that consist of the essential subunits GluRIIC, GluRIID and GluRIIE and either GluRIIA or GluRIIB. The latter showing differences in their single channel properties and synaptic currents [DiAntonio et al. 1999; DiAntonio 2006]. The PSD is also comprised of scaffolding proteins, cytoskeletal proteins and associated signaling proteins. Clustering of neurotransmitter receptors and scaffolding proteins is mediated by Discs-large (Dlg) protein [Budnik et al. 1996], the *Drosophila* homologue of mammalian PSD-95 protein [El-Husseini et al. 2000]. Dlg was shown to regulate structure and function of type I glutamatergic synapses [Budnik et al. 1996]. It is also responsible for proper localization of the potassium channel Shaker [Tejedor et al. 1997] and the homophilic cell adhesion molecule Fasciclin II (FasII) [Thomas et al. 1997]. FasII is the *Drosophila* homologue for mammalian N-CAM and functions in growth cone guidance [Menon et al. 2013] and synaptic stabilization [Schuster et al. 1996]. At the postsynaptic side type I boutons are surrounded by a system of membranes called the subsynaptic reticulum (SSR), which appears to form a halo

surrounding the boutons [Petersen et al. 1997]. Dlg is expressed at the SSR and in association to presynaptic membranes [Lahey et al. 1994]. FasII expression in the SSR is restricted to the postsynapse [Schuster et al. 1996].

Synaptic plasticity

A remarkable feature of synapses is that they are highly dynamic. During development synapses undergo an activity-dependent review. Competition results in progressive changes in synaptic structure. The initial overproduction of synapses is followed by a period of selective elimination [Zhang and Poo 2001]. This leads to weakening and loss of some synapses, but also to strengthening and maintaining of others [Wyatt and Balice-Gordon 2003]. Long-term plasticity in synaptic function (hours or days) leads to structural alterations [Guo and Zhong 2006], whereas short-term changes (milliseconds to minutes) involve the modulation of presynaptic transmitter release or postsynaptic transmitter detection [Zucker 1989].

Molecular mechanisms that regulate NMJ development are inherently similar between vertebrates and *Drosophila* [Keshishian et al. 1996; Featherstone and Broadie 2000]. In *Drosophila* each muscle cell is innervated by an identified motor neuron and this input persists throughout development [Keshishian et al. 1996]. Therefore, the number of boutons and the size of the NMJ innervating the muscle has to be expanded due to a tight coupling of synaptic and muscle growth [Davis and Bezprozvanny 2001; Menon et al. 2013].

NMJ formation

During larval development diverse mechanisms like neuronal activity, target derived signals and glial activity [Packard et al. 2002; Marques and Zhang 2006; Fuentes-Medel et al. 2012] drive synaptic growth. From hatching of the embryo to late third instar larvae, muscle

surface area increases up to 100-fold. The final increase of AZs then matches this fundamental growth [Menon et al. 2013]. New boutons either locate between preexisting boutons or at the end of a branch of the NMJ. They arise by asymmetric budding, symmetric division or by *de novo* formation from the axonal membrane (Figure 13, [Zito et al. 1999; Menon et al. 2013]).

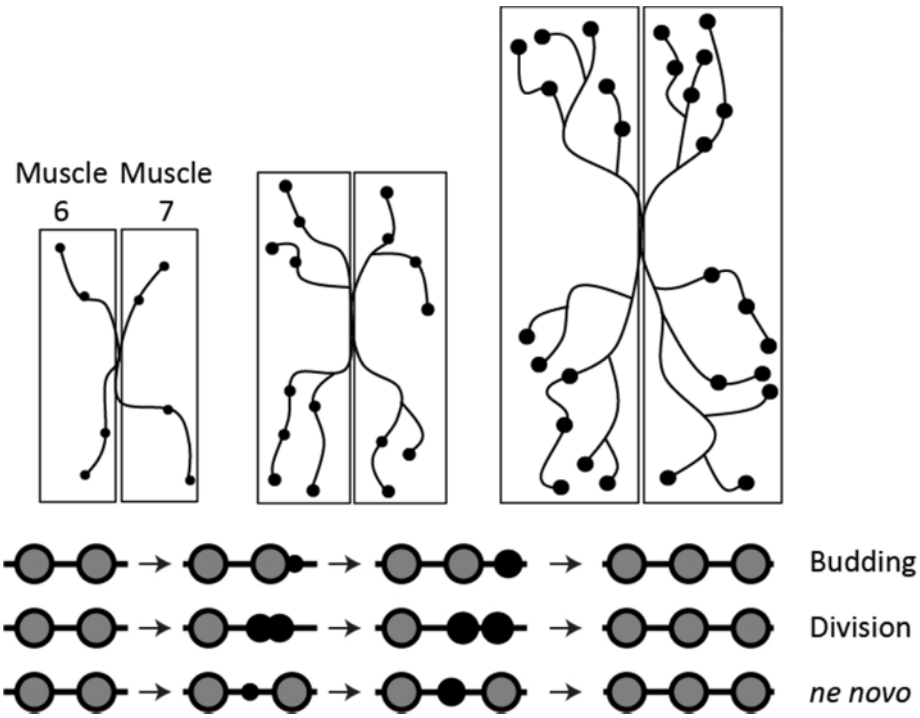

Figure 13: Schematic overview of bouton formation mechanisms.

The expansion of NMJ 6/7 during larval growth is characterized by increasing branch and bouton numbers. New boutons can be added by three different mechanisms: asymmetric budding of an already existing bouton, symmetric division of a bouton or *de novo* formation out of the neuronal membrane at the NMJ [Zito et al. 1999]. Image is modified from [Menon et al. 2013].

The development of NMJs begins with an initial contact of motor neurons to the muscle surface, which then extents in size to both sides, anterior and posterior, at embryonic stage 17 [Schuster et al. 1996]. By hatching the NMJ contains AZs with T-bars and is physiologically mature [Broadie and Bate 1993; Schuster et al. 1996].

Mutants with hyperexcitable neurons show increased number of synaptic boutons, suggesting a positive regulation of synaptic activity to NMJ growth [Budnik et al. 1990;

Mosca et al. 2005]. Steward and McLean have shown that the population density of *Drosophila* larvae also has an impact on synaptic morphology [Stewart and McLean 2004]. NMJ branch length and bouton number decrease with increasing larval population [Stewart and McLean 2004].

In *Drosophila,* synaptic growth and stabilization is dependent on MAP Futsch [Roos et al. 2000] and the neuronal cell adhesion molecule FasII, which is strongly expressed at synaptic terminals [Schuster et al. 1996]. *FasII* null mutants show maturation of the NMJ with building new AZs only until the first instar larva. After that, NMJ outgrowth stops [Schuster et al. 1996]. Larvae lacking Futsch show a dispersed MT and Futsch staining and cannot form MT loops that are necessary for proper bouton formation [Roos et al. 2000].

During larval development the formation of NMJs underlies a complex system that leads to stabilization of some transient structures und retraction of others. Transient structures contain synaptopods, presynaptic debris and ghost boutons. These structures can be observed during normal growth of the NMJ and seem to be remnants of the refinement process of the nervous system [Menon et al. 2013].

Ghost boutons are immature boutons that are not surrounded by postsynaptic elements and contain vesicles, but no AZs. These boutons can be stained for horseradish peroxidase antibody (HRP, binds to neuronal membranes), FasII, SV marker and Synapsin, but rarly show Brp immunoreactivity. They likely represent an immature bouton that can differentiate into a mature bouton [Ataman et al. 2008]. In contrast, synaptic footprints show areas where presynaptic structures have retracted (Figure 14). In this stage the postsynaptic specialization is still visible. The frequency of synaptic footprints is around 18% in early larval development and even lower in third instar larva [Eaton et al. 2002].

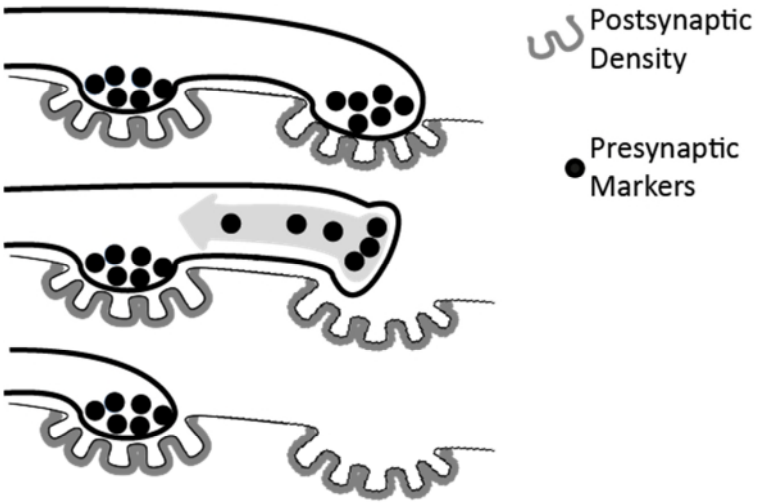

Figure 14: Presynaptic retraction resulting in a "footprint"

Schematic presentation of a hypothesized series of events in a retracting NMJ that results in a "footprint". Thereby presynaptic retraction is more rapid than postsynaptic disassembly. The synaptic "footprint" is consequently a transient state during retracting NMJs. Figure is modifed from [Eaton et al. 2002].

1.6.2 Neurodegeneration in *Drosophila* NMJs - presynaptic retraction and Wallerian-like degeneration

Studies of NMJ retraction in *Drosophila* are based on mutants that affect NMJ stability. Genetic loss of different proteins, which are necessary for stable NMJs, show a common kind of neuronal retraction. In a state prior to retraction of the neuromuscular terminal, Futsch and MT staining is reduced. Then, the AZ marker Brp and the vesicular glutamate transporter (VGlut) disappear. In the end, the neuronal membrane and FasII structure are disturbed [Graf et al. 2011]. Thereby, the presynaptic part of the NMJ retracts from the muscle fiber in a distal-to-proximal manner towards the axon and postsynaptic specializations are left unopposed (Figure 14, [Eaton et al. 2002; Eaton and Davis 2005; Pielage et al. 2005; Massaro et al. 2009]).

Classically Wallerian degeneration is defined as degeneration of axons after a distal injury that follows the original nerve transection experiments from Waller [Waller 1850]. Here, synaptic boutons, located at the NMJ distal to the site of nerve transection, become

morphologically separated from one another [Xiong and Collins 2012]. In between 12h after injury, they become also devoid of presynaptic proteins like Brp and GluRIIC and Futsch [Xiong and Collins 2012]. Influx of extracellular calcium was shown to be necessary and sufficient to trigger Wallerian degeneration [George et al. 1995].

As chemical or genetic inhibitors of apoptosis cannot block Wallerian degeneration [Finn et al. 2000; Whitmore et al. 2003; Osterloh et al. 2012], it appears to be a mechanism that is molecularly distinct from apoptosis. The term Wallerian-like degeneration means the degeneration of axons in the absence of transection or crush injury with Wallerian-like morphology. Wallerian degeneration can be slowed down by the wallerian degeneration slow (Wld^S) protein. Wld^S is a fusion protein of the 70 N-terminal amino acids of Ube4b with full-length Nmnat1 [Coleman et al. 1998; Conforti et al. 2009] that can delay degeneration of injured axons by ten-fold [Coleman and Freeman 2010]. Wld^S is not present in wild type animals.

Most probably the mechanism, by which NMJs degenerate, is influenced by the trigger that leads to neuronal degeneration.

1.6.3 Animal models of non-functional Khc protein

Clinically, SPG10 has been classified as a neurodegenerative disorder [Reid et al. 2002]. However, experimental data derived from *Kif5a* knockout mice, KIF5A mutant zebrafish and *Drosophila khc* null mutant provide evidence for neurodevelopmental defects [Hurd and Saxton 1996; Xia et al. 2003; Karle et al. 2012; Nakajima et al. 2012; Campbell et al. 2014]. However, morphological changes observed in the respective khc^{N262S} mutant *Drosophila* larvae seem to be primarily degenerative in nature [Füger et al. 2012].

Kif5A *knockout mouse models*

Kif5a knockout mouse models die shortly after birth. Karle and colleagues reported severe deficits in neurodevelopment with impaired neurite outgrowth in cultured motor neurons from *Kif5a* knockout mice, while axonal swellings were not prominent [Karle et al. 2012].

Postnatal conditional knockout of *Kif5a* in mice results in severe seizures [Xia et al. 2003; Nakajima et al. 2012]. The conditional *Kif5a* knockout mouse model of Nakajima and colleagues died at approximately three weeks of age [Nakajima et al. 2012]. They showed abnormal trafficking of inhibitory $GABA_A$ receptors to the neuronal membrane in the brain, a seemingly neurodevelopmental defect. Nakajima and colleagues suggested this to be the possible cause of the reported epileptic seizures [Nakajima et al. 2012].

Xia and colleagues reported a similar conditional knockout model for which 75% of the knockout mice had seizures and died at the age of around three weeks [Xia et al. 2003]. The remaining mice however, survived for three months or longer. These mice displayed age dependent neurodegeneration, accumulation of neurofilaments and hindlimb paralysis. Though, Nakajima and colleagues could not confirm a survival of *Kif5a* knockout mice after four weeks [Nakajima et al. 2012]. Consequently, developmental defects dominate in these mouse models of HSP.

Kif5A mutant zebrafish model

In zebrafish, KIF5A mutations truncating the tail domain of the protein led to seizures and to higher sensitivity. Additionally, the posterior lateral line nerve (pLLn), the longest motor neuron, was shorter and thinner compared to controls (Campbell et al., 2014). These pathologic alterations can thereby also be classified as neurodevelopmental delay.

Khc mutant Drosophila *models*

Hurd and colleagues suggested a reduced outgrowth as reason for less synaptic boutons in *khc*$^{-/-}$ *Drosophila* larvae [Hurd and Saxton 1996].

In summary, this means that so far the developmental delay was the major pathological factor of HSP animal models.

Füger and colleagues established a *Drosophila* model with ectopic overexpression of the dominant negative Khc mutation *Khc*^{N262S} [Füger et al. 2012]. The larvae showed a tail-flip phenotype and axonal traffic jams with enrichment of markers for synaptic vesicles (VGlut, CSP), dense core vesicles (ANF) and AZ particles (Brp), autophagosomes (ATG8) and lysosomes (LAMP). The mitochondrial flux in axons was reduced in both directions and NMJ size was reduced [Füger et al. 2012]. The electrophysiological transmission at the synapses was reduced and NMJs were retracting [Füger et al. 2012]. In this *Drosophila* model of SPG10 neurodegeneration is the predominant pathology.

Compared all available animal models of HSP, this approach resembles most the patients' situation. As the clinical evaluation resulted in a degenerative pathology of HSP, the predominantly degenerative pathology of the fly model of Füger and colleagues fits best for examinations of the origin of the disease. Unfortunately the above mentioned model dies early and is only accessible shortly before death [Füger et al. 2012]. This led to the idea to create a *Drosophila* model with lower expression levels of the mutant protein to achieve less severe affected larvae. Aim of this study was to shed light on the pathological progression events that lead to the HSP like symptoms in larvae: the posterior paralysis.

2 AIMS

The point mutation Khc^{N256S} causing SPG10 acts dominant negative on dimer forming wild type Khc. Few animal models of KIF5A loss exist [Hurd and Saxton 1996; Xia et al. 2003; Karle et al. 2012; Nakajima et al. 2012], but can hardly simulate a partial loss of function of wild type Khc protein, as it is thought to happen in patients of SPG10. Furthermore these models hint at neurodevelopmental defects, whereas HSP is clinically classified as a neurodegenerative disease [Salinas et al. 2008; Novarino et al. 2014]. Therefore the establishment of ectopic overexpression of *khc* bearing the corresponding point mutation in *Drosophila* (khc^{N262S}) is a major advantage in SPG10 research. Aim of this study was to create a fly model of SPG10, which contains an amount of mutant Khc that resembles more closely the situation in heterozygous SPG10 patients. Expressing khc^{N262S} or $khc^{wt+N262S}$ at moderate levels allows the analysis of pathologic steps developing the slow progression of paralysis of the posterior part of the larval body. First question to answer was, if neurodevelopmental delay and neurodegeneration occur in parallel. As Kinesin-1 is an anterograde transport protein, transport of axonal cargo to the posterior part of the larvae will be analyzed. Furthermore the morphology of NMJs of posterior segments of the larvae is an important indicator for their functionality. The most important known cargo of Khc is mitochondria. As mitochondria are important for a number of processes essential for neuronal function, it will be important to clarify the effectiveness of mitochondrial transport. Reduced exchange and less or non-functional mitochondria at synapses could be the reason for impaired locomotion [Hurd and Saxton 1996] and could be the initiator of neuronal degeneration, which was described for *Drosophila* larvae expressing mutant *khc* [Füger et al. 2012].

3 MATERIALS AND METHODS

3.1 Chemicals

All chemicals were purchased from Roth (Karlsruhe, Germany), Sigma (St. Louis, USA) or Applichem (Darmstadt, Germany), if not stated otherwise. Primer were ordered from MWG-Biotech AG (Ebersberg, Germany).

3.2 Solutions and buffers

- Solution A — 0.1M TrisHCl, pH 9.0; 0.1M EDTA; 1% SDS
- Ca^{2+} free HL3 — 70mM NaCl, 5mM KCl, 20mM $MgCl_2$, 10mM $NaHCO_3$, 5mM trehalose, 115mM saccharose, 5mM HEPES, pH 7.2
- Phosphate buffered saline (PBS) — 136.9mM NaCl, 2.7mM KCl, 1.5mM KH_2PO_4, 6.5mM, $Na_2HPO_4 \bullet 2H_2O$
- PBST — PBS with 0.05% Triton TX100

3.3 Cloning of pUAST-LifeAct-mTurquoise

All cloning steps were performed as previously described [Sambrook et al. 1989]. Restriction enzymes were purchased from New England Biolabs (Frankfurt am Main, Germany). Shrimp Alcaline Phosphatase (SAP) and T4 Ligase were purchased from Roche Diagnostics GmbH (Mannheim, Germany). QIAprep® Spin Miniprep Kit, QIAquick® Gel

Extraction Kit, QIAquick® PCR Purification Kit and QIAfilter® Plasmid Maxi Kit from QIAGEN GmbH (Hilden, Germany) were used for purification.

Both vectors (Backbone: pUAST and Insert: pLifeAct-mTurquoise N1) were cut with restriction enzymes XbaI and EcoRI. After dephosphorylation with SAP backbone vector (pUAST) and insert (LifeAct-mTurquoise N1) were ligated together. Finally, a restriction digest and sequencing was used to prove the correct integration of the insert. The pUAST-LifeAct-mTurquoise N1 vector was sent for injection into *Drosophila* embryos to BestGene (Chino Hills, USA).

3.4 Isolation of genomic DNA

Genomic DNA was isolated from a single or 10 adult flies (same sex and genotype). First, flies were frozen in an Eppendorf tube at -80°C for at least 5min. After addition of 100µl (200µl for 10 flies) solution A, flies were homogenized using a plastic pistil and incubated at 70°C for about 30min. After adding 14µl (28µl for 10 flies) of 8M KAc and a cautious shaking, they were incubated another 30min. on ice. After centrifugation for 15min. with 13,000rpm at 4°C, supernatant was gently mixed with 100% isopropanol and once again centrifuged at 10,000rpm for 5min. The pellet was washed two times with 500µl 70% EtOH and dried at room temperature for 30min. The pellet was then solved in dH_2O and DNA content was measured using a NanoDrop™ spectrophotometer (Thermo Fisher Scientific, USA).

3.5 *Drosophila* culture conditions

Flies were raised on standard corn meal/agar medium (0.8% agar, 14.3% dried yeast, 10% soy flour, 21.3% treacle, 8% malt extract, 8% corn meal, 0.63% propionic acid) seeded with yeast. They were maintained at 25°C in plastic bottles (Greiner Bio-One).

3.6 The Gal4/UAS system for targeted gene expression in *Drosophila*

The establishment of the Gal4/UAS system in flies enabled the possibility to express genes of interest in a temporal- and tissue-specific manner. Brand and Perrimon established the ectopic expression of genes under the control of a specific driver. Gal4 was identified in yeast (*Saccharomyces cerevisae*) and functions as a transcription factor for genes with an upstream activating sequence (UAS, [Brand and Perrimon 1993]). If both, Gal4 and a UAS, are expressed in one fly, the gene with the UAS gets expressed under the control of Gal4 driver. The key feature of the technique is that the transcription factor (Gal4) is separated from the targeted gene (with UAS). Only the combination of both by a cross of two transgenic *Drosophila* lines (Figure 15) leads to their activation. Thereby a huge library of different Gal4 and UAS lines could be built up that can be combined in every conceivable combination. Additionally, it is also possible to maintain stocks containing lethal target genes. Importantly, the expression of Gal4 in *Drosophila* has no overt deleterious phenotypic effects [Duffy 2002].

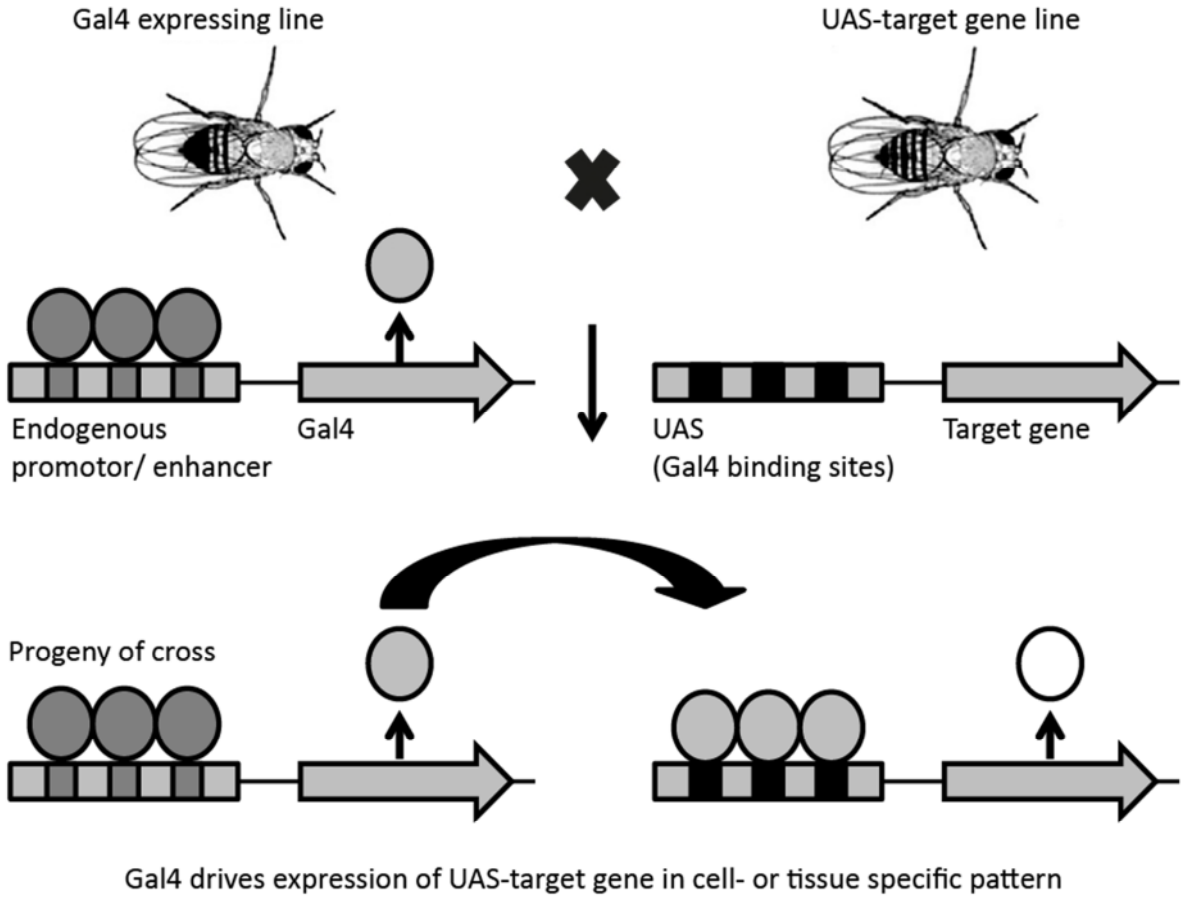

Figure 15: Directed gene expression through Gal4/UAS system

The yeast transcriptional activator Gal4 can bind to an UAS and induces expression of the following gene. Gal4 can be expressed under the control of the requested promotor. Only the progeny combines the driver and the target gene and therefore, expresses the desired gene. Image is modified from [Phelps and Brand 1998].

In *Drosophila* the activity of Gal4 is temperature dependent. With keeping the flies at 16°C minimal activity is reached, whereas a temperature of 29°C provides minimal effect on viability of the flies and maximal Gal4 activity [Duffy 2002]. This increases the flexibility of this system and is particularly interesting for studies that aim to examine mild phenotypes with lower expression levels of the targeted gene.

3.7 *Drosophila* larvae used for analysis

Transgenic fly stocks were obtained from the Indiana University Stock Center (Bloomington, IN), unless otherwise specified. Table 3 lists all fly strains used in this study.

Table 3: Fly strains used in this study

	Allel	Chromosome	Donor/ BDSC number	Reference
Deficiencies	w^{1118}	X	BL 3605	[Castiglioni 1951]
	khc^{8}	II	BL 1607	[Saxton et al. 1991]
	khc^{k13314}	II	BL 11084	[Spradling et al. 1999]
Driver	D42-Gal4	III	BL 8816	[Gustafson and Boulianne 1996]
UAS-Constructs	UAS-khc^{wt}	III	intern	[Füger et al. 2012]
	UAS-khc^{N262S}	III	intern	[Füger et al. 2012]
	UAS-GluRIIA-C1-genomic-GFP	III	S. Sigrist	[Rasse et al. 2005]
	pacman-BRP-GFP	III	S. Sigrist	unpublished
	UAS-IVS-myr-tdTomato	III	BL 32221	[Trichas et al. 2008]
	UAS-mito-GFP	II	BL 8442	[Barkus et al. 2008]
	UAS-LifeAct-mTurquoise	III		this study
Exon-Trap Line	Dlg-GFP	X	Flytrap CC01936	[Buszczak et al. 2007]

UAS-*khc*^{wt}, UAS-*khc*^{N262S} and UAS-*khc*^{wt} in combination with UAS-*khc*^{N262S} were expressed in a wild type background using the motor neuron driver D42-Gal4 [Sanyal 2009]. As control D42-Gal4 was crossed to wild type (w^{1118}) flies for heterozygous expression of D42-Gal4. To create *khc* null larvae (*khc*$^{-/-}$) the two alleles *khc*^{8} and *khc*^{k13314} were combined.

The *khc*^{8} allele [Saxton et al. 1991] carries an ethyl methanesulfonate induced point mutation (C948T) which leads to an early stop codon in the *khc* gene (R210STOP). In the *khc*^{k13314} allele a transposon (P{lacW}Khc^{k13314}) that disrupts the *khc* gene was inserted in minus orientation at position 2R:12159268 [Spradling et al. 1999]. The UAS-IVS-myr-tdTomato construct leads to UAS-controlled expression of a membrane tagged myristoylated tandem Tomato fluorescent protein [Trichas et al. 2008]. LifeAct is a nontoxic actin marker that does not interfere with actin dynamics *in vivo* [Riedl et al. 2008]. The genetic combination of LifeAct with mTurquoise is described above.

For a list of all genotypes used in this study and abbreviations used see Table 4. Expressing an additional copy of *khc*^{wt} makes no difference to control regarding behavior, survival, NMJ and axonal morphology [Füger et al. 2012].

Table 4: Genotypes used in this study

Genotype	Abbreviation
w^{-}/w^{-};+/+;D42-Gal4/+	control
w^{-}/w^{-};+/+;D42-Gal4/ UAS-khc^{wt}	khc^{wt}
w^{-}/w^{-};+/+;D42-Gal4,UAS-khc^{wt}/UAS-khc^{N262S}	khc$^{wt+N262S}$
w^{-}/w^{-};+/+;D42-Gal4/UAS-khc^{N262S}	khc^{N262S}
w^{-}/w^{-};khc^{8}/khc^{13314};+/+	khc$^{-/-}$

Table 5 shows the exact genotypes used in this study, listed according to Figure numbers.

Table 5: Genotypes according to figure numbers

Figure number	Genotype
16A-C; 20A,B; 22B,C,E,F; 28	w^-/w^-;+/+;D42-Gal4/+ w^-/w^-;+/+;D42-Gal4,UAS-khc^{wt}/UAS-khc^{N262S} w^-/w^-;+/+;D42-Gal4/UAS-khc^{N262S}
17A-C	w^-/w^-;+/+;D42-Gal4, IIA-GFP/+ w^-/w^-;+/+;D42-Gal4, IIA-GFP/UAS-khc^{N262S}
18A,B; 19A-D; 23A,C; 24	Dlg-GFP/w^-;+/+;D42-Gal4/+ Dlg-GFP/w^-;+/+;D42-Gal4,UAS-khc^{wt}/UAS-khc^{N262S} Dlg-GFP/w^-;+/+;D42-Gal4/UAS-khc^{N262S}
20C	w^-/w^-;+/+;D42-Gal4/Brp-GFP w^-/w^-;+/+;D42-Gal4,UAS-khc^{wt}/Brp-GFP, UAS-khc^{N262S} w^-/w^-;+/+;D42-Gal4/Brp-GFP, UAS-khc^{N262S}
21A-E	w^-/w^-;+/UAS-mito-GFP;D42-Gal4/+ w^-/w^-;+/UAS-mito-GFP;D42-Gal4,UAS-khc^{wt}/UAS-khc^{N262S} w^-/w^-;+/UAS-mito-GFP;D42-Gal4/UAS-khc^{N262S}
22A,D; 23B	Dlg-GFP/w^-;+/+;D42-Gal4/+ w^-/w^-;+/+;D42-Gal4/+ Dlg-GFP/w^-;+/+;D42-Gal4,UAS-khc^{wt}/UAS-khc^{N262S} w^-/w^-;+/+;D42-Gal4,UAS-khc^{wt}/UAS-khc^{N262S} Dlg-GFP/w^-;+/+;D42-Gal4/UAS-khc^{N262S} w^-/w^-;+/+;D42-Gal4/UAS-khc^{N262S}
25	w^-/w^-;+/+;D42-Gal4/UAS-mTurquoise-LifeAct w^-/w^-;+/+;D42-Gal4,UAS-khc^{wt}/UAS-mTurquoise-LifeAct , UAS-khc^{N262S} w^-/w^-;+/+;D42-Gal4/UAS-mTurquoise-LifeAct, UAS-khc^{N262S}

Figure number	Genotype
26; 27	Dlg-GFP/w^-;+/+;+/D42-Gal4, UAS-myr-tdTomato Dlg-GFP/w^-;+/+;D42-Gal4,UAS-khc^{wt}/UAS-myr-tdTomato, UAS-khc^{N262S} Dlg-GFP/w^-;+/+; D42-Gal4, UAS-myr-tdTomato /UAS-khc^{N262S}
29	w^-/w^-;+/+;D42-Gal4/+ w^-/w^-;+/+;D42-Gal4/UAS-khc^{N262S}
31; 34; 35C,D	w^-/w^-;+/+;D42-Gal4/+ w^-/w^-;+/+;D42-Gal4/UAS-khc^{N262S} w^-/w^-;khc^8/khc^{13314};+/+
32; 33; 35F,G	Dlg-GFP/w^-;+/+;D42-Gal4/+ Dlg-GFP/w^-;+/+;D42-Gal4/UAS-khc^{N262S} Dlg-GFP/w^-;khc^8/khc^{13314};+/+
35A,B,E	Dlg-GFP/w^-;+/+;D42-Gal4/+ w^-/w^-;+/+;D42-Gal4/+ Dlg-GFP/w^-;+/+;D42-Gal4/UAS-khc^{N262S} w^-/w^-;+/+;D42-Gal4/UAS-khc^{N262S} Dlg-GFP/w^-;khc^8/khc^{13314};+/+ w^-/w^-;khc^8/khc^{13314};+/+
36A	w^-/w^-;khc^8/khc^{13314};+/+
36B,C; 38	Dlg-GFP/w^-;khc^8/khc^{13314};+/+

3.8 Behavioral analysis

3.8.1 Imaging and scoring of the tail-flip phenotype

Individual larvae were placed on a thin slice of apple juice agar at 25°C. They were imaged while crawling with a DCM510 (SkopeTek, P.R. China) camera integrated in a custom-

built stereomicroscope. Tail-flipping phenotype was scored visually. A score of 1 represents a weak phenotype, a score of 5 complete paralyses excluding the mouth.

3.8.2 Righting assay

Larvae of variable size (and age) were recovered from food and washed in 15% sucrose. After 2min. for acclimatization on apple juice agar plates larvae were placed ventral side up. The time they needed for coming into crawling position/ dorsal side up was recorded in seconds [Daigle et al. 2013]. At least 50 larvae were assayed per genotype. Each larva was assayed three times. The average righting time per larva was used for further analysis. 60s was used as a cut-off for the calculation of the average. N represents the number of larvae analyzed.

3.8.3 Quantification of larval size and stage

Larvae of each genotype were kept at 25°C for four days and washed in 15% sucrose for analysis.

3.9 Larval body wall muscle preparation

Larvae of either sex were used for all experiments except for immunostaining of larvae expressing native Dlg-GFP (Flytrap CC01936, [Buszczak et al. 2007]). In this case only females were used (Dlg-GFP is located on the X chromosome). For statistical analysis of area fraction swelling, Futsch intensity, axonal VGlut, VGlut intensity at the NMJ, axonal Brp intensity, Brp intensity at the NMJ, NMJ size, AZs per NMJ, PSDs per NMJ, bouton size, AZs per bouton, PSDs per bouton, % abnormal membrane morphology and % Futsch innervated NMJ area of all genotypes, three experiments were pooled. Within these three experiments

larvae were dissected on the same day, stained in the same tube, mounted on the same slide and imaged using the same settings.

3.9.1 Larval body wall dissection

Larvae were fixed on a rubber dissection pad with insect pins (Austerlitz, Slavkov, Czech Republic) and covered with ice cold calcium free hemolymph-like solution (HL-3, [Stewart et al. 1994]). Larvae were cut open along the dorsal midline with dissection spring scissors (NO.15005-08, Fine Science Tools, Vancouver, Canada). Everything except the body wall muscles and the brain and axons (when needed for analysis) was removed with fine forceps (A1 231-20, Fine Science Tools, Vancouver, Canada) and the epidermis was pinned down at the sides [Rasse et al. 2005; Schmid et al. 2008; Kern et al. 2013]. Larvae were fixed with 4% paraformaldehyde in phosphate buffered saline for 3min. (native green fluorescent protein, GFP, epifluorescence detection) or for 10min. Larvae that were stained for Futsch were dissected with solutions at room temperature and fixed for 3min. in Bouin's Solution (Sigma; HT10132). After the fixation time larval filets were washed with PBST (0.05% Triton-X 100 in PBS) and were then also kept in PBST until immunostaining procedure.

3.9.2 Immunostaining procedure

After 30min. of blocking with 5% normal goat serum (NGS) in PBST, larval filets were stained with primary antibodies at 4°C overnight. The antibodies were diluted in 5% NGS in PBST (dilutions for each antibody see Table 6). After three short and three 30min. washing steps with PBST, larvae were incubated with secondary antibodies (diluted in 5% NGS in PBST) for two hours at room temperature. Then larvae were washed in three short and three long washing steps and incubated for 30min. in VectaShield mounting medium (Vector

Laboratories, Burlingame, USA). Finally, larvae were mounted in VectaShield® on glass object slides.

Table 6: Primary and secondary antibodies used for immunohistochemistry

Primary Antibodies

Antigen	Antibody	Host	Dilution	Fixation	Donor	Reference
Bruchpilot	Nc82	mouse	1:100	10min. PFA	DSHB*	[Wagh et al. 2006]
DV-Glut C-term		rabbit	1:2000	3min. Bouin's	H. Aberle	[Mahr and Aberle 2006]
Futsch	22C10	mouse	1:150	3min. Bouin's	DSHB	[Hummel et al. 2000]
Fasciclin II	1D4	mouse	1:50	10min. PFA	DSHB	[Hummel et al. 2000]
GluRIIC		rabbit	1:2000	10min. PFA	intern	[Kern et al. 2013]

Secondary Antibodies

Antigen	Antibody	Host	Dilution	Fixation	Donor
HRP**	Cy3	goat	1:500	over night	DiAnova
mouse	Atto-647N	goat	1:500	over night	Fluka/Sigma
rabbit	Alexa-405	goat	1:500	over night	Invitrogen
rabbit	Alexa-488	goat	1:500	over night	Molecular Probes

*DSHB Developmental Studies Hybridoma Bank
**HRP Horseradish peroxidase (plant glycoprotein common on neuronal membranes of *Drosophila*, [Snow et al. 1987; Paschinger et al. 2009]).

3.10 Imaging of *Drosophila* larvae

3.10.1 Imaging of fixed larvae

NMJs and axons were recorded using a Zeiss LSM 710 Confocal Microscope using 40x Plan-Apochromat 1.3 N.A. oil objective. Pinhole was set to 1 Airy Disc and voxel dimensions (x/y/z) of 100 × 100 × 500nm were used. Images used for deconvolution were recorded with voxel dimensions (x/y/z) of 100 × 100 × 200nm.

3.10.2 Life imaging

In vivo imaging was essentially performed as previously described [Füger et al. 2007] at a Zeiss LSM 710 Confocal Microscope using 40x Plan-Apochromat 1.3 N.A. oil objective. Pinhole was set to 1 Airy Disc and voxel dimensions (x/y/z) of 100×100×500nm were used. Brp-GFP was recorded at a speed corresponding to 1 stack per 10sec. Overall 10 Z-planes were recorded. The total time window was no more than 60min. For glutamate receptor imaging at two different time points the GFP-tagged *Drosophila* glutamate receptor subunit IIA (GluRIIA-GFP) was expressed under the native promotor [Rasse et al. 2005]. The imaging for this experiment was done by Shabab Hannan und kindly provided from him for this study. The pinhole was 35µm and an average of eight was taken. For counting mitochondria at the NMJ and measuring mitochondrial flux in the axon, UAS-mito-GFP and UAS-IVS-myr-tdTomato were expressed using the motor neuron driver D42-Gal4. Living larvae were recovered from food and pinned on a small Sylgard® plate, which sticked to a glass objective slide. They were dissected in Ca^{2+} free HL3 essentially as described above. Here the insect pins used for fixation of the larva were trimmed and pushed completely into the Sylgard® plate. After putting a cover slip onto the larva, it was imaged directly after dissection [Smith et al. 2012]. As the mitochondrial density in axons is high especially in controls, a part of the

axon was bleached by high laser intensity (488nm) for about 30sec. Directly after bleaching, 12 confocal z-planes were imaged once a minute during a time period of 10-12min. Images were recorded using a Zeiss LSM 710 Confocal Microscope using 40x Plan-Apochromat 1.3 N.A. oil objective. Pinhole was set to 1 Airy Disc and voxel dimensions (x/y/z) of 100×100×750nm were used and four times averaged. Stacks with movement were aligned using ImageJ plugin StackReg (Philippe Thevenaz, Biomedical Imaging Group, Swiss Federal Institute of Technology Lausanne; www.epfl.ch/thevenaz/stackreg). Laser intensities were adjusted such that none of the genotypes gave an oversaturated image and then kept constant within one dataset. Shabab Hannan did *in vivo* imaging of GluRIIA receptor fields.

3.11 Sample preparation for EM of NMJs

Larval fillets were prepared for EM analysis as previously described [Füger et al. 2012]. In brief, larvae were fixed with 4% paraformaldehyde for 10min. and incubated with 2.5% glutaraldehyde overnight, postfixed with 1% osmium tetroxide in 100mM phosphate buffer (pH 7.2) for 1h, rinsed with water and treated with 1% aqueous uranyl acetate for 1h at 4°C. Next dehydration was done with an ethanol series and larval fillets were kept in fluid epon overnight. Then muscles were dissected and single muscles were embedded in epon and polymerized for 48h at 60°C. Ultrathin sections were stained with uranyl acetate and lead citrate and viewed in a Philips CM10 electron microscope. EM was done by Dr. Jeannine Kern, Raphael Zinser and Matthias Flötenmayer.

3.12 Data Analysis

3.12.1 Data processing

ImageJ 1.46r was used for data analysis and processing (US National Institutes of Health; http://rsb.info.nih.gov/ij/download.html). Common settings were chosen in single data sets, avoiding oversaturation in any of the genotypes. If necessary, brightness and contrast were adjusted. Partly, images were scaled by a factor of 2, next a Gaussian blur filtering was applied (pixel radius = 2 or 1) or scaled after the Gaussian blur filtering. As last step relevant sliced of the image stacks were maximum-projected. In images processed for visualization purposes, gamma values were adjusted to 0.75.

The area of NMJs was analyzed by HRP staining. Area of binary masks of stacks that were processed like described above was measured using ImageJ. Measurements of fluorescence intensity of HRP, Futsch, or AZs were made such, that the binary mask of HRP was superimposed (minimum projection) with the maximal projected image. Thereby, original fluorescent intensities could be measured.

Number of boutons was counted manually.

The number of synapses was quantified either by counting PSDs, which were visualized by staining for the GluRIIC or GluRIIA [Qin et al. 2005] or scoring AZs that were visualized by staining for Brp [Kittel et al. 2006; Wagh et al. 2006]. For automatic counting images were processed as described above. Then grey value filter was applied and points were counted using Delta2D software (DECODON GmbH, BioTechnikum Greifswald, Germany). For PSD counting Delta2D settings were: background 7, spot size 2 and sensitivity 100; for AZ counting setting were: background 7, spot size 1 and sensitivity 100.

The area of high HRP intensities in axons and NMJs was quantified setting a threshold such, that control images did only show a minority of pixels over the set threshold. Then a binary mask with pixels above the set threshold was created and the percentage of total area to area with pixels above the threshold was quantified.

The number of mobile Brp packages and flux of mitochondria were counted manually from images processed as described above.

The area innervated by MTs was quantified by manually deleting areas that were not covered by Futsch staining from the original binary HRP mask and then quantify the area of the new binary HRP mask.

3.12.2 Quantification of larval size

Within one experiment all larvae were stained in one tube. For being able to distinguish larvae of different genotypes after common staining, the genotypes were marked with cutting away a unique part the body wall. Complete larval size was therefore quantified with a factor multiplied with the muscle length of segment A5. This factor was calculated by measuring length of whole larval body wall length and muscle length in control larvae that were not cut.

3.12.3 Normalization of values

NMJ area, AZ number and PSD number was normalized to larval length using the following formula:

$$\text{Normalized value} = \frac{\text{value}}{\text{larval length}} * \text{average larval length of the group}$$

Number of mitochondria was normalized to NMJ area using the same formula.

3.12.4 Deconvolution

Images were deconvolved using AutoQuant X.2.2.2. 3D volume rendering was created using Imaris 7.6.1.

3.12.5 Statistical analysis

Statistical significance was tested with JMP from SAS Institute GmbH (Böblingen, Germany). In normal distributed data sets with more than two groups, significance was determined by one-way ANOVA analysis followed by Dunnett's multiple comparison test. In data sets with only two groups significance was tested by Students T-Test. The standard error of mean is shown as a box and standard deviation as a black line. The following alpha levels were used for all tests: * $p<0.05$; ** $p<0.01$; *** $p<0.001$. *p*-values < 0.05 were considered to be statistically significant.

4 RESULTS

4.1 Establishment of a slow progressing SPG10 model

In an earlier study Füger and colleagues established the first SPG10 fly model expressing a mutant Khc protein (Khc^{N262S}) [Füger et al. 2012]. In this model a high expression rate of mutant khc^{N262S} led to a very fast progressing pathology and an early lethality of larvae. The high expression rate was achieved by keeping the larvae at 29°C, where the efficiency of the Gal4-UAS system is higher than at 25°C. Analyzing this model aimed the investigation of pathological events directly preceding larval paralysis and death. Major characteristics are a severe larval tail-flip, axonal swellings and traffic jam of several cargos, reduced axonal flux of mitochondria in both directions and less mitochondria at the NMJ [Füger et al. 2012].

For a more detailed investigation of initial pathological events leading to paralysis of the posterior segments, a delayed disease progression that circumvents larval lethality was required. Therefore, a slow progressing model was established in this study by keeping the larvae at 25°C, leading to a lower expression rate of mutant Khc protein. In this model lethality is shifted to pupal or adult stage and young larvae represent a comparatively early stage of SPG10 pathology in flies. This model uses the same motor neuron driver (D42-Gal4) as the fast progressing model.

4.1.1 Introductory remarks on the analysis of the slow progressing SPG10 model

To investigate different disease stages during development, a range of larval sizes was analyzed. As the pathology in khc^{N262S} expressing larvae is progressing during ageing,

larvae were divided in two groups of different ages: a younger group between 1.25 and 2.75mm in length and an older group between 2.75 and 4mm.

Control larvae (w^-/w^-;+/+;D42-Gal4/+) and those expressing *khc*$^{wt+N262S}$ (w^-/w^-;+/+;D42-Gal4, UAS-khc^{wt}/UAS-khc^{N262S}) molt from larval stage L2 to the next larval stage L3 at a size around 2.5mm. Larvae expressing *khc*^{N262S} (w^-/w^-;+/+;D42-Gal4/UAS-khc^{N262S}) molt from L2 to L3 at a size of about 2mm. All larvae analyzed had an age between three and four days and were raised and maintained at 25°C. As defects of mutant Khc in *Drosophila* larvae seem to be length dependent [Füger et al. 2012], size matched and not larval stage matched larvae were taken for analysis.

The analysis of the *khc*$^{wt+N262S}$ larvae was performed, because a suppression of the phenotype due to the additional expression of *khc*^{wt} was expected. Nearly all patients of SPG10 are heterozygous for their mutation [Reid et al. 2002; Lo Giudice et al. 2006; Schüle et al. 2008; Tessa et al. 2008; Goizet et al. 2009]. With equal expression of both alleles [Ding et al. 2004] wild type Khc dimers, homodimeric mutant dimers and heterodimeric motors that contain wild type and mutant subunits at a stoichiometry of 1:1:2 are expected [Ebbing et al. 2008]. *In vitro* assays have shown that dominant inherited *khc*^{N256S} shows reduced gliding velocity depending on the ratio of mutant to wild type protein [Ebbing et al. 2008]. Therefore, expressing an additional copy of wild type Khc (UAS-Khc$^{wt+N262S}$) should lead to a higher proportion of homodimeric wild type dimers of Khc and ameliorate the phenotype.

4.1.2 Behavioral deficits of larvae expressing *khc*$^{wt+N262S}$ and *khc*^{N262S}

In patients mutant KIF5A leads to a slow progressing spasticity and paralysis of the lower limbs [Harding 1993]. Fast progressing SPG10 model larvae and *khc* null mutant larvae also show posterior paralysis [Hurd and Saxton 1996; Füger et al.

2012]. To characterize body posture and locomotor behavior of slow progressing SPG10 model larvae, they were imaged while crawling. Righting assay was performed to determine the orientation and motoric skills of the larvae.

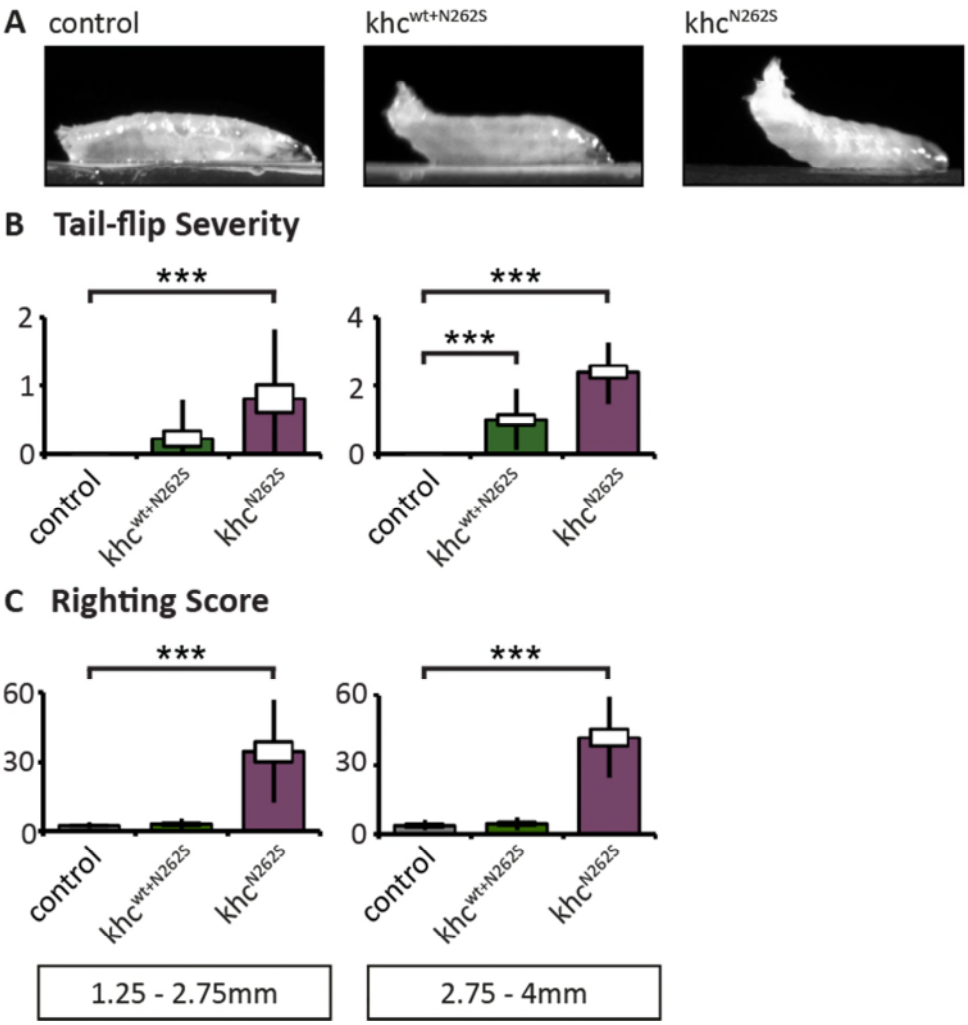

Figure 16: Behavioral analysis of slow progressing SPG10 model larvae

(A) *Khc*$^{wt+N262S}$ and *khc*^{N262S} expressing larvae display a posterior paralysis, also called tail-flip phenotype. **(B)** Quantification of tail-flip severity reveals that small *khc*$^{wt+N262S}$ expressing larvae only show a mild tail-flip, whereas large larvae of the same genotype and larvae expressing *khc*^{N262S} display a more severe manifestation of the phenotype. **(C)** Only larvae expressing *khc*^{N262S} show deficits in righting compared to controls. Larval sizes are summarized in the individual panels. Statistical significance was determined using a one way ANOVA test followed by Dunnett's multiple comparison test. The standard error of mean is shown as a box, the standard deviation as a black line. ***p<0.001.

Behavioral analysis revealed that larvae expressing *khc*^{N262S} or *khc*$^{wt+N262S}$ display posterior paralysis, also called tail-flip phenotype (Figure 16A, B), which was also seen in

other mutant *Drosophila* larvae with deficits in axonal transport [Hurd and Saxton 1996; Hanein et al. 2008; Füger et al. 2012; Ikenaka et al. 2012; Lo Giudice et al. 2014]. The righting assay showed that the khc^{N262S} larvae, which display strong posterior paralysis, were slower in righting than controls (Figure 16C). However, no significant difference in righting speed was detected between controls and $khc^{wt+N262S}$ larvae, which display milder posterior paralysis (Figure 16B, C). The tail-flip phenotype of larvae of the slow progressing SPG10 model is comparable with larvae of the fast progressing SPG10 model. Consequently, there is also a parallel to SPG10 patients that develop spasticity and paralysis of the lower limbs.

4.1.3 Decreased synaptogenesis of larvae expressing $khc^{wt+N262S}$ and khc^{N262S}

Khc knockout (KO) mouse models suggest a delay in neuronal development [Xia et al. 2003; Karle et al. 2012; Nakajima et al. 2012], whereas SPG10 is clinically classified as a neurodegenerative disorder [Salinas et al. 2008; Novarino et al. 2014]. *In vivo* imaging of slow progressing SPG10 model larvae was performed to investigate parallels to the developmental defects in KO mouse models. In *Drosophila* neurodevelopment the genesis of new PSDs seems to take place previously to the formation of the presynaptic specialization of the NMJ [Rasse et al. 2005]. Therefore, a genomic construct of the glutamate receptor subunit IIA C-terminally tagged with GFP [Rasse et al. 2005] was used to visualize newly formed synapses at the NMJ in between a time window of 24h. The GluRIIA construct was chosen, because it is expressed at physiological levels and reliably labels PSDs [Rasse et al. 2005]. Anesthetizing the larvae during imaging and recovery afterwards allowed imaging of NMJ 26/27 in segment A4 of mid L2 and early L3 larvae.

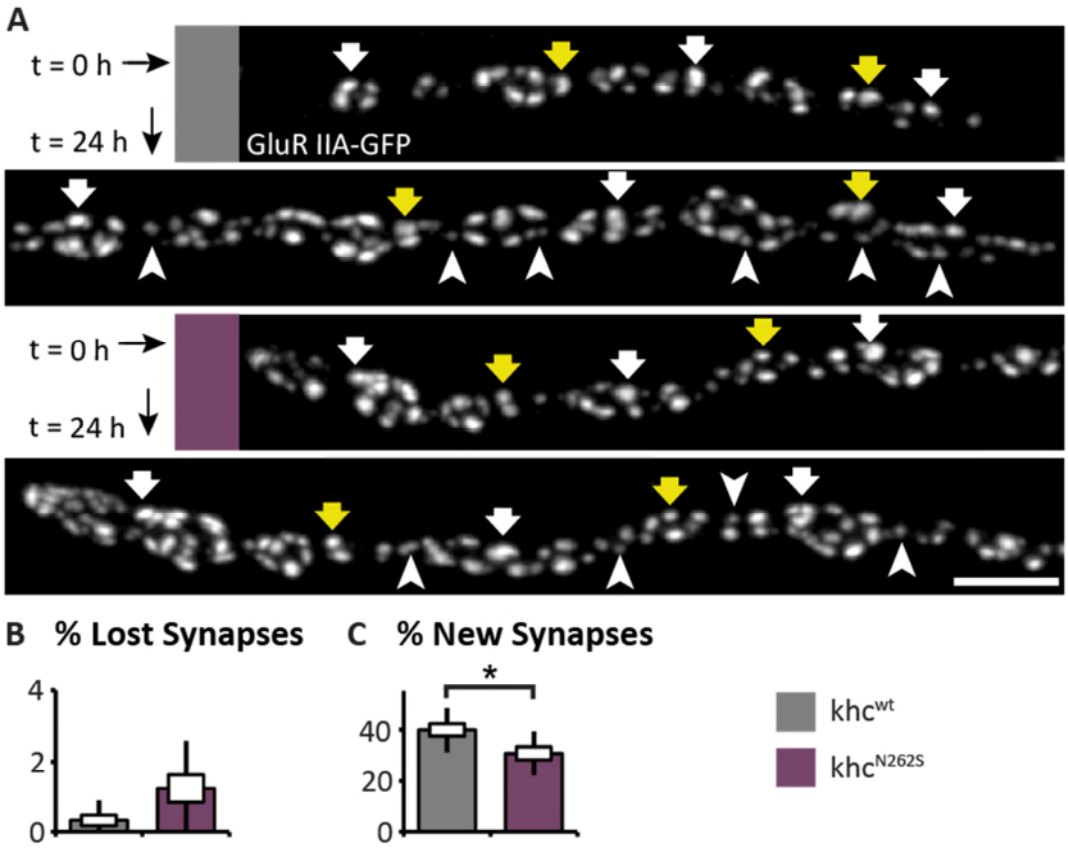

Figure 17: Synaptogenesis visualized by GluRIIA-GFP

(A) Confocal images show several boutons of the NMJ 26/27 in segment A4 at two time points. Larvae are expressing a genomic construct of the GluRIIA C-terminally tagged with GFP. The first time point (t=0) is at mid-second instar and second time point (t=24h) at mid-third instar. White and yellow arrows point at synapses that were stable between the two imaging time points and thus were used as landmarks. White arrowheads highlight some newly formed synapses. Scale bar: 5µm. **(B)** Quantification of degraded synapses in between the 24h time period is shown. No significant difference was determined between larvae expressing khc^{N262S} and control larvae expressing khc^{wt}. **(C)** Quantification of the rate, at which new synapses were formed, showed a significant decrease in khc^{N262S} larvae compared to controls. Images were kindly provided by S. Hannan. Statistical significance was determined using a Student's T-Test. The standard error of mean is shown as a box, the standard deviation as a black line. * $p<0.05$.

As the expression of an additional copy of khc^{wt} makes no difference to control regarding behavior, survival, NMJ and axonal morphology [Füger et al. 2012], this genotype was here used as control. By determining synapses that were found at both time points (Figure 17A, alternating white and yellow arrows), newly formed synapses and the ones that disappeared could be counted. Analysis of rates of synapse disassembly revealed no increased disassembly of PSDs between control larvae expressing an additional copy of khc^{wt}

and those expressing *khc*^{N262S} (Figure 17B). However, significantly decreased rates of synapse formation were observed in *khc*^{N262S} larvae (Figure 17C), demonstrating a mild developmental delay.

4.1.4 Abnormalities in axonal transport and components of the synaptic transmission machinery at the NMJ of larvae expressing *khc*$^{wt+N262S}$ and *khc*^{N262S}

Khc is an important motor protein for axonal transport (details see section 1.2.5) and the integrity of axonal MT architecture is essential for Kinesin-1-based transport [Bettencourt da Cruz et al. 2005; Yao et al. 2011]. Therefore, the morphology of axons regarding the structure of neuronal membranes (HRP) and MTs (Futsch, *Drosophila* homologue for the mammalian MAP1B) was investigated. An accumulation of HRP immunoreactivity was also shown in axons of larvae with mutant Khc [Hurd and Saxton 1996; Füger et al. 2012].

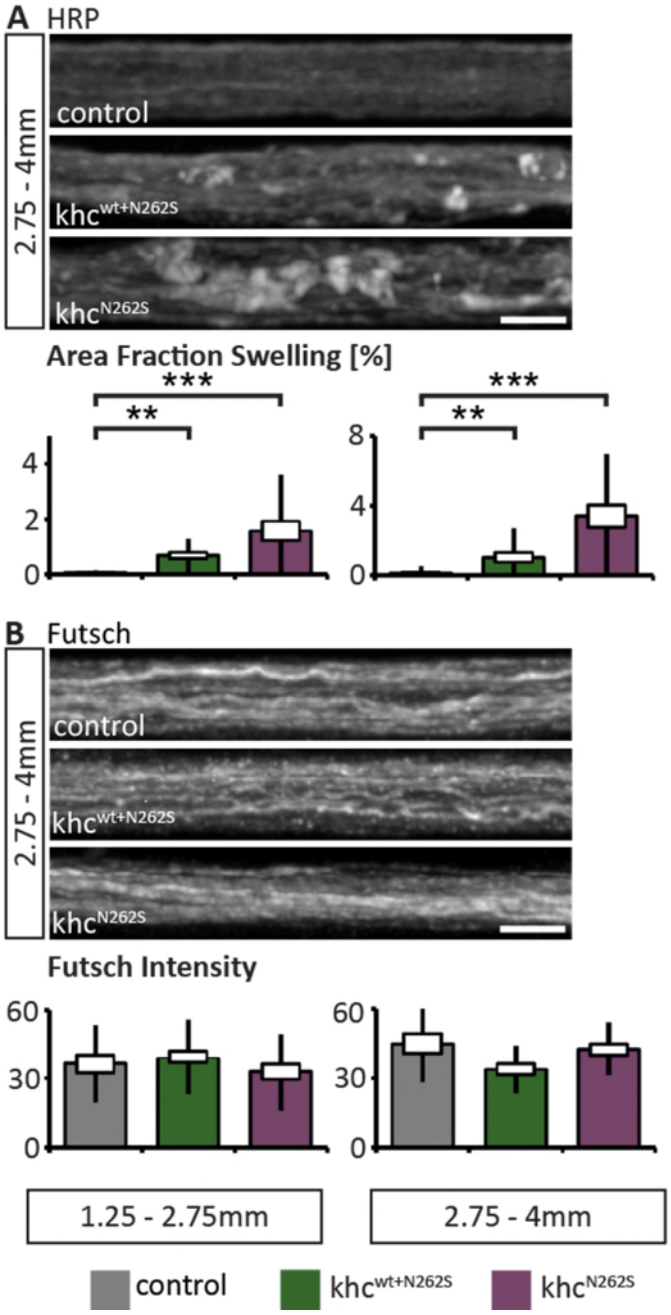

Figure 18: Structure of neuronal membranes and MT integrity in the axon

(A) Confocal images of segmental nerves stained for HRP. Quantification of the area fraction of high HRP intensity showed a significant higher percentage of increased HRP intensity of mutant larvae in both sizes compared to controls. **(B)** As Kinesin-1 is moving on MTs, segmental nerves were also stained for the MT-associated protein Futsch. Quantification of Futsch intensity did not show a significant difference between the genotypes. Larval sizes are summarized in the individual panels. Scale bar: 5µm. Statistical significance was determined using a one way ANOVA test followed by Dunnett's multiple comparison test. The standard error of mean is shown as a box, the standard deviation as a black line. ** $p<0.01$; ***$p<0.001$.

Staining for the neuronal membrane marker HRP revealed local inhomogeneity in axons of *khc* mutant larvae. This is indicative for altered neuronal membranes and may be

used as a biomarker for the presence of axonal swellings [Füger et al. 2012]. The percentage of area of strong HRP intensity in axons compared to average HRP intensity was significantly higher in small and large $khc^{wt+N262S}$ or khc^{N262S} larvae compared to control (Figure 18A). Füger and colleagues also detected an accumulation of HRP immunoreactivity in axons of *khc* mutant larvae and showed by EM that various vesicles are also accumulating in regions, where the axon diameter is increased [Füger et al. 2012].

Comparison of axonal Futsch abundance showed no significant difference between any of the investigated genotypes (Figure 18B). The axonal swellings of SPG10 model larvae did therefore not develop from altered MT cytoskeleton in axons.

However, it is not clear whether the accumulation of HRP signal originates in the accumulation of transport vesicles that are also labeled by HRP antibody or if the neuronal membrane surrounding each axon changed its composition. To test whether the membranous accumulations in axons of the slow progressing SPG10 model larvae also contain cargo accumulations, segmental nerves were stained for HRP as neuronal marker and for VGlut, which was used as a marker for SVs. As changes in axonal transport could also lead to a synaptic defect, NMJ 6/7 of segment A5 was also stained with these two antibodies.

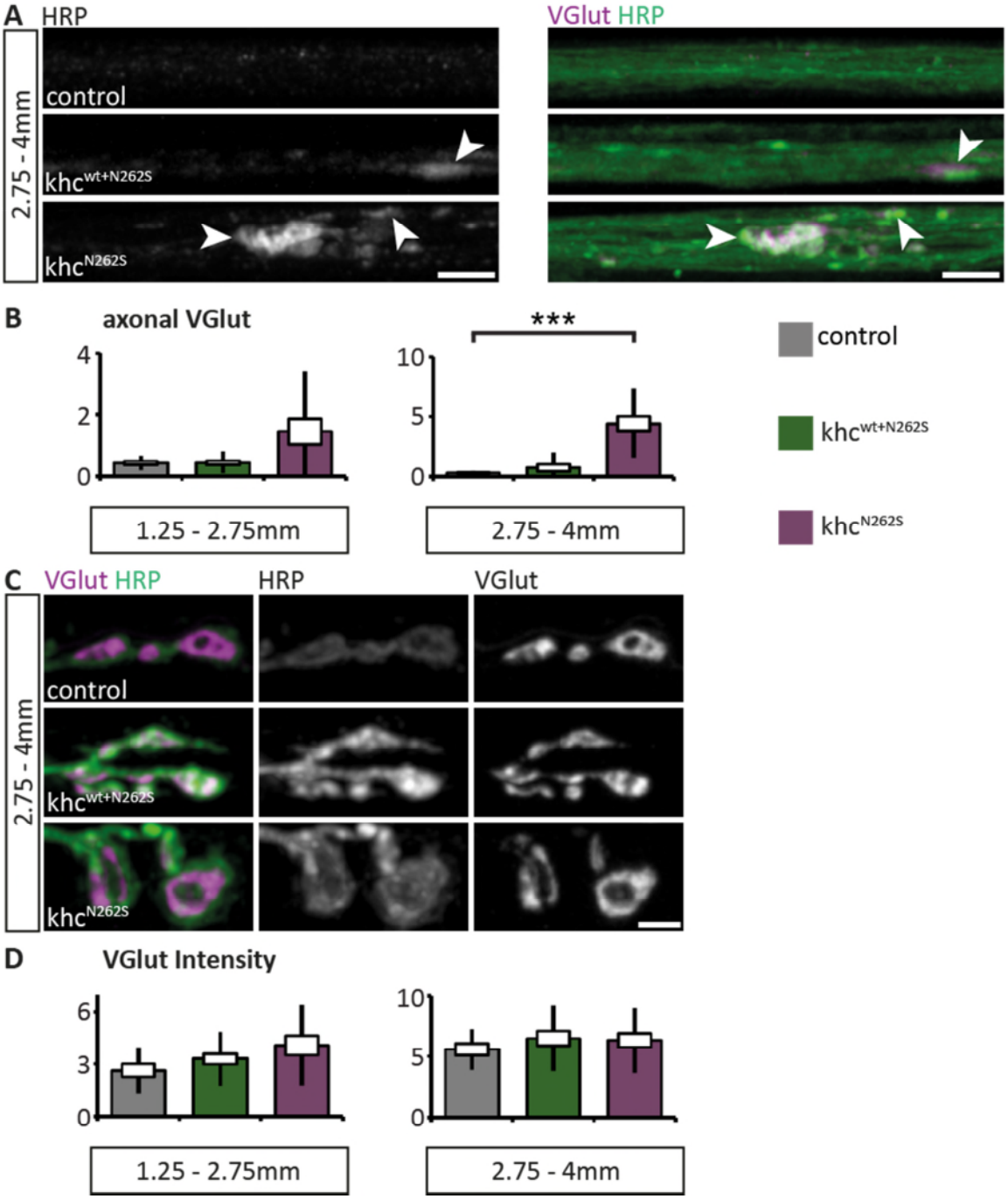

Figure 19: Axonal accumulation of Brp and amount of Brp at the NMJ in larvae expressing *khc^{N262S}*

(A) Confocal immunofluorescence images showing segmental nerves stained for VGlut (grey and magenta) and HRP (green). **(B)** Quantification shows that VGlut intensity in axons was significantly increased in large *khc^{N262S}* expressing larvae. **(C)** Confocal immunofluorescence images showing several synaptic boutons stained for VGlut (magenta and grey) and HRP (green and grey) in NMJ 6/7 of segment A5. Quantification of VGlut intensity at the NMJ revealed no significant difference between the genotypes. Larval sizes are summarized in the individual panels. Scale bar in segmental nerves: 5µm. Scale bar in boutons: 3µm. Statistical significance was determined using a one way ANOVA test followed by Dunnett's multiple comparison test. The standard error of mean is shown as a box, the standard deviation as a black line. ***p<0.001.

Quantification of VGlut intensity revealed an increased intensity primarily in axons of large *khc*^{N262S} expressing larvae (Figure 19A, B). Most HRP positive areas in segmental nerves of larvae expressing *khc*^{N262S} collocate with VGlut signal. This supports the hypothesis that the accumulation of HRP immunoreactivity originates from accumulation of cargo vesicles and not from altered neuronal membrane surrounding the axon. Analysis of total VGlut abundance at the NMJ 6/7, segment A5 revealed no significant alterations between the genotypes (Figure 19C). Thus, SVs can be transported to the synapse and the abundance of SVs can be maintained despite the existence of axonal swellings.

It was previously demonstrated that Brp, although primarily transported by the Kinesin-3 Unc-104 [Kern et al. 2013], accumulates in- and outside of axonal swellings in the fast progressing SPG10 model [Füger et al. 2012]. Brp is a marker for AZ precursor vesicles and is located to AZs at the NMJ. To test, if it also accumulates in the slow progressing SPG10 model, segmental nerves and NMJ 6/7 segment A5 were stained for Brp. As with VGlut, segmental nerves and NMJs were both imaged to relate eventual differences in Brp transport with Brp abundance at the NMJ.

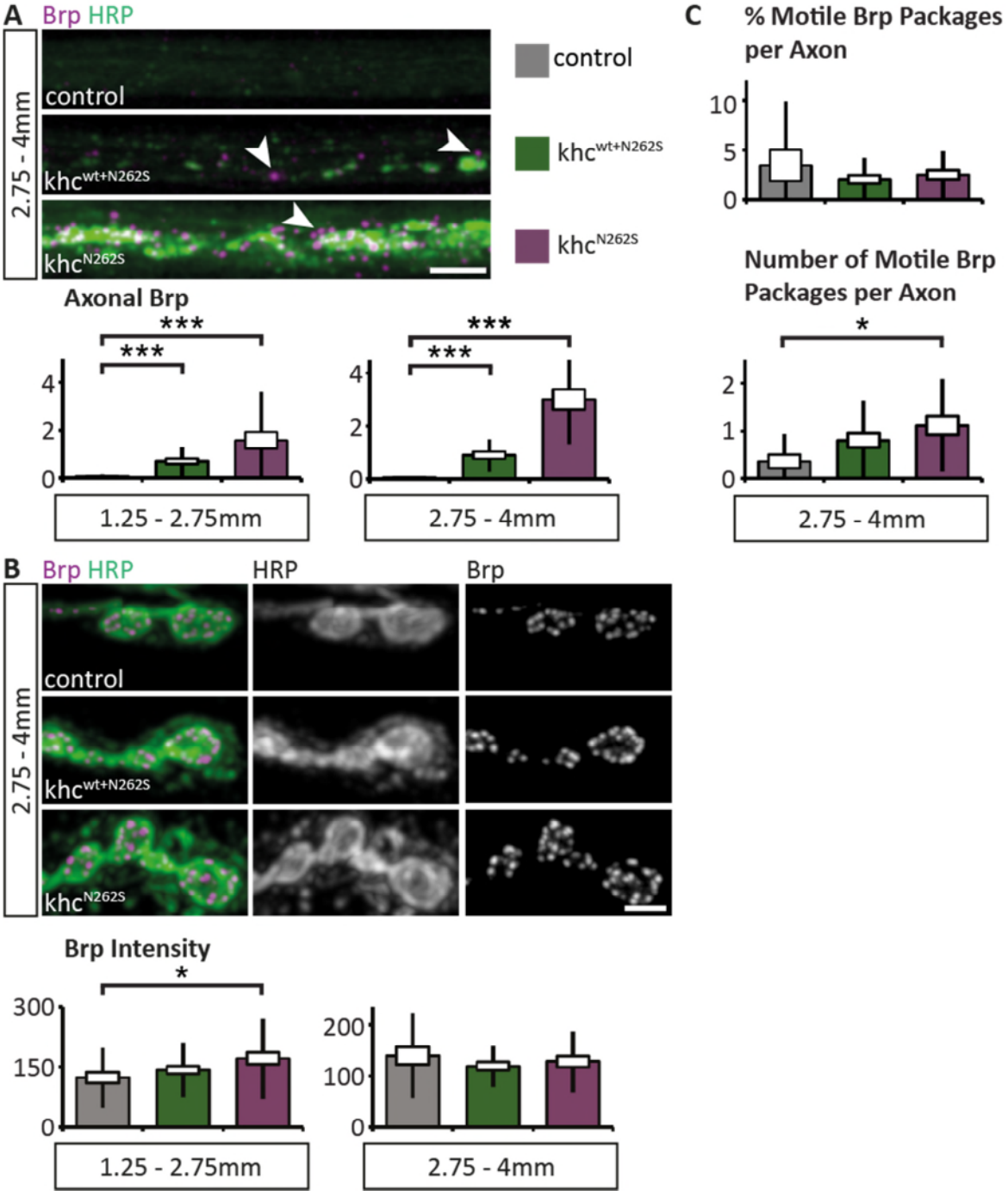

Figure 20: Axonal accumulation of Brp and amount of Brp at the NMJ in larvae expressing *khc^{N262S}*

(A) Segmental nerves stained for Brp, a marker for AZ precursor vesicles (magenta) and HRP (green). Quantification shows that axonal Brp levels were increased in *khc$^{wt+N262S}$* and *khc^{N262S}* expressing larvae of all sizes compared to control. **(B)** Confocal immunofluorescence images showing several synaptic boutons NMJ 6/7 segment A5 stained for Brp (magenta and grey) and HRP (green and grey). Quantification of Brp intensity showed a significant increase of Brp in NMJs of *khc^{N262S}* expressing larvae. **(C)** Quantification of % motile Brp packages *in vivo* in segmental nerves shows no significant difference, but the total number of motile Brp packages is significantly increased in *khc^{N262S}* expressing larvae. Larval sizes are summarized in the individual panels. Scale bar in segmental nerves: 5µm. Scale bar in boutons: 3µm. Statistical significance was determined using a one way ANOVA test followed by Dunnett's multiple comparison test. The standard error of mean is shown as a box, the standard deviation as a black line. * p<0.05; ** p<0.01; ***p<0.001.

Increased axonal Brp abundance is also observed in small and large *khc*$^{wt+N262S}$ and *khc*^{N262S} larvae of the slow progressing model (Figure 20A). This increased level of Brp might be indicative for a more generalized impairment of axonal transport. Alternatively, it might indicate that increased trafficking of Brp might be part of a homeostatic compensatory response to the synaptic deficits that lead to impaired locomotion (Figure 16). The observation that Brp abundance at the NMJ is also significantly increased in small and large *khc*^{N262S} larvae (Figure 20B) supports the latter hypothesis. *In vivo* imaging of GFP-tagged Brp was used to further address this question. The overall percentage of motile Brp packages is low in nerves of both mutant and control larvae and no significant difference was detected between the genotypes (Figure 20C, top). As Brp is thought to have a very slow turnover of at least eight hours (Stefan Sigrist, personal communication), it is not expected to see high trafficking rates in the given time window of no more than 60min. However, the absolute numbers of Brp packages in axons were higher in mutant larvae than in controls and hence, also the total number of motile Brp packages was higher (Figure 20C, bottom). Thus, expression of mutant *khc* leads to a compensatory increase of Brp transport to the NMJ.

4.1.5 Reduced mitochondrial supply to the NMJ of larvae expressing *khc*$^{wt+N262S}$ and *khc*^{N262S}

As Kinesin-1 is the major motor protein for axonal transport of mitochondria, *in vivo* imaging was performed to measure mitochondrial transport in axons of *khc*^{N262S} and *khc*$^{wt+N262S}$ expressing larvae. The expression of mito-GFP in small larvae allowed imaging of axons *in vivo* as previously described [Smith and Taylor 2011].

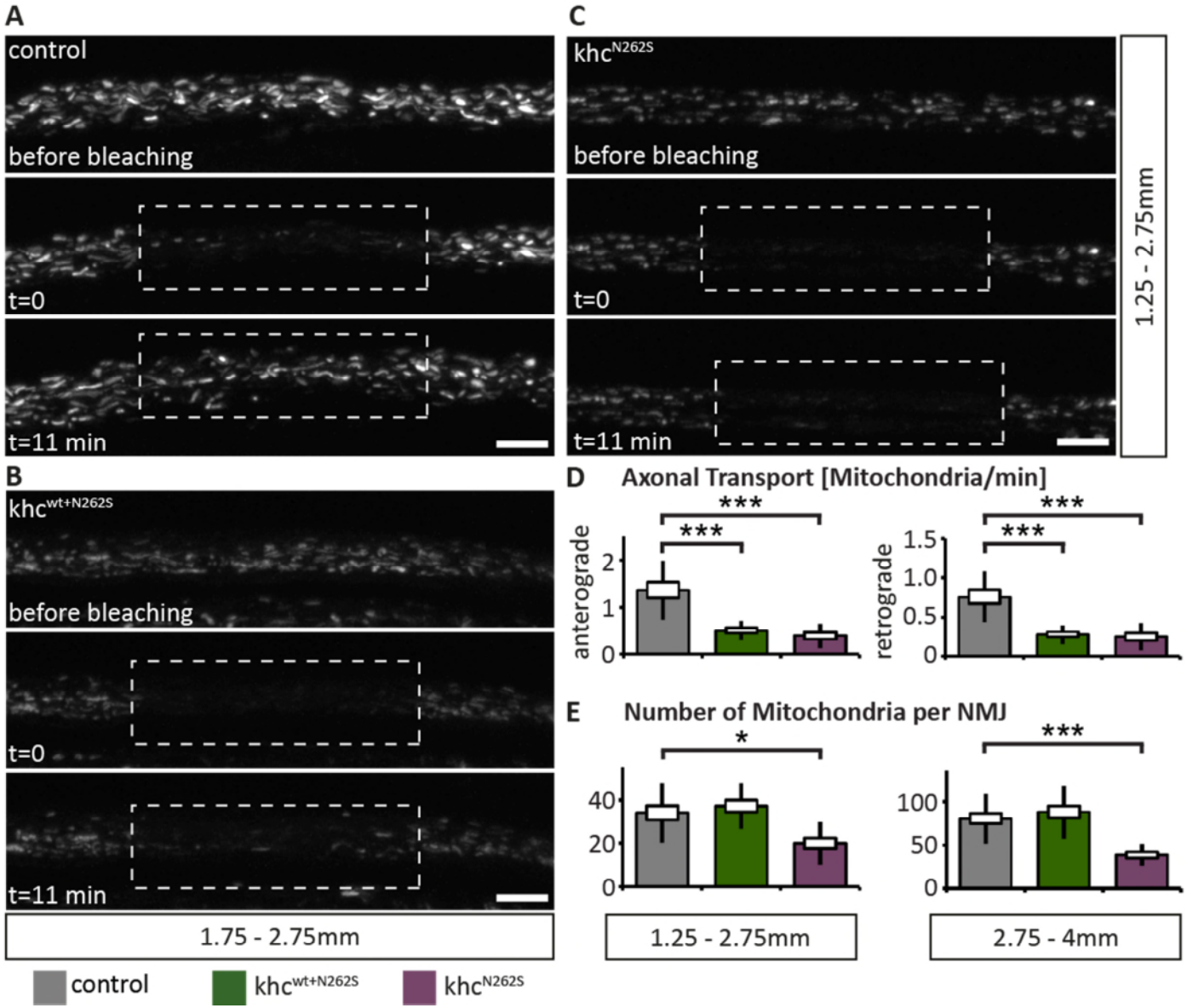

Figure 21: Defects in axonal transport and reduced numbers of mitochondria at the NMJ

(A)-(C) Confocal images show segmental nerves of larvae expressing a genomic construct of mitochondrial located GFP. Segmental nerves were imaged once before bleaching of the white box and directly after bleaching (t=0) for up to 15min. **(A)** In the control mitochondria filled the bleached gap after t=11min. **(B)** Larvae expressing *khc*$^{wt+N262S}$ could partly refill the gap after this time. **(C)** In larvae expressing *khc*^{N262S} the bleached gap is still clearly visible after t=11min. Scale bar: 5µm. **(D)** Quantification of axonal transport of mitochondria revealed severe defects in both mutant genotypes in anterograde, as well as retrograde direction in small larvae. **(E)** The number of mitochondria at the NMJ is just reduced in larvae expressing *khc*^{N262S}. Statistical significance was determined using a one way ANOVA test followed by Dunnett's multiple comparison test. The standard error of mean is shown as a box, the standard deviation as a black line. * p<0.05; ***p<0.001.

After bleaching a part of the axon, moving mitochondria that enter the bleached zone can be easily counted. In control axons the bleached zone of the axon was almost completely refilled with transported mitochondria after 11min. (Figure 21A). In larvae expressing $khc^{wt+N262S}$, there was only a minor recovery after this time (Figure 21B). Worst affected were larvae expressing khc^{N262S}, which showed minimal recovery during the given time period (Figure 21C). Quantification of axonal flux of mitochondria showed a significant decrease of transported mitochondria per minute in either direction (retrograde and anterograde) of both: $khc^{wt+N262S}$ and khc^{N262S} expressing larvae (Figure 21D). Disturbed axonal transport of mitochondria leads to reduced exchange of mitochondria at the NMJ. Additionally, it could lead to reduced numbers of mitochondria at the NMJ. Quantification of the number of synaptic mitochondria revealed indeed a significant decrease in both small and large larvae expressing khc^{N262S}, but no differences in larvae expressing $khc^{wt+N262S}$ compared to the control (Figure 21E). Thus, the expression of khc^{N262S} leads to reduced axonal transport of mitochondria and partially to a reduced number of mitochondria at the NMJ.

4.1.5.1 Altered morphology of the NMJ of larvae expressing $khc^{wt+N262S}$ and khc^{N262S}

Expression of khc^{N262S} leads to severely impaired axonal transport in larvae of slow progressing SPG10 model. As a consequence proper supply of the NMJ through axonal transport is probably not ensured. Results obtained in the fast progressing SPG10 model showed reduced NMJ size and synapse number [Füger et al. 2012] and the *Drosophila* $khc^{-/-}$ mutant was also shown to have smaller NMJs [Hurd and Saxton 1996]. To clarify if these defects occur also in slow progressing SPG10 model larvae, NMJs were stained for neuronal membranes (HRP), AZs (Brp) and PSDs (GluRIIC).

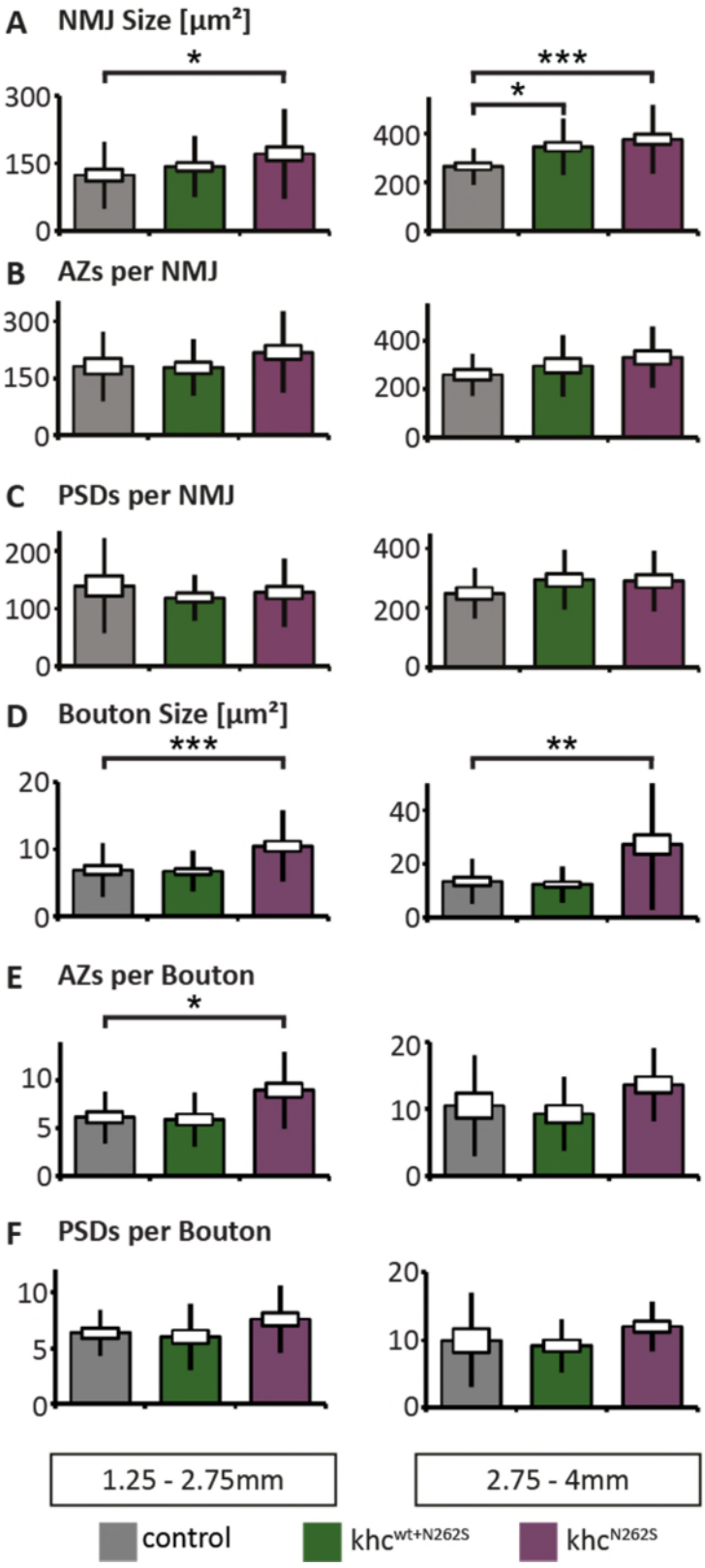

Figure 22: Structural characterization of the NMJ 6/7 segment A5

(A) Quantification of NMJ size revealed significantly larger NMJs in mutant larvae except for the small *khc*$^{wt+N262S}$ expressing larvae that had NMJs of the same size as controls. Quantification of AZs **(B)** and PSDs **(C)** per NMJ did not show a significant difference between the genotypes. **(D)** Bouton size was significantly increased in *khc*^{N262S} expressing larvae, whereas **(E)** increase in AZs per bouton was only significant in small *khc*^{N262S} expressing larvae. In large larvae the slight increase was not significant. **(F)** PSDs per bouton were not increased

compared to control. Larval sizes are summarized in the individual panels. Statistical significance was determined using a one way ANOVA test followed by Dunnett's multiple comparison test. The standard error of mean is shown as a box, the standard deviation as a black line. * p<0.05; ***p<0.001.

Consistent with milder effects of the slow progressive SPG10 model, no significant reduction of NMJ size (Figure 22A), number of AZs (Figure 22B) or PSDs (Figure 22C) was observed in segment A5 NMJ 6/7 of larvae that expressed $khc^{wt+N262S}$ or khc^{N262S} compared to control. Interestingly, in khc^{N262S} expressing larvae NMJ size was even increased compared to controls (Figure 22A). Average bouton sizes in small and large khc^{N262S} expressing larvae were also increased compared to controls (Figure 22D). Analysis of AZs per bouton revealed that bouton enlargement was accompanied by increased numbers of AZs per bouton of small khc^{N262S} larvae, but this difference was not statistically significant in large larvae (Figure 22E). Furthermore, there is no statistical difference in the numbers of PSDs per bouton between the investigated genotypes (Figure 22F). Thus, the structural characterization of the NMJ of the slow progressing SPG10 model did not show a decreased NMJ size or less synaptic components compared to the control. In contrast NMJs were even larger compared to controls.

4.1.6 Altered structure of neuronal membranes and microtubule innervation of larvae expressing $khc^{wt+N262S}$ and khc^{N262S}

In former studies of larvae with mutant Khc, the staining for HRP at the NMJ was non-uniform with frequent areas of high HRP intensities [Hurd and Saxton 1996; Füger et al. 2012]. A closer look at NMJs in larvae expressing khc^{N262S} alone or in combination with khc^{wt}, which were stained for neuronal membranes, revealed also high inhomogeneity in HRP immunoreactivity (Figure 23). To quantify eventual NMJ disassembly, NMJs were stained for HRP and the MT marker Futsch.

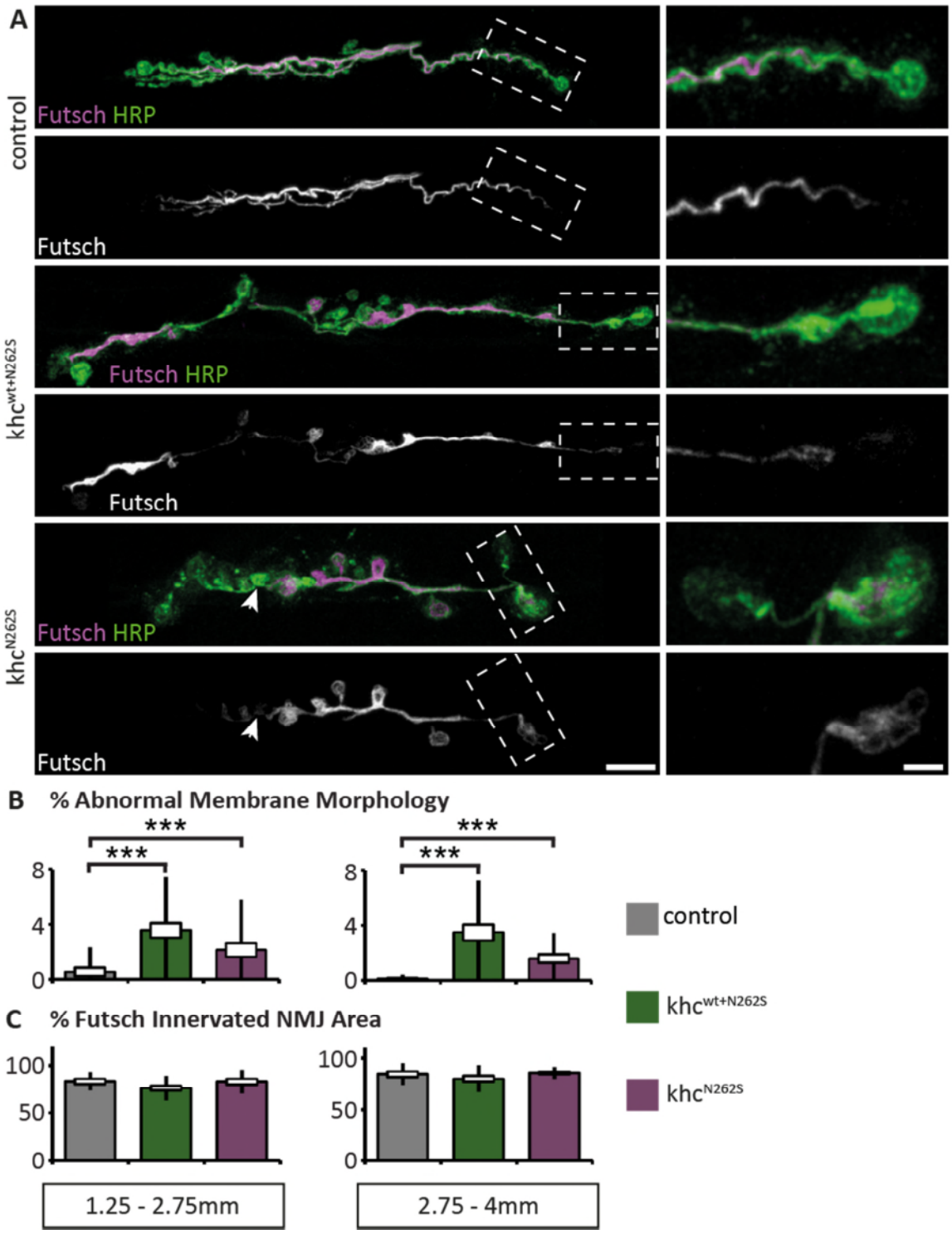

Figure 23: Altered neuronal membrane morphology and MT innervation at the NMJ

(A) Confocal immunofluorescence images showing abnormal membrane morphology (arrowhead) stained for HRP (green) and Futsch (magenta and grey). Enlargements on the right panel show abnormal membrane morphology of terminal boutons. **(B)** Quantification of increased HRP intensities show a significant increase in both size groups of mutant larvae compared to controls. **(C)** Futsch innervation in terminal boutons was not significantly altered in mutant larvae compared to controls. Larval sizes are summarized in the individual panels. Scale bar: 10µm and 3µm in enlargements. Statistical significance was determined using a one way ANOVA test followed by Dunnett's multiple comparison test. The standard error of mean is shown as a box, the standard deviation as a black line. ***p<0.001.

Confocal images of NMJs of *khc*^{N262S} expressing larvae show a dramatic increase in HRP labeled membranes at several boutons (Figure 23A,B) in small and large larvae. To find out if these membrane accumulations at the NMJ correlate with altered MT cytoskeleton, NMJs stained for HRP and Futsch were further analyzed. The quantification of Futsch loss from terminal boutons revealed no significant differences between the genotypes in the percentage of HRP area innervated by Futsch (Figure 23C). Thus, there is abnormal accumulation of HRP at the NMJ, but no clear local MT retraction from terminal boutons.

NMJs of *khc*^{N262S} mutant larvae frequently exhibited unusually large boutons (Figure 22D). Interestingly, the Futsch structure inside these large boutons seems to be different than in boutons of controls.

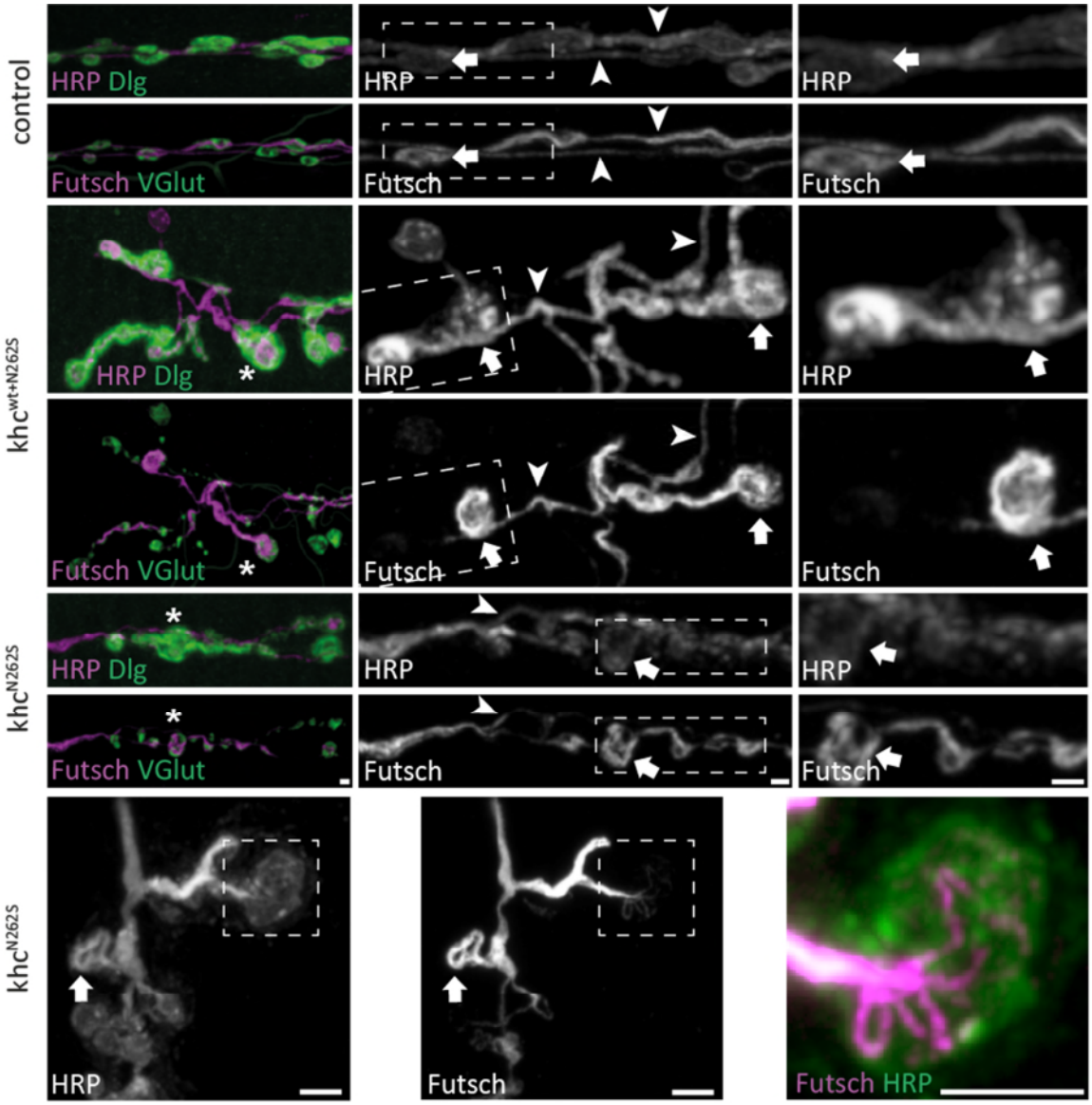

Figure 24: Altered Futsch structure at the NMJ

Confocal immunofluorescent images of several boutons (NMJ 6/7, Segment A5) and enlargements thereof are shown. Larvae between 2.75–4mm in length expressing a genomic Dlg-GFP construct were stained for neuronal membranes (HRP), SVs (VGlut) and MTs (Futsch) as indicated. Giant boutons that were observed in both mutant genotypes ($khc^{wt+N262S}$ and khc^{N262S}) were frequently filled with MTs (arrows). Stars mark boutons positive for Dlg and positive for the SV marker VGlut that contain disorganized Futsch structures. In inter-bouton areas Futsch staining had a cable-like appearance (arrowheads) in all genotypes. The proportion of disorganized, fragmented or lost Futsch staining was bigger in large boutons, while a cable like or loop structure was more frequent in normal sized boutons. Scale bar: 3.5µm.

A high proportion of large boutons in both, khc^{N262S} and $khc^{wt+N262S}$ expressing larvae, was surrounded by the SSR positive for discs large (Dlg) and was positive for the SV marker VGlut (Figure 24, star). Conspicuously, NMJs of *khc* mutant larvae frequently had boutons that were filled with disorganized MT (Figure 24, arrows), whereas this was never seen in the

control, where MTs form cables or loops inside boutons. However, Futsch staining in inter-bouton areas (Figure 24, arrowheads) had a normal cable-like shape in all genotypes. Such locally disorganized MT cytoskeleton was also seen in disassembling NMJs [Pielage et al. 2005] and other forms of neurodegeneration or retraction [Zhai et al. 2003; Massaro et al. 2009]. Hence, the abnormal Futsch structure could be a sign for NMJ disassembly in slow SPG10 model larvae.

4.1.7 Normal distribution and intensity of actin at the NMJ of larvae expressing *khc*$^{wt+N262S}$ and *khc*^{N262S}

The structure of the MT cytoskeleton in larvae expressing *khc*^{N262S} is altered (Figure 24) and hence, also the transport possibilities at the NMJ are likely impaired. Besides MTs, the actin cytoskeleton plays also an important role as short range transport rails at the NMJ. F-actin is important for various functions maintaining synaptic activity (Figure 2 and Figure 7). It is located preferentially near the plasma membrane [Hirokawa et al. 2010], whereas MTs are located more in the center of the NMJ branches and boutons. To clarify the status of the actin cytoskeleton NMJ 6/7, segment A5 of larvae expressing the actin marker LifeAct tagged with mTurquoise was imaged. LifeAct was shown to collocate to actin without disturbing actin or other cellular functions [Riedl et al. 2008].

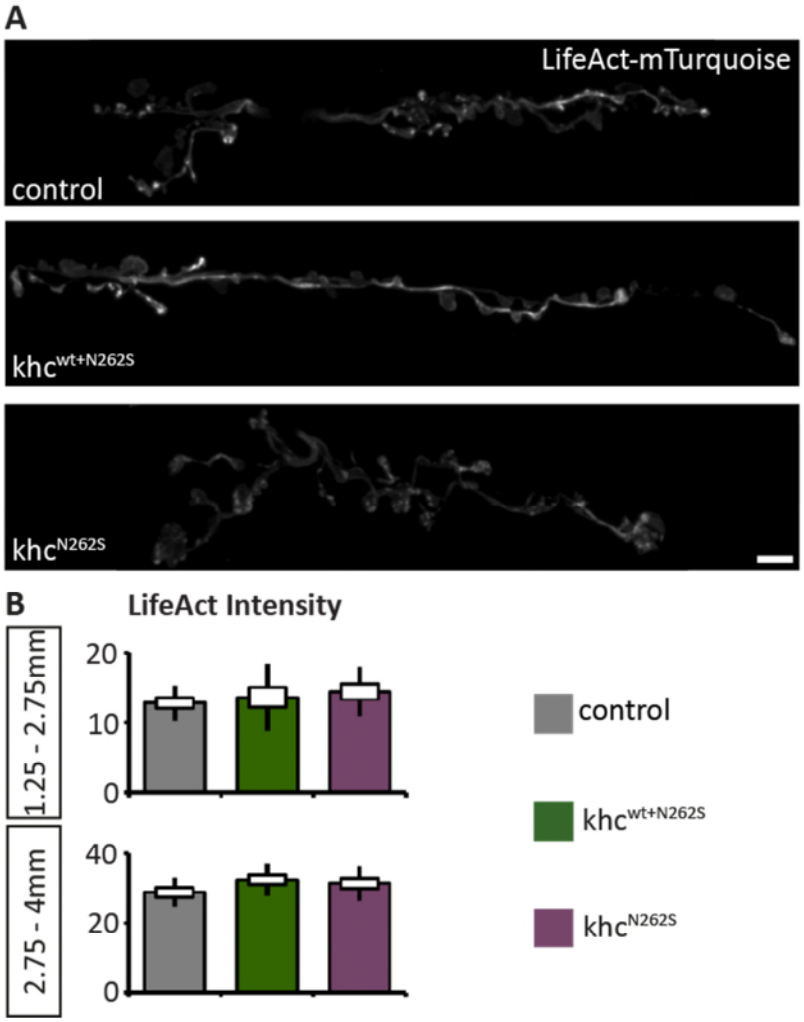

Figure 25: Intensity and distribution of actin at the NMJ

(A) Confocal images of *in vivo* imaged larvae (2.75 - 4mm) expressing the actin marker LifeAct tagged with mTurquoise fluorescence. **(B)** Overall intensity of LifeAct was not significantly altered in Khc mutant larvae compared to control. The non-uniform distribution can be found in all genotypes. Scale bar: 5µm. Quantification of overall intensity at the NMJ shows no significant differences between the genotypes. Statistical significance was determined using a one way ANOVA test followed by Dunnett's multiple comparison test. The standard error of mean is shown as a box, the standard deviation as a black line.

The overall intensity of LifeAct was not significantly different in larvae expressing *khc*^{N262S} compared to control (Figure 25). The distribution of actin in the NMJ is not uniform, but shows regions with high fluorescent intensity and areas, where signal is low in all three genotypes. Thus, the morphology of the actin cytoskeleton seems not to be affected by impaired Khc function.

4.1.8 Formation and development of dystrophic or giant boutons

The average bouton size of larvae expressing *khc*^{N262S} is enlarged compared to controls (Figure 22D). Interestingly, this average enlargement originates from the existence of very large (giant) boutons and small dystrophic boutons among normal sized boutons (compare Figure 20B, Figure 24 and Figure 27). The frequent occurrence of giant boutons led to the question, if they persist once formed or if they collapse and develop into dystrophic boutons. To clarify this question, *in vivo* imaging at two successive time points was performed. To visualize neuronal membranes, larvae were expressing a membrane-tagged tdTomato fluorescence protein together with Dlg-GFP for visualizing the SSR.

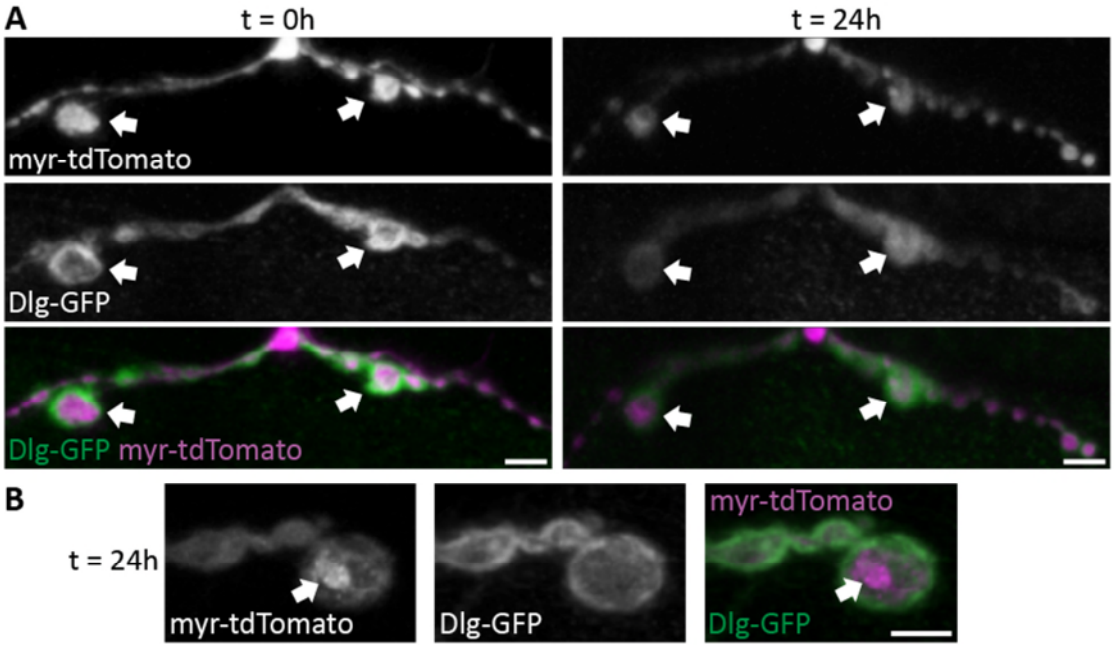

Figure 26: *In vivo* imaging of giant bouton development

In vivo confocal images of larvae expressing a membrane (myr-) tagged tdTomato and Dlg-GFP. **(A)** Images of *in vivo* imaging in between 24h timespan of *khc*^{N262S} expressing larvae. The giant bouton shown in the left panel at time point t=0 gets slightly smaller, but does not develop into a small dystrophic bouton with prominent neuronal membrane accumulations at the second imaging time point 24h later (right panel). **(B)** *In vivo* confocal images of a giant bouton that contains aggregated neuronal membranes inside a bouton (t=24h). Scale bars: 5µm

Here, giant boutons appear to develop out of normal sized boutons and – once formed – stay until pupation with only minor decrease in size (Figure 26A). They did not seem to be the origin of dystrophic boutons by collapsing together. Nevertheless, giant boutons sometimes contain areas where neuronal membranes are highly enriched (Figure 26B). Studying the development of boutons with such high HRP intensity of *khc*^{N262S} expressing larvae *in vivo* revealed that dystrophic boutons did not change morphology once formed.

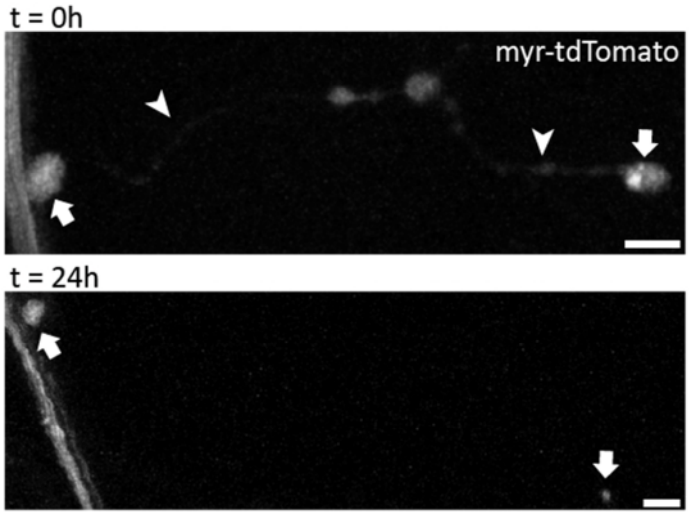

Figure 27: Disassembly within 24h of NMJ 4 of larvae expressing *khc*^{N262S}

In vivo confocal images of NMJ 4 of larvae expressing *khc*^{N262S} and a membrane (myr-) tagged tdTomato within 24h. The thin connection (arrowheads) between the boutons (all normal sized) is disappeared at the second time point (t=24h). The dystrophic terminal bouton and the bouton located directly next to the innervating axon (arrows) are the only ones left at the second imaging time point, 24h later. Scale bars: 5µm

In vivo confocal imaging of NMJ 4 of larvae expressing *khc*^{N262S} and a membrane tagged tdTomato showed that disassembly of NMJs with dystrophic boutons can occur within 24h (Figure 27). At time point t=0 a thin line of neuronal membranes connects the (normal sized) boutons to the innervating axon. 24h later only a small dot that marks the former terminal bouton and the bouton next to the axon were visible. The terminal bouton already showed accumulated neuronal membrane at time point t=0, the bouton next to the

axon just got smaller. This first set of experiments suggests that normal sized boutons either form giant boutons that almost keep their size until pupation, or they form dystrophic boutons. However, further experiments are required to confirm the development and physiological role of giant and dystrophic boutons in *khc*^{N262S} expressing larvae.

4.1.9 Altered FasII structure in disassembling boutons

Boutons that contain areas with highly disorganized Futsch structure were also shown in other mutant larvae with disassembling NMJs [Pielage et al. 2005]. Füger and colleagues reported synaptic degeneration in larvae of the fast progressing SPG10 model [Füger et al. 2012]. To validate the hypothesis that NMJ disassembly happens in larvae expressing *khc*^{N262S} at 25°C with a slower pathological progression, NMJ 6/7 was stained for PSDs, HRP and Fasciclin II (FasII), a peri-synaptic cell adhesion molecule, which is expressed in the pre- and postsynapse. An intact FasII structure has previously been shown to be important for NMJ stability [Schuster et al. 1996; Pielage et al. 2005, 2006]. Hence, defects in cell adhesion are established markers for early stages of NMJ degeneration [Pielage et al. 2008].

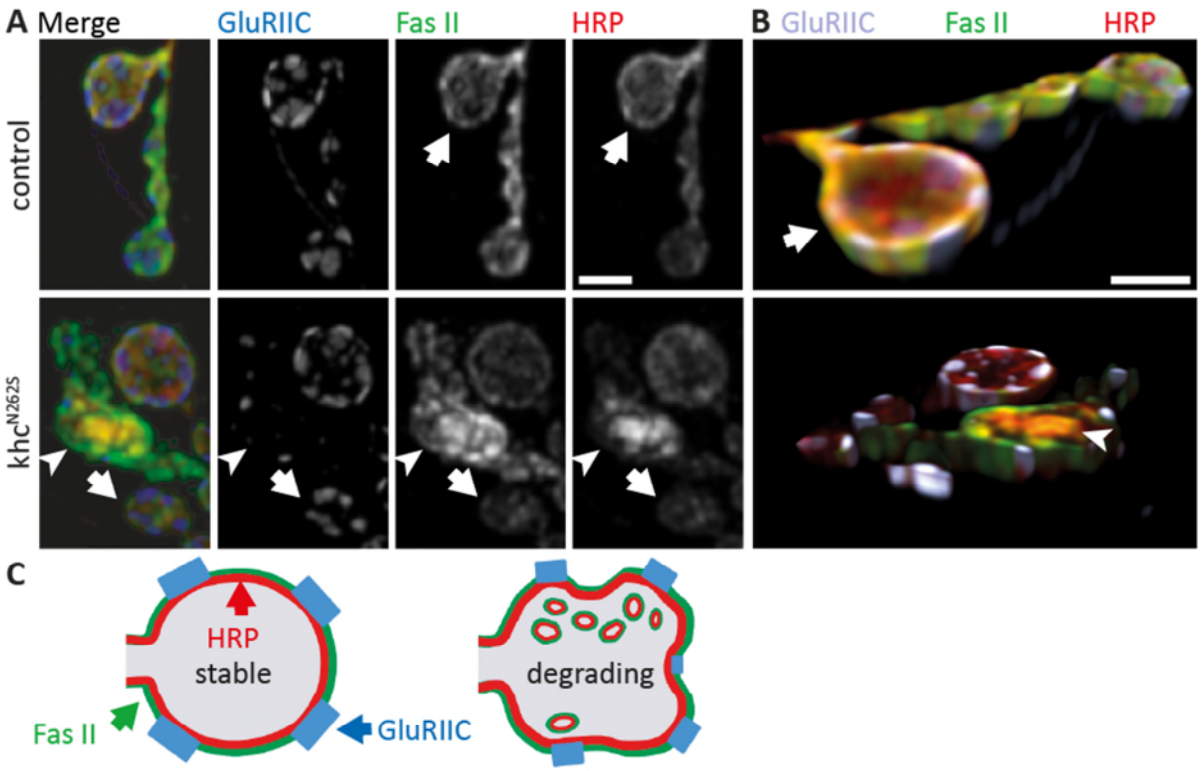

Figure 28: Morphological characteristics of disassembling boutons

Defects in cell adhesion were assessed by staining 2.75 – 4mm large *khc*^{N262S} expressing and control larvae for HRP, the PSD marker GluRIIC and the peri-synaptic cell adhesion molecule Fasciclin II (FasII). **(A)** At stable boutons FasII formed a honeycomb network that surrounds PSDs (arrows). At boutons that are putatively undergoing dissociation, as indicated by increased HRP intensity and diminished size of PSD fields (arrowheads), the FasII network was disturbed. Scale bar: 2µm. **(B)** Internalization of the presynaptic membrane was visualized using 3D volume rendering after deconvolution. HRP staining that normally localizes only to the membrane (arrow) extended into the interior of the bouton (arrowhead). Deconvolution was done using AutoQuant X 2.2.2, 3D volume rendering was created using Imaris 7.6.1 Scale bar: 1µm **(C)** Schematic representation of a stable bouton (left) and a bouton that is in the process of degradation (right).

Normally, FasII forms a honeycomb-like network that surrounds PSDs at synaptic boutons. The disruption of this network has been shown to precede NMJ retraction [Pielage et al. 2008]. Indeed, disruptions of the FasII network could be observed at boutons that displayed increased HRP intensities in NMJs of *khc* mutant larvae (Figure 28A, arrowhead). In stable regions normal shaped FasII network surrounded PSDs (Figure 28A, arrow). Analysis of 3D volume rendering following deconvolution provided evidence for the presence of internal presynaptic membrane at boutons that show high HRP intensities in maximum intensity projections (compare Figure 23A, B, Figure 26B and Figure 28B). A schematic representation

of the structure of mutant and control boutons shows the different shape and the accumulation of internal vesicles in the putatively degrading bouton (Figure 28C). Thus, disrupted FasII network and accumulation of neuronal membranes seem to be signs for synaptic disassembly, which also occurs in larvae expressing *khc*^{N262S} at 25°C.

4.1.10 Ultrastructural analysis of NMJ disassembly of larvae expressing *khc*$^{wt+N262S}$ and *khc*^{N262S}

EM analysis was used to further investigate the frequent morphological alterations of HRP staining in boutons of SPG10 model larvae. Internal lab data show that the alterations in HRP staining occur more frequently in NMJ 4 of larvae kept at 29°C. For technical reasons third instar larvae expressing *khc*$^{wt+N262S}$ were taken for EM analysis.

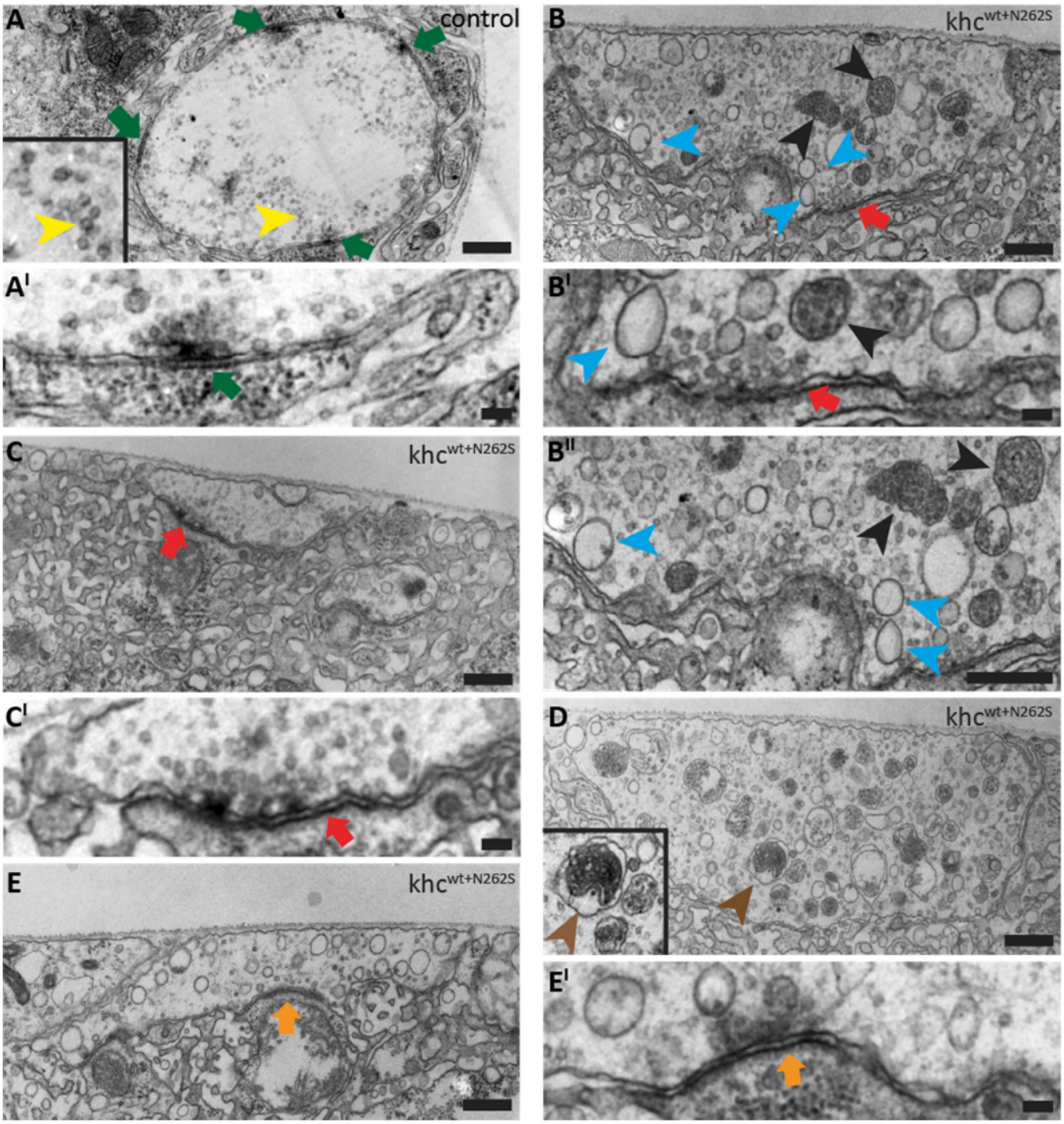

Figure 29: Ultrastructural analysis of NMJ disassembly

NMJ 4, segment A4 of larvae raised and maintained at 29°C was analyzed with EM. **(A)** Boutons of control larvae were round and contained small clear SVs near the synaptic membrane (yellow arrowheads). Green arrows show AZs that conformed to a flat plane. **(B)** Boutons of mutant larvae showed frequently large vesicles that were either clear (cyan arrowhead) or densely filled (black arrowhead). **(C, E)** AZs of mutant larvae also had a different shape compared to that of controls. They were "bumpy" or curved towards the center of the bouton (red and orange arrows). **(D)** Autolysosome structures were also present in boutons of mutant larvae. Images were kindly provided by J. Kern. Scale bars: 100nm

While control boutons contained primarily small SVs (Figure 29A, yellow arrowhead), mutant NMJs were characterized by boutons that were densely filled with membranous

organelles such as multi-vesicular bodies (black arrowheads), autolysosome structures (brown arrowheads) and large clear vesicles (cyan arrowheads) (Figure 29B-D). Additionally, another characteristic of NMJs undergoing degeneration and disassembly could be observed [Pielage et al. 2008]: Wild type AZs typically conformed to a flat plane (Figure 29A, green arrow), whereas curved AZs have been associated with NMJ disassembly [Pielage et al. 2008]. Indeed, AZs in mutant larvae were frequently either "bumpy" (Figure 29B, C, red arrows) or curved towards the center of the bouton (Figure 29E, orange arrow). The intense HRP staining in several boutons of larvae expressing khc^{N262S} could originate from the accumulation of vesicles surrounded by neuronal membranes. Therefore, these areas of high HRP staining could be another evidence for NMJ degeneration in the slow progressing SPG10 model larvae.

4.2 Correlation of the amount of functional Khc to pathological severity

Analysis of larvae expressing khc^{N262S} either alone or in combination with khc^{wt} showed common characteristics for both genotypes. Axonal swellings, high Brp levels and reduced mitochondrial transport were detectable in axons of both mutant genotypes and both larval sizes. Another common feature was areas of high HRP intensity at the NMJ. The tail-flip phenotype and larger NMJ size was only significantly altered in large larvae expressing $khc^{wt+N262S}$ and both sizes of larvae expressing khc^{N262S}. Defects in the righting assay, larger bouton size, Brp accumulation and less mitochondria at the NMJ were only shown for small and large larvae expressing khc^{N262S}. Finally, VGlut accumulations in axons were only significantly altered in large larvae expressing khc^{N262S} (compare Figure 30).

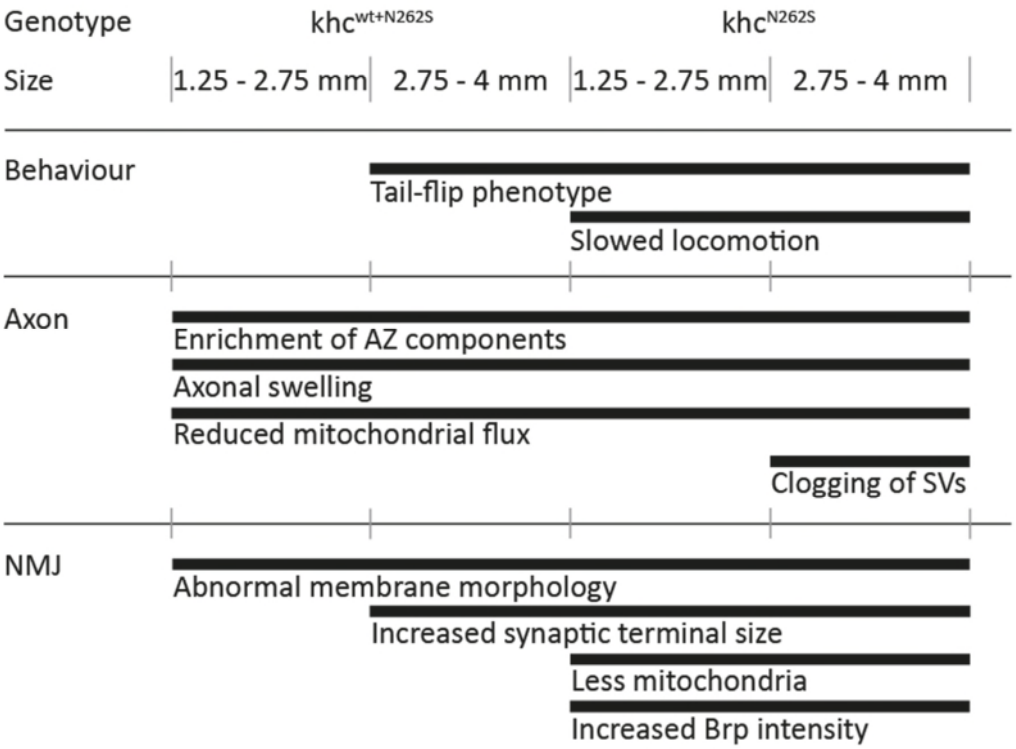

Figure 30: Correlation of the amount of functional Khc to larval pathology

High Brp levels, axonal swellings and reduced mitochondrial flux in axons as well as abnormal membrane morphology at the NMJ were common for all mutant genotypes and for both size groups. The tail-flip phenotype and larger NMJs were detected in large larvae expressing *khc*$^{wt+N262S}$ and on both size groups of larvae expressing *khc*^{N262S}. Defects in locomotion, less mitochondria and increased amounts of Brp at the NMJ were only present in both size groups of larvae expressing *khc*^{N262S}. Finally, clogging of SVs was only significantly higher in large larvae expressing *khc*^{N262S}.

Summarizing the results in larvae with ectopic overexpression of mutant Khc a correlation of the amount of functional Khc, the age of larvae and the severity of pathology could be suggested. Füger and colleagues previously demonstrated that pathological changes observed following expression of *khc*^{N262S}, are caused by antimorphic effects that disturb the function of endogenous Khc [Füger et al. 2012]. Larvae deficient for *khc* should consequently represent a good model to study defects that occur late during pathogenesis of loss of functional Khc. To this aim the next part of this study focuses on the pathology of larvae deficient for *khc*.

4.3 *Khc*$^{-/-}$ mutant larvae as model for late stage SPG10 pathology

Khc null mutant larvae were generated through a combination of the two alleles *khc*^{8} and *khc*^{k13314} (*khc*$^{-/-}$). Larvae were raised and maintained at 25°C. *Khc*$^{-/-}$ larvae grow slower than controls and die as early third instar larvae. Therefore, they were compared to size matched controls and – for comparison of different Khc mutants – *khc*^{N262S} expressing larvae.

4.3.1 *Khc*$^{-/-}$ larvae display severe tail-flip and righting deficits

Hurd and Saxton described for their *khc* null mutant a severe tail-flip phenotype [Hurd and Saxton 1996]. Larvae expressing *khc*^{N262S} have also shown a tail-flip phenotype and additionally, deficits in righting. To confirm the tail-flip phenotype of *khc*$^{-/-}$ larvae behavioral analyses, including the righting assay, were performed.

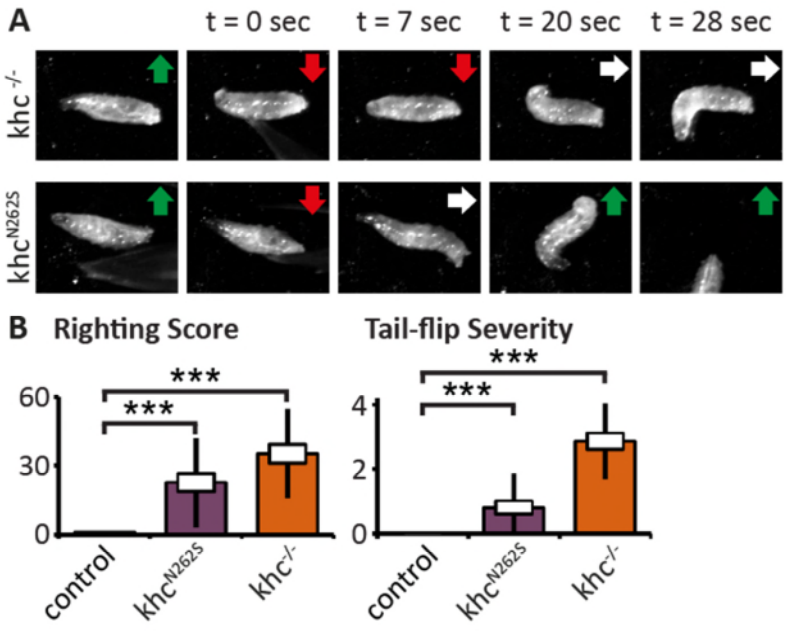

Figure 31: behavioral analysis of *khc*$^{-/-}$ larvae

Small *khc*$^{-/-}$ larvae (1.25 to 2.75mm), raised and maintained at 25°C, were compared to size-matched *khc*^{N262S} expressing larvae and controls. **(A)** Exemplary results obtained in the righting assay are shown as a series of images. Color-coded arrows indicate orientation of the larvae during the righting assay. Green arrow: normal posture, red arrow: ventral side up, white arrow: lateral side up. **(B)** *Khc*$^{-/-}$ larvae displayed a severe tail-flip and moved slower as scored by the righting assay. Quantification of the time in seconds larvae need to turn from

ventral side up to dorsal side up was significantly longer than for controls. The control of posterior body segments was also severely impaired compared to controls. Statistical significance was determined using a one way ANOVA test followed by Dunnett's multiple comparison test. The standard error of mean is shown as a box, the standard deviation as a black line. ***p<0.001

In addition to the tail-flip phenotype of *khc*$^{-/-}$ larvae, indeed, behavioral analysis revealed also a defect in righting score. As shown in a time series of images taken during the righting assay, *khc*$^{-/-}$ larvae are only half turned at a time point, when *khc*^{N262S} expressing larvae already crawl away (Figure 31A). Furthermore, the level of posterior paralysis is even higher than in small larvae expressing *khc*^{N262S} (Figure 31B).

4.3.2 Axonal swellings and MT integrity in axons of *khc*$^{-/-}$ larvae

Hurd and colleagues described axonal swellings and abnormal accumulation of Khc, but no abnormal structure of MTs in segmental nerves of *khc*$^{-/-}$ larvae. To confirm that there are swellings, but no alteration in MT abundance in axons of *khc*$^{-/-}$ larvae, segmental nerves were stained for MT marker Futsch and neuronal membrane marker HRP.

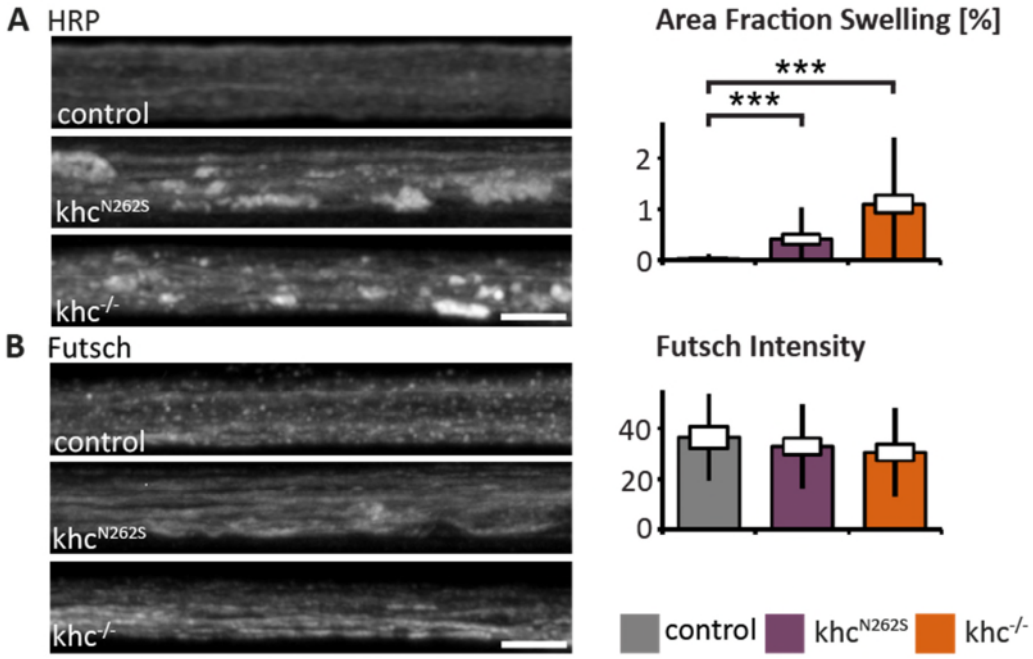

Figure 32: Axonal swellings and axonal MTs in *khc*$^{-/-}$ larvae

(A) Confocal images show segmental nerves stained for neuronal membranes (HRP). Quantification of the area fraction of bright HRP staining revealed a significant higher proportion of axonal swellings in *khc*$^{-/-}$ larvae than in controls. **(B)** Confocal images show segmental nerves stained for Futsch. Quantification of the total level of axonal Futsch intensity showed no significant differences between the genotypes. Scale bar: 5µm. Statistical significance was determined using a one way ANOVA test followed by Dunnett's multiple comparison test. The standard error of mean is shown as a box, the standard deviation as a black line. ***p<0.001

Khc$^{-/-}$ larvae display severe axonal swellings (Figure 32A), but the integrity of the MT cytoskeleton in the axon seems not to be affected (Figure 32B).

4.3.3 Accumulation of axonal cargo and reduced synaptic supply of *khc*$^{-/-}$ larvae

Hurd and Saxton described for their *khc* null mutant axonal swellings containing kinesin, mitochondria and large, likely fused vesicles [Hurd and Saxton 1996]. To find out if cargos of Kinesin-1 or other transport proteins get stalled in these axonal swellings, as it is the case in larvae expressing *khc*^{N262S} and if this also leads to a diminished supply to the NMJ, segmental nerves and NMJs were stained for VGlut, Brp and HRP.

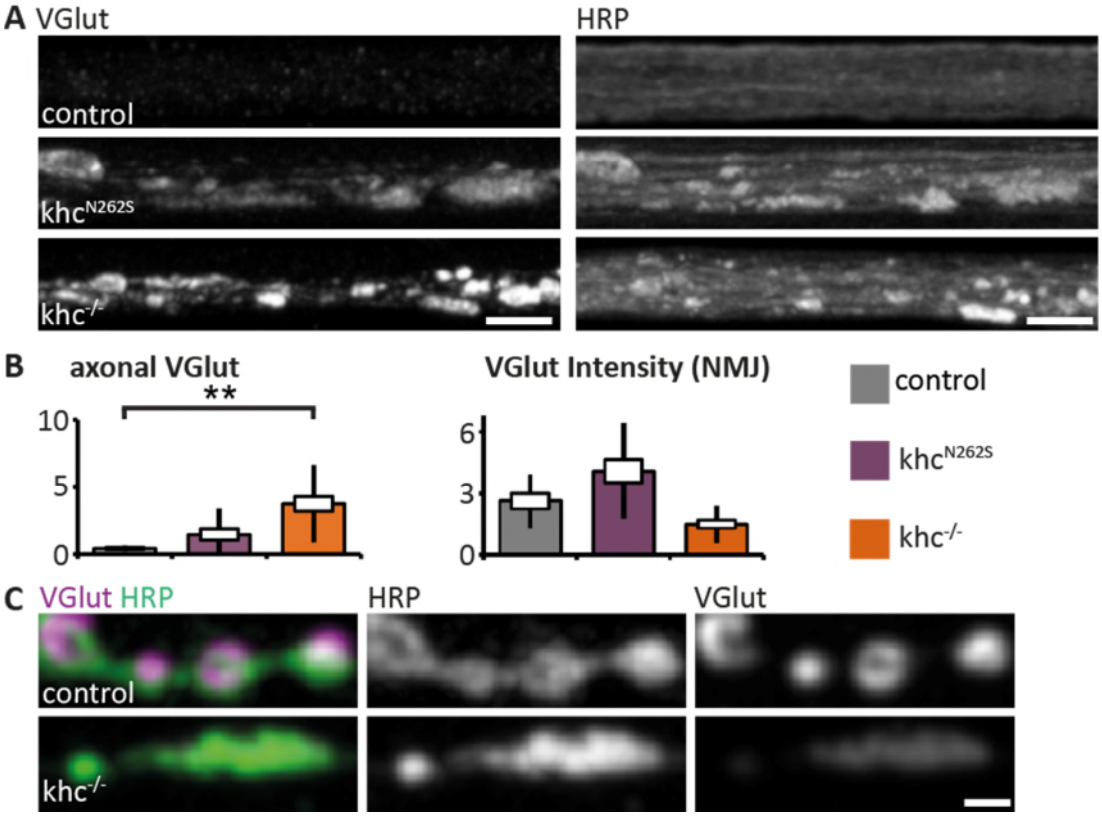

Figure 33: Axonal accumulation of VGlut and amount of VGlut at the NMJ in *khc*$^{-/-}$ larvae

(A) VGlut accumulation is mostly collocated with HRP enrichments in axons of both mutant genotypes. **(B)** Quantification of the axonal intensity of VGlut immunoreactivity revealed a significant higher amount of VGlut in axons in *khc*$^{-/-}$ larvae than in controls. **(C)** NMJs of *khc*$^{-/-}$ larvae show only a tendency towards reduced VGlut intensity compared to controls. Scale bars in segmental nerves: 5µm, scale bars in boutons: 1.5µm. Statistical significance was determined using a one way ANOVA test followed by Dunnett's multiple comparison test. The standard error of mean is shown as a box, the standard deviation as a black line. ** $p<0.01$

Segmental nerves of larvae expressing *khc*^{N262S}, as well as *khc*$^{-/-}$ larvae, showed mostly collocated staining of VGlut and HRP (Figure 33A). In line to this, the quantification of VGlut intensity in axons revealed a significant higher amount of VGlut in axons of *khc*$^{-/-}$ larvae than in controls (Figure 33B, left). The enriched VGlut intensity in nerves of *khc*$^{-/-}$ larvae in axonal swellings leads to the assumption that traffic jams persist at sides of axonal swellings. Quantification of the amount of VGlut at the NMJ showed a tendency towards less VGlut in NMJs of *khc*$^{-/-}$ larvae (Figure 33B, right) and consequently suggests the traffic jam hypothesis. As an example for cargos not transported by Khc, but by the Kinesin-3 Unc-104 [Kern et al. 2013], segmental nerves were also stained for the AZ marker Brp.

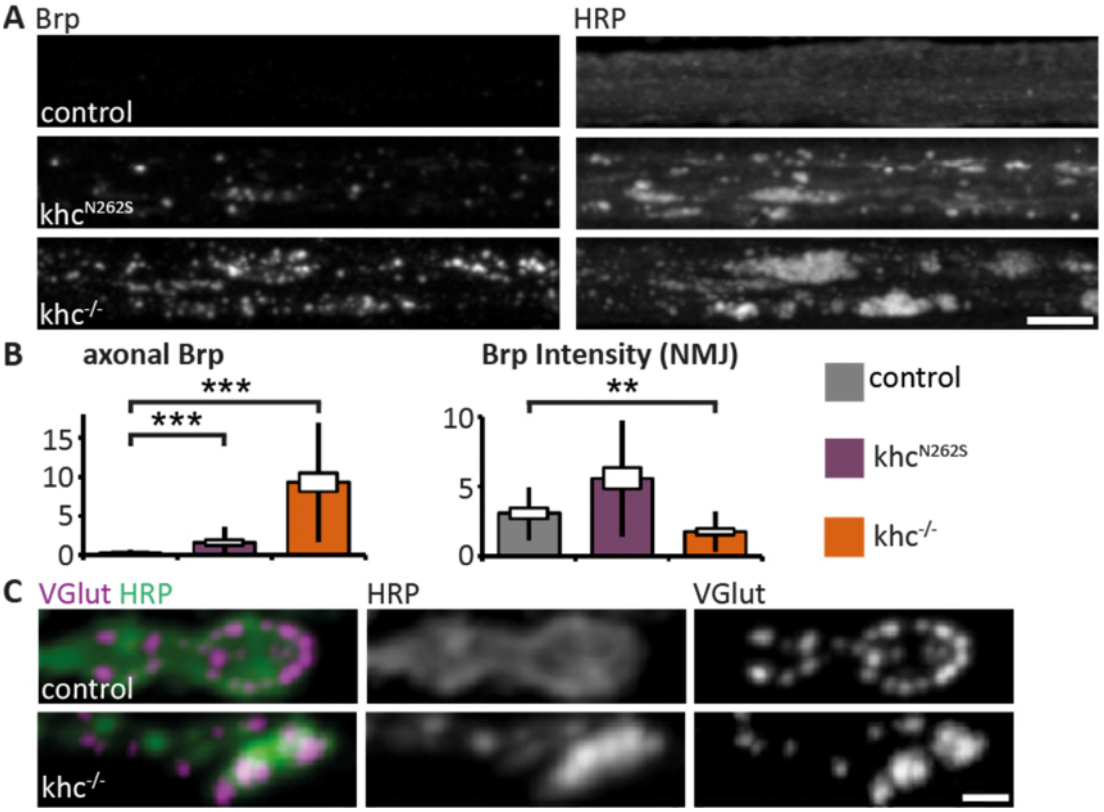

Figure 34: Axonal accumulation of Brp and amount of Brp at the NMJ in *khc*$^{-/-}$ larvae

(A) Confocal images show segmental nerves stained for Brp (AZs). Brp packages are present inside, as well as outside axonal swellings. **(B)** Quantification of Brp intensity in the axon showed even higher amount of Brp as in *khc*^{N262S} expressing larvae. **(C)** Staining of Brp at the NMJ revealed less Brp in NMJs of *khc*$^{-/-}$ larvae than in controls and *khc*^{N262S} expressing larvae. Scale bars in segmental nerves: 5µm, scale bars in boutons: 1.5µm. Statistical significance was determined using a one way ANOVA test followed by Dunnett's multiple comparison test. The standard error of mean is shown as a box, the standard deviation as a black line. ** p<0.01; ***p<0.001

As in larvae expressing *khc*^{N262S}, Brp accumulates in the axon in- and outside of axonal swellings of *khc*$^{-/-}$ larvae (Figure 34A). But in contrast to the examined *khc*^{N262S} expressing larvae where Brp intensity at the NMJ was even higher than in controls, *khc*$^{-/-}$ larvae show less Brp at the NMJ (Figure 34B,C). The same phenomenon was also shown for larvae expressing *khc*^{N262S} that were kept at 29°C and are therefore more severely affected. Thus, in *khc*$^{-/-}$ larvae seems to be a general defect of axonal transport (Figure 33 and Figure 34), which also leads to diminished supply to the NMJ.

4.3.4 Reduced HRP area and synapse number with MT retraction at the NMJ of *khc*$^{-/-}$ larvae

Hurd and Saxton reported less boutons in *khc*$^{-/-}$ larvae [Hurd and Saxton 1996]. To test whether the HRP area of *khc*$^{-/-}$ larvae is smaller and if the NMJ shows further defects as a result of the lack of Khc, NMJs were stained for HRP, AZs (Brp) and PSDs (GluRIIC).

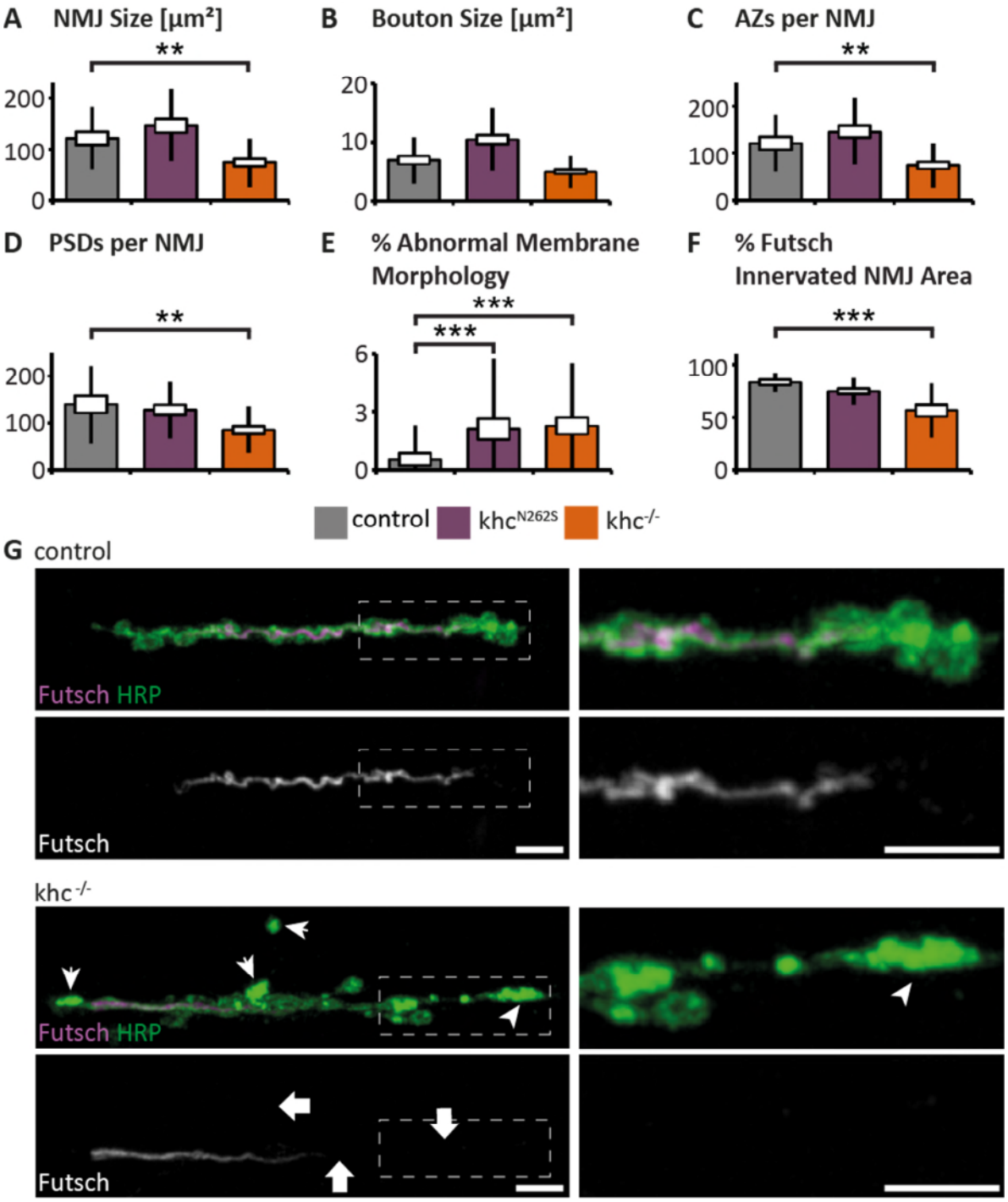

Figure 35: *Khc*$^{-/-}$ larvae display strong signs for NMJ degeneration

(A) Quantification of NMJ size showed significant smaller NMJs and **(B)** a tendency towards smaller boutons in *khc*$^{-/-}$ larvae compared to controls. **(C)** The number of AZs, as well as **(D)** the number of PSDs was also significantly reduced in NMJs of *khc*$^{-/-}$ larvae compared to controls. **(E-G)** NMJ 6/7 of segment A5 of mutant and control larvae was stained for neuronal membranes (HRP) and MT marker Futsch. **(E)** Quantification of area of high HRP staining showed significant differences of both mutant larvae compared to control. **(F)** The NMJ area innervated by Futsch is only significantly reduced in *khc*$^{-/-}$ larvae. **(G)** Abnormally increased membrane staining (arrowheads) and loss of MT from terminal regions of the NMJ (arrows) was frequently observed at boutons of *khc*$^{-/-}$ larvae. Scale bar: 5µm. Statistical significance was determined using a one way ANOVA test followed by Dunnett's multiple comparison test. The standard error of mean is shown as a box, the standard deviation as a black line. ** p<0.01; ***p<0.001.

The quantification of HRP area (Figure 35A) could confirm a smaller NMJ size of *khc*$^{-/-}$ larvae compared to controls, but no differences in bouton size (Figure 35B). Counting AZs and PSDs per NMJ also revealed a reduced number of both in NMJs of *khc*$^{-/-}$ larvae compared to controls (Figure 35C,D). Additionally, *khc*$^{-/-}$ larvae showed a high percentage of abnormal bright HRP staining as it was also seen for larvae expressing *khc*^{N262S} (compare Figure 23A and Figure 35E). The reduction of NMJ size could either derive from diminished outgrowth or from retraction of the NMJ. Retracting MTs were shown to be an early marker for disassembling NMJs [Eaton et al. 2002]. Therefore, NMJs were stained for HRP and MT marker Futsch. To score for retracting MTs from the terminal sides of the NMJ, which Eaton and colleagues suggest as a sign for the retraction of the NMJ [Eaton et al. 2002], the percentage of Futsch innervated NMJ area was quantified. Indeed the percentage of the by Futsch innervated NMJ area was significantly reduced in *khc*$^{-/-}$ larvae compared to control (Figure 35F). Hence, NMJs of *khc*$^{-/-}$ larvae show clear signs of synaptic retraction, which could be an explanation for the smaller NMJ size.

4.3.5 NMJ disassembly in *khc*$^{-/-}$ larvae

To point out more details about the morphology of NMJ degeneration in a *khc*$^{-/-}$ background, larvae were stained for Brp and GluRIIC together with HRP or Dlg with Futsch and HRP.

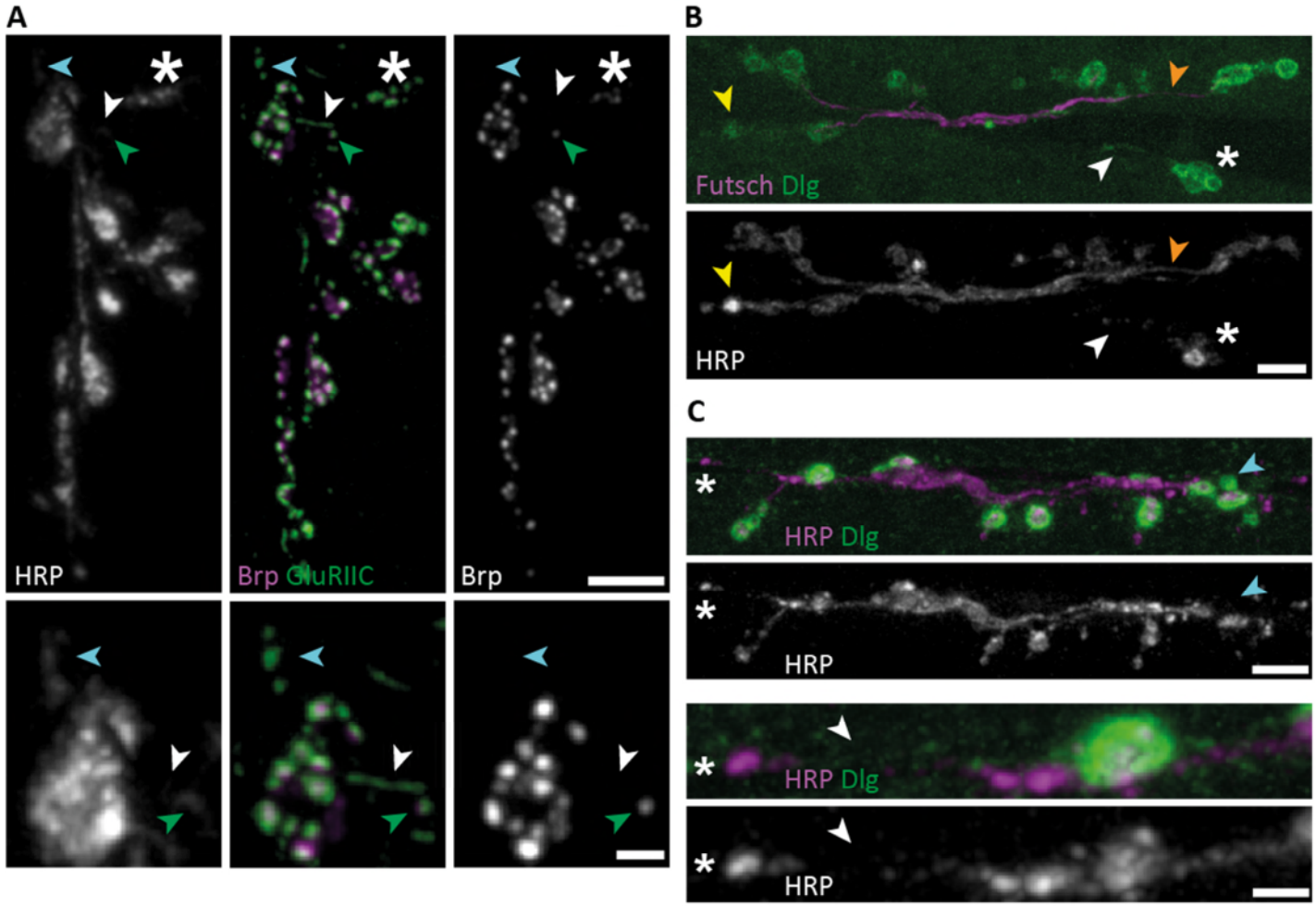

Figure 36: NMJs of *khc*$^{-/-}$ larvae degenerate locally

(A)-(C) Confocal images showing NMJ 6/7 of segment A5 of *khc*$^{-/-}$ larvae. **(A)** Larvae were stained for HRP (grey), Brp (magenta and grey) and GluRIIC (green). White arrowheads point on the missing connection of boutons. White stars mark the boutons separated from the remaining NMJ and positive for HRP and GluRIIC, but with a lack of Brp signal. Green arrowheads are showing a GluRIIC and Brp positive bouton where very low HRP signal is visible. Blue arrowheads point at GluRIIC fields that show reduced HRP staining, but a complete loss of Brp. **(B)** Confocal images from larvae that expressed SSR marker Dlg-GFP (green) and were stained for HRP (grey) and MT associated protein Futsch (magenta). MTs were just innervating less than 60% of the NMJ. White arrowheads and white stars mark a branch that has no MT connection to the remaining NMJ. Yellow arrowheads show a region with bright HRP signal that suggests membranous structures being accumulated. Orange arrowheads point at a region of the NMJ, which could be on the way to be disconnected, because of very thin Futsch signal. **(C)** Confocal images from larvae that were expressing Dlg-GFP (green) and were stained for HRP (grey). An isolated bouton is marked with a white star; lost HRP connection to the remaining NMJ is marked by a white arrowhead in the enlargement below. The blue arrowhead is showing a synaptic footprint (negative for HRP, but positive for Dlg), which was rarely seen in NMJs of *khc*$^{-/-}$ larvae. Scale bars: 5µm and 1.5µm in zoom-in.

Further analysis of NMJ 6/7 of *khc*$^{-/-}$ larvae revealed many aspects of NMJ disassembly. Isolated boutons that were not connected to the NMJ through neuronal membranes (Figure 36A, white star and arrowhead), but were positive for pre- and postsynaptic markers did exist as well as classical retracting parts (Figure 36A, blue arrowhead), where postsynaptic marker and neuronal membrane were present, but presynaptic markers were missing. Otherwise, there were also regions that were possibly on the way to disassemble with showing few Brp packages and low HRP signal, but normal postsynaptic marker (Figure 36A, green arrowhead). NMJs that were stained for Dlg as marker for SSR together with HRP and Futsch showed bright HRP signal (Figure 36B, yellow arrowhead). This staining revealed that disconnected branches of NMJs also completely missed MT cytoskeleton (Figure 36B, white star and arrowhead). Furthermore, branches that were connected to the remaining NMJ through neuronal membranes and showed only very thin Futsch cables could be in the process to disconnect (Figure 36B, orange arrowhead). Figure 36C shows a second example for disconnected NMJ branches (Figure 36C, white star and arrowhead), but also shows one of the rarely seen footprints at NMJs of *khc*$^{-/-}$ larvae (Figure 36C, blue arrowhead). Footprints count to the classical signs for neuronal retraction [Eaton et al. 2002]. Schematic representations of the different forms of NMJ disassembly in comparison with healthy NMJs are shown in Figure 37.

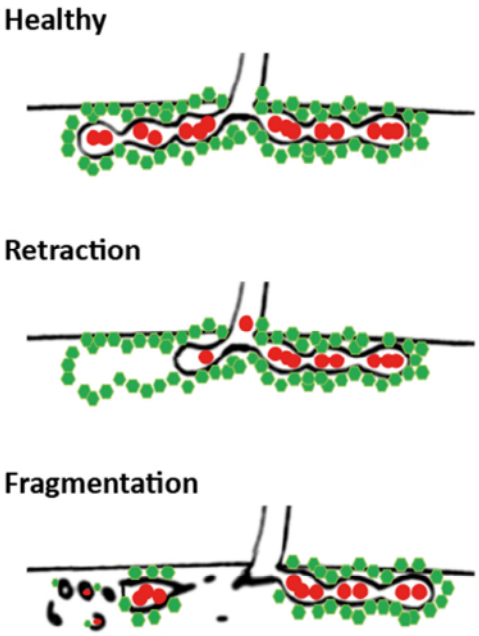

Figure 37: Schematic representation of disassembling NMJs

Schematic representations of the different forms of NMJ disassembly in comparison with healthy NMJs are shown.

4.3.6 Unusual molecular anatomy of NMJ disassembly of *khc*$^{-/-}$ larvae

For further analysis of the nature of synaptic disassembly of *khc*$^{-/-}$ larvae, NMJ 4 was imaged. The motor neuron that innervates muscle 4 is branched from that innervating muscles 6/7 and is slightly longer because NMJs 4 are farer away from the symmetrical middle of the larvae where all axons are led along (compare Figure 12). In some studies NMJ 4 seems to be more vulnerable to synaptic defects than NMJ 6/7 [Tsai et al. 2008; Liu et al. 2010]. Larvae were expressing the SSR marker Dlg-GFP and NMJs were stained for HRP, Futsch and VGlut.

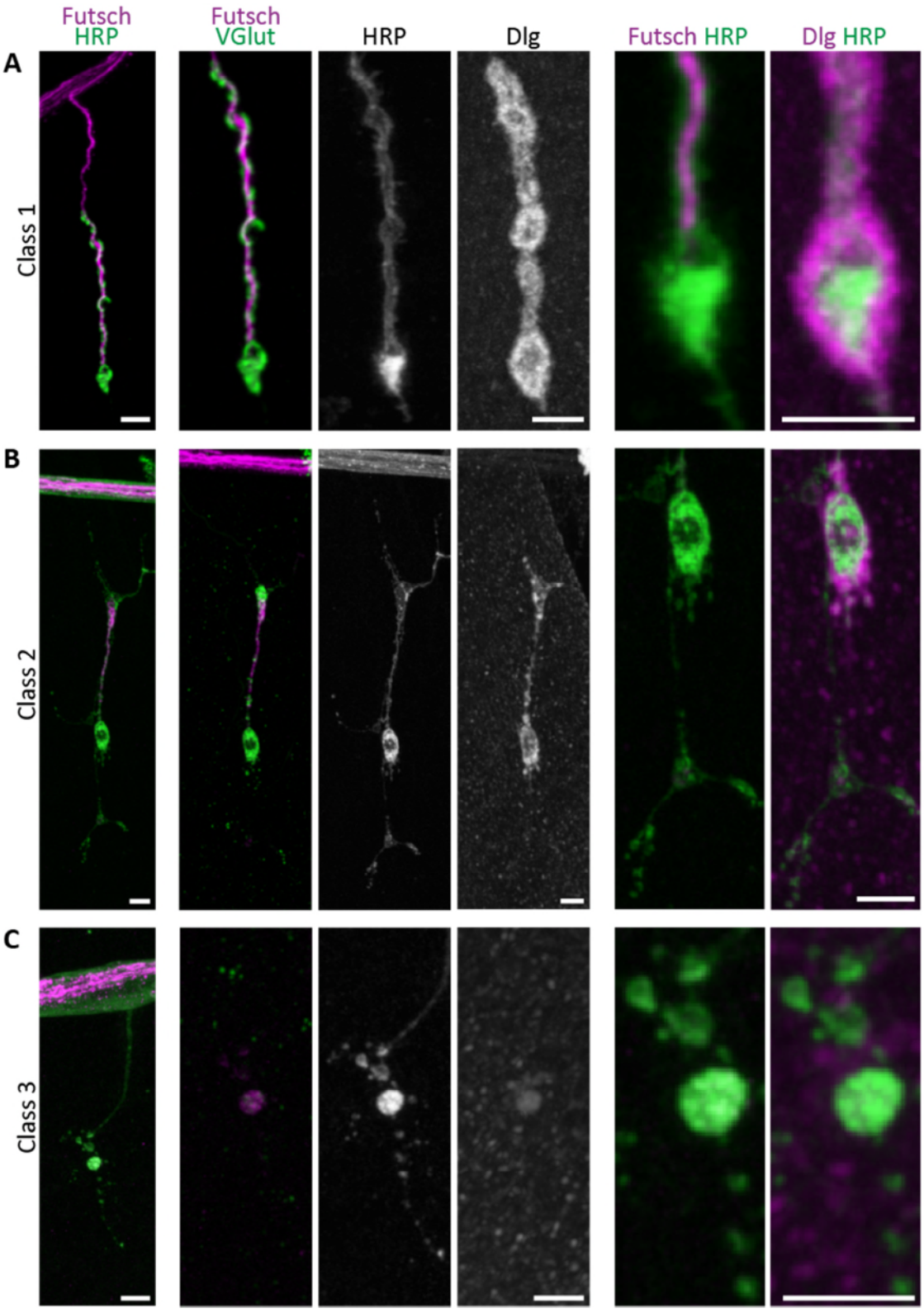

Figure 38: NMJ disassembly in NMJ 4 of *khc*$^{-/-}$ larvae

Confocal images of *khc*$^{-/-}$ mutants showing different magnifications of the NMJ on muscle 4 in three different panels. The different stainings are indicated once on top of the image. **(A)** NMJs categorized in class 1 are positive for Futsch, VGlut, HRP and Dlg in the whole NMJ and their connection to the axon is intact. Abnormal bright HRP staining is frequent in the terminal bouton. **(B)** NMJs categorized in class 2 show a thin HRP connection to the axon, whereas MTs are just present in the middle of the NMJ. Dlg can be tattered and regions of the NMJ retract and are positive for HRP, but negative for MTs and Dlg. Class 2 NMJs are at least to 50% innervated by MTs, but the connection

to the axon is either devoid of MTs or displays membrane fragmentation. **(C)** NMJs categorized in class 3 are completely negative for VGlut and Dlg and the connection to the axon is lost. MTs are just present in the central bouton and the neuronal membrane is fragmented all over the NMJ. Scale bars: first image 5µm, first zoom-in 1.5µm and second zoom-in 6µm.

Interestingly, the imaged NMJs 4 of segments A2 to A5 showed different degrees of severity of NMJ disassembly. Therefore, all imaged NMJs of segments A2 to A5 were assigned to one of the following three classes: class 1 for structurally intact NMJs that were just showing dystrophic boutons (Figure 38A) as they were already described for *khc*$^{-/-}$ larvae [Hurd and Saxton 1996]; class 2 for NMJs that were structurally not connected to the innervating axon through MTs, but might have a thin connection through neuronal membranes (Figure 38B). In this category a quarter of all boutons were negative for VGlut or Dlg. In class 3 NMJs were collected that were fragmented and had no connection to the innervating axon (Figure 38C). In this class one third of all boutons were negative for VGlut and a quarter was negative for Dlg. The analysis of the distribution of these different classes revealed that class 1 NMJs were located on segments A2 or A3, class 2 NMJs were found on segments 2,3 and 4, whereas class 3 NMJs were primary located on segments A4 or A5. Thus, the analysis showed that NMJ 4 seems to be indeed more vulnerable for synaptic defects in *khc*$^{-/-}$ larvae than NMJ 6/7. This hints at a dependency on the distance to the brain, which is highest at segment A5. Such a correlation was also shown for the fast progressing SPG10 model (Füger et al. 2012).

In *khc*$^{-/-}$ larvae neurodegeneration could be detected in the form of normal neuronal retraction, but predominantly as a Wallerian-like NMJ disassembly. This is characterized by structural dissociation of single boutons of the NMJ without retracting in a distal-to-proximal manner towards the innervating axon [Xiong and Collins 2012], which would be the case in conventional retraction of *Drosophila* NMJs (Figure 14, [Eaton et al. 2002]).

4.4 Data collection and summary

In summary, most pathological features occurred in larvae expressing *khc*$^{wt+N262S}$ or *khc*^{N262S} as well as in *khc*$^{-/-}$ larvae. As visualized in Figure 39, small *khc*$^{wt+N262S}$ larvae can be seen as the least affected group of larvae analyzed in this study. The graphic shows the increasing severity of pathology with position of the groups to the right. In each group of larvae listed to the right direction, some additional defects were added.

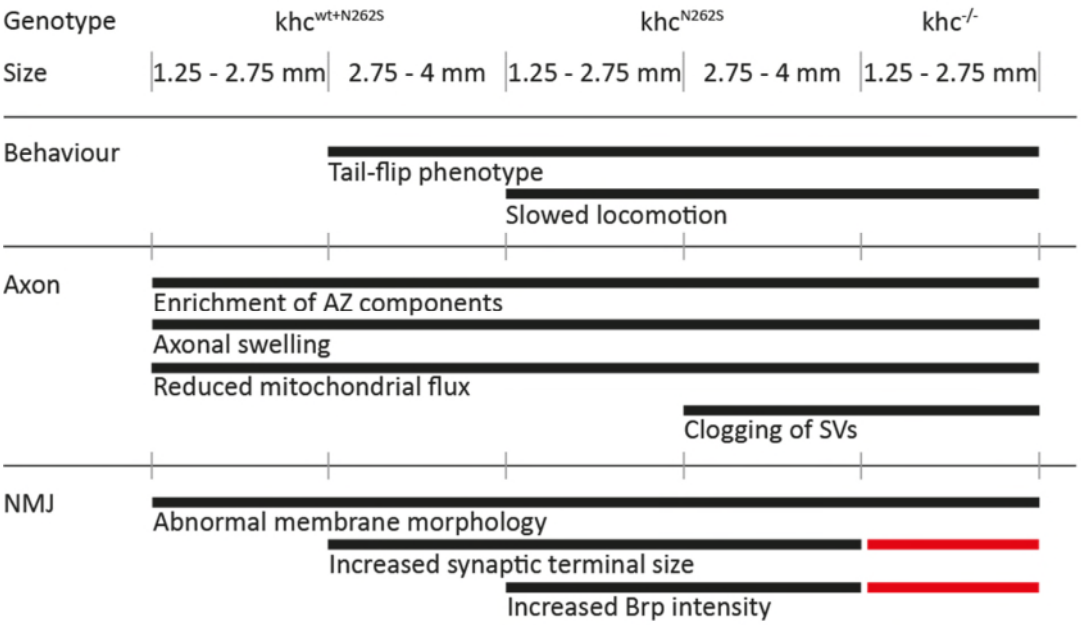

Figure 39: Common pathological feature of larvae expressing *khc*$^{wt+N262S}$ or *khc*^{N262S} and *khc*$^{-/-}$ larvae

The graphic lists all in this study analyzed groups of larvae indicated by genotype and size on the top. The severity of pathology is increasing with position of the groups to the right with small larvae expressing *khc*$^{wt+N262S}$ representing the least affected group and *khc*$^{-/-}$ larvae representing the most affected group. Red lines indicate the opposite of the black lines (decreased NMJ size instead of increased NMJ size and decreased Brp intensity instead of increased Brp intensity). Data is derived from this study except mitochondrial traffic in axons of *khc*$^{-/-}$ larvae, which was examined by Hurd and Saxton [Hurd and Saxton 1996].

In between the four groups of larvae expressing *khc*^{N262S} alone or in combination with *khc*^{wt}, pathologic alterations that were seen in a milder affected group appeared again in more severely affected groups to the right. The most conspicuous difference between larvae

expressing *khc*^{N262S} and *khc*$^{-/-}$ larvae was that NMJ size and Brp number at the NMJ was increased in the first and decreased in the latter group.

5 DISCUSSION

HSPs are a group of heterogeneous neurological disorders caused by a length-dependent, distal degeneration of corticospinal tract axons [Blackstone et al. 2011]. These defects in axon maintenance and function then lead to weakness and spasticity of lower extremities, bladder disturbances and to a lesser extent sensory impairments [Harding 1983; Fink 2003; Martin et al. 2012]. The underlying molecular cell biology of HSPs reveals disrupted neuronal trafficking, organelle morphogenesis and distribution (compare Figure 1).

5.1 Mild neurodevelopmental delay as common ground with other animal models of HSP

Clinically, HSPs have been classified as neurodegenerative disorders [Salinas et al. 2008; Novarino et al. 2014]. However, experimental data derived from *kif5a* knockout mice, Kif5A mutant zebrafish and a *Drosophila khc* null mutant are less conclusive and provide evidence for neurodevelopmental, rather than neurodegenerative defects [Hurd and Saxton 1996; Xia et al. 2003; Wang and Brown 2010; Karle et al. 2012; Nakajima et al. 2012; Campbell et al. 2014]. There the developmental delay was the major pathological factor of HSP animal models. The present study and previous work of larvae expressing khc^{N262S} alone or in combination with khc^{wt} [Füger et al. 2012] could show a mild neurodevelopmental delay and the degeneration of the NMJs in a fly model of HSP.

As already mentioned in the introduction, synapses are continuously further differentiated and remodeled. With growing muscles NMJs are adding a similar number of AZs matching the muscle surface and volume [Menon et al. 2013]. In a time window of 24h control larvae built up about 40% new synapses, whereas larvae expressing mutant *khc* only

formed 30% (Figure 17). The observed developmental delay in *khc*^{N262S} expressing larvae is, however, only minor compared to the degeneration effects. At the same time *khc*^{N262S} expressing larvae depleted about three times the amount of synapses compared to depletion rate of synapses in controls. However, this difference was not significant. Therefore, *khc*^{N262S} expressing larvae likely show only a mild delay in development compared to controls.

In this study, for the first time the parallel occurrence of both, neurodevelopmental and neurodegenerative defects in the same model, could be proven. However, more detailed analyses are needed to reveal, whether similar neurodegenerative defects may also occur in vertebrate models of HSP.

5.2 Increased NMJ size – a contradiction to neurodegeneration?

The major difference of the SPG10 model of this study compared to previously published fly models [Hurd and Saxton 1996; Füger et al. 2012] is the expected amount of functional Kinesin-1. The model of the present study expressed less mutant *Khc*^{N262S} and presumably contains more functional Kinesin-1, than previously published *khc* mutant larvae. In contrast to these other *Drosophila* models of mutant Khc, where NMJ size was reduced [Hurd and Saxton 1996; Füger et al. 2012], larvae of this study show even larger NMJ areas compared to control (Figure 22A). This might be a compensatory effect of the NMJ to circumvent the dysfunctional synaptic transmission that leads to posterior paralysis. This compensation may develop because of the slow progression of pathology in the present model in contrast to fast progressive pathology in previous *Drosophila* models.

5.3 Compensatory increase of Brp particles at the NMJ of *khc*^{N262S} expressing larvae

Brp is important for proper AZ assembly, calcium channel clustering [Kittel et al. 2006] and the size of the readily releasable vesicle pool at the synapse in *Drosophila* [Matkovic et al. 2013]. In axons of control larvae Brp appears as sparse and small packages. In *khc* mutant larvae, Brp was enriched in the axon and at the NMJ (Figure 20).

Brp seems to be primarily transported by Unc-104 (Kinesin-3). Larvae mutant for Unc-104 show reduced amounts of Brp at the NMJ and in axons, but an enrichment of Brp in motor neuron cell bodies, which could be rescued by pan-neural expression of wild type Unc-104 [Pack-Chung et al. 2007; Kern et al. 2013].

Interestingly, an axonal enrichment of Brp was also reported for *dMiro* null mutant larvae, while the number of synapses at the NMJ of those larvae revealed no difference to the control [Guo et al. 2005]. *dMiro* is important for the axonal transport of mitochondria. Consequently, another common feature of both larvae is the reduced number of mitochondria at the NMJ (Figure 21, [Guo et al. 2005] and also an abnormal locomotion, hinting to a synaptic defect at posterior NMJs [Guo et al. 2005]. Therefore, lacking mitochondria at the NMJ could be the trigger for axonal Brp enrichment in both, *dMiro* and *khc* mutants.

Using *in vivo* imaging of GFP-tagged Brp, it could be shown that the axonal transport of Brp was not disturbed, but the total number of transported particles was even increased compared to control (Figure 20C).

The nature of Brp movement in control larvae was comparable to the movement of putative AZ precursor vesicles containing Bassoon in time-lapse confocal microscopy of rat

cultured hippocampal neurons [Shapira et al. 2003]. Brp seems to correspond to neuronal CAZ-associated structural protein (CAST) isoforms in mammals [Wagh et al. 2006]. In vertebrates, Bassoon and Piccolo are thought to organize the AZ together with RIM1, Munc-13 and CAST [Dresbach et al. 2001; Ohtsuka et al. 2002].

As Brp was enriched in the axons of all mutant larvae used in this study (Figure 39) and the axonal transport of Brp particles seems to be enhanced, rather than generating a traffic jam, the hypothesis of a compensatory upregulation of Brp transport to NMJs seems natural. In models of presynaptic strengthening, where only GluRIIB is expressed, lacking the GluRIIA subunit, the amount of Brp at NMJs increased within 10min. [Weyhersmuller et al. 2011]. Thereby the absolute number of Brp packages was, just like in *khc*^{N262S} expressing larvae of this study, not increased (compare Figure 20 and Figure 22, [Weyhersmuller et al. 2011]). This shows that a compensatory response in *Drosophila* NMJs is possible within a few minutes. As Brp is transported by Unc-104 and not by Khc [Kern et al. 2013], the upregulated transport also suggests a communication between different transport proteins.

5.4 The tail-flip phenotype and spastic posterior paralysis

A common phenotype of *Drosophila* models with axonal transport deficits is the tail-flip body posture, also called dystonic posterior paralysis [Hurd and Saxton 1996; Gindhart et al. 1998; Martin et al. 1999; Bowman et al. 2000]. Homozygous mutant larvae lacking Kinesin-1 or Dynein exhibit intense axonal organelle jams. Larvae deficient for the amyloid protein precursor-like (APPL) protein also show axonal traffic jams, but to a much lesser extent than Kinesin-1 or Dynein mutant larvae [Gunawardena and Goldstein 2001]. As APPL deficient larvae do not show tail-flipping or paralysis, it is thought that the extent of

blockage within axons may determine the severity of the phenotype [Gunawardena and Goldstein 2001].

Normal larval crawling originates in the rhythmic contraction of dorsal and ventral muscle groups. The lateral muscles in the adjacent posterior segment contract concurrently [Heckscher et al. 2012]. Most probably abnormal contraction of the posterior body wall muscles leads to flipping of the posterior part of the larvae while crawling and impairs locomotion. In HSP patients also the long motor neurons that innervate the lower part of the body are affected, whereas shorter ones mostly do not show any impairments [Blackstone et al. 2011]. The varying degree of effects in different muscle groups could derive from the different length of innervating axons just like in humans.

In *Drosophila*, this could be due to the fact that most dorsal muscles are innervated by axons that are longer than those innervating the ventral muscles (compare Figure 12 and Figure 40).

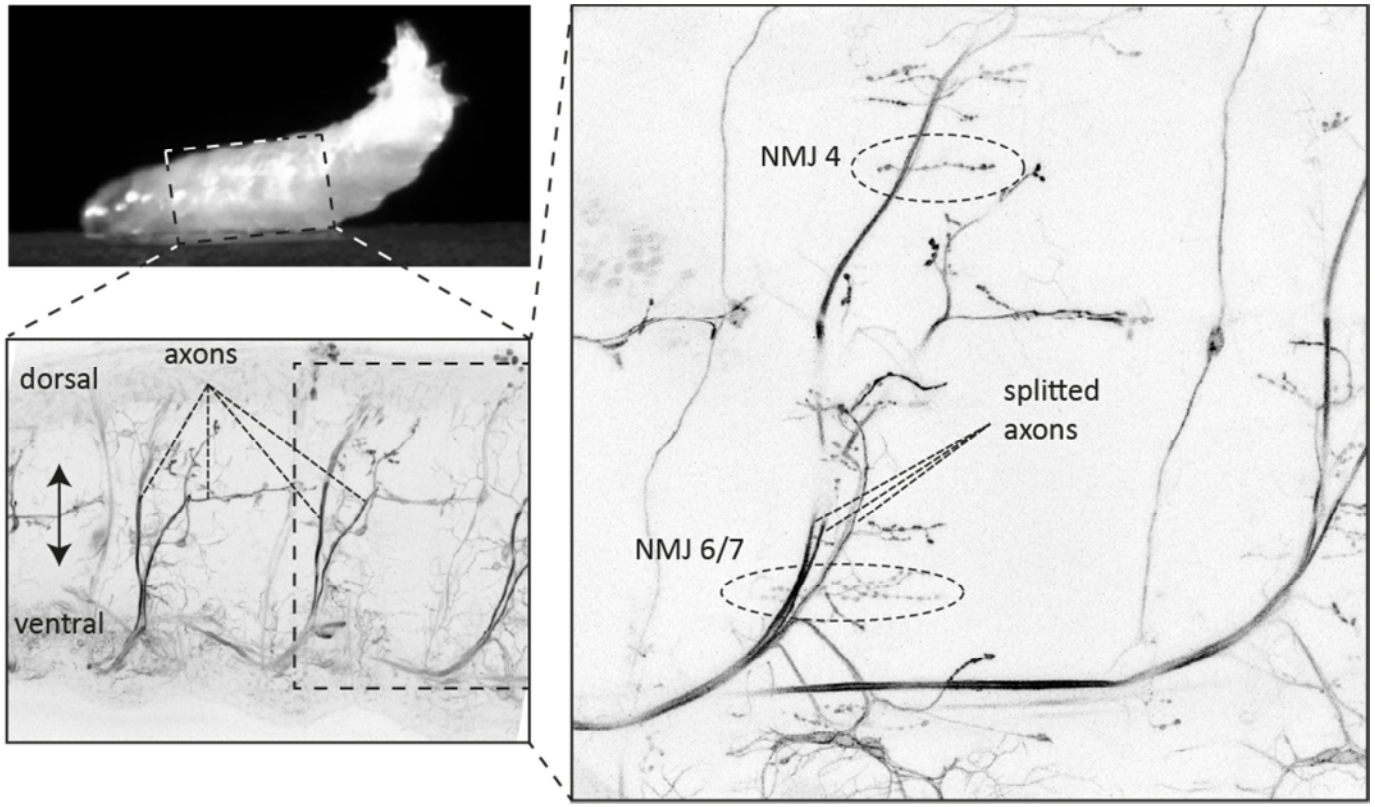

Figure 40: Location of motor neurons innervating NMJ 6/7 and NMJ 4 in third instar larvae

On the left side on the top, a third instar *Drosophila* larva with a tail-flip is shown. On the left side on the bottom, an *in vivo* image of two segments of a larva expressing a neuronal membrane tagged tdTomato is shown. On the ventral side nerves are guided to the respective segment and then split to lead to the muscle they innervate. On the right side a single segment and the corresponding axons and NMJs are shown. As the axons split after leaving the ventral middle line, NMJ 6/7 is innervated by a different axon than NMJ 4.

When arriving at the designated segment nerves split into several different branches, which innervate different muscles (Figure 40, [Menon et al. 2013]). Per segment three different motor neurons are leaving the CNS: the segmental nerve root (SN), the intersegmental nerve root (ISN) and the transverse nerve (TN) [Menon et al. 2013]. They innervate lateral and ventral muscles (SN) or dorsal (ISN) and ventrolateral muscles (ISNb). Each motor neuron pathway is genetically determined and in each larvae the same [Menon et al. 2013]. As NMJ 4 is located at the dorsal side and the bundles of axons are guided to the respective segment at the ventral side of the larvae, axons innervating NMJ 4 are considerably longer than axons innervating NMJ 6/7.

In the *Drosophila* model of this study the aberrant larval crawling is triggered by a pathogenic mutation, which in patients leads to spastic paralysis of the lower extremities. The *Drosophila* larval nervous system does not contain upper and lower motor neurons and therefore, spastics cannot be explained by increased reflex activity. Still the origin of the abnormal contraction lies most probably in the innervating axon and not in the brain, since reduced transport rates at long distances are the major defect in animal models. Therefore, the tail-flip phenotype in the SPG10 model is more a spastic posterior paralysis than a dystonic posterior paralysis, which would originate in the brain.

5.5 Axonal traffic jams – a common feature of *kif5a* mutants

Neurons, perhaps more than any other cell, heavily depend on effective intracellular transport. Cargo that is transported along axons of control larvae distributes smoothly throughout the axon. In the SPG10 models of this study, enrichment of neuronal membranes in large aggregates in the axon is an early feature of pathology, when delivery of presynaptic markers like VGlut and Brp to the NMJ is not diminished (Figure 19 and Figure 20).

Disruption of axonal transport seems to be a common mechanism in a number of neurodegenerative diseases including motor neuron disorders [De Vos et al. 2008]. Post-mortem analysis of two HSP patients with mutations in SPG4 (Spastin) also showed strong axonal swellings in the cortico spinal tract. Spastin is responsible for MT severing and bundling [Kasher et al. 2009], indicating that defects in axonal transport may underlie the disease process in SPG4. Axons of cultured motor neurons of *kif5a* knockout mice show an accumulation of neurofilaments [Uchida et al. 2009; Wang and Brown 2010; Karle et al. 2012] and *kif5A* mutant zebrafish had axonal swellings and acetylated tubulin accumulations [Campbell et al. 2014]. Axonal traffic jams and the tail-flip phenotype are typical for deficits in axonal transport [Hurd and Saxton 1996; Martin et al. 1999; Horiuchi et al. 2005; Karle et al. 2012]. However, it is also conceivable that the membrane accumulations seen in the SPG10 model of this study could be directly linked to the impaired mitochondrial flux observed in larvae of the same stage (Figure 21). As vesicle transport seems to be mainly maintained by ATP, which is generated by glycolysis, mitochondria are not needed for energy supply during vesicle transport [Zala et al. 2013]. The transport of mitochondria, however, does not depend of glycolysis. Thereby, a high number of mitochondria that are stationary bound to MTs, could trigger the generation of traffic jams for other cargos, too. Therefore, further research in this field can also be of importance for many other diseases that involve axonal transport problems, including Alzheimer's disease, Parkinson's disease and ALS [De Vos et al. 2008].

5.6 The formation of dystrophic NMJs

HRP stained neuronal membranes distributed uniformly throughout the NMJ in control larvae. In all *khc* mutants analyzed in this study ($khc^{wt+N262S}$, khc^{N262S} and $khc^{-/-}$) even

the small larvae show highly irregular HRP staining with accumulations at several boutons (Figure 39). As shown by 3D reconstruction, these areas were located at the center of the bouton (Figure 28). EM analysis has shown an increased amount of different kinds of vesicles inside boutons of larvae expressing *khc*$^{wt+N262S}$ (Figure 29). Such dystrophic boutons were also shown for *khc* null mutant larvae (Figure 35, [Hurd and Saxton 1996], *glued* mutant larvae [Lloyd et al. 2012] and a*nkyrin* mutant larvae [Pielage et al. 2008]. Ankyrin provides a link between intercellular adhesion and cytoskeletal stabilization in neurons. Larvae expressing a large isoform of Ankyrin show retracting NMJs with inhomogeneous HRP staining as well as disorganized NMJ structure [Pielage et al. 2008]. Ultrastructural analysis of these larvae revealed an abnormal accumulation of membranes as well as curved AZs [Pielage et al. 2008] that indicate sites of NMJ disassembly. Lloyd and colleagues also report inhomogeneous HRP staining in larvae deficient for Glued, the major subunit of Dynactin. They also show a dependence of the severity of this phenotype on the gene dosage of Khc, because Khc functions synergistically with Glued at terminal boutons [Lloyd et al. 2012]. The related phenotypes of mutants of the SPG10 model of this study (Khc), another transport protein (Glued) and a scaffolding protein (Ankyrin) hint at common pathological pathways leading to membrane accumulation and NMJ degeneration. Possibly, an interaction between Glued and Khc, which could be necessary for proper transport, cannot take place when one partner is missing or non-functional.

5.7 Irregular MT cytoskeleton, FasII staining and giant boutons as signs for neurodegeneration

The MT cytoskeleton and MT-associated proteins like Futsch are crucial for the delivery of cargo to synapses and thereby for synaptic growth and stability [Hummel et al.

2000; Roos et al. 2000]. In control larvae MTs form a cable-like structure with loops at sides of nerve branching and at terminal boutons [Roos et al. 2000]. NMJs of large larvae expressing mutant Khc revealed strongly jumbled MT organization with Futsch accumulating at several boutons, whereas it was lucking at others (Figure 24). A resembling phenotype is shown in NMJs with altered FasII expression [Ashley et al. 2005]. Asymmetric expression of FasII at the pre- and postsynapse was accompanied by giant boutons and aberrant MT cytoskeleton. These giant boutons also stained brightly for HRP and showed altered FasII structure [Ashley et al. 2005], like larvae expressing khc^{N262S} of this study do. Pielage and colleagues also describe disorganized MT and FasII structures at NMJs with knocked-down β-Spectrin, which is essential for synaptic stability [Pielage et al. 2005]. These results suggest that regions at the NMJ of larvae expressing khc^{N262S}, which show alterations of MT cytoskeleton or irregular FasII staining, were instable and could be on the way to degenerate.

5.8 Disrupted axonal transport of mitochondria as trigger for the initiation of NMJ disassembly?

Presynaptic mitochondria are important for the sequestration of calcium, which is especially important during synaptic depression, post-tetanic potentiation [David and Barrett 2003] and for ATP production that can overcome the high energy demands of vesicle recycling at the presynapse (Figure 7, [Verstreken et al. 2005]). Mitochondria are thought to be mainly synthesized and degraded in the motor neuron cell body [Sheng and Cai 2012]. Hence, the delivery of mitochondria to the NMJ is crucial for many functions of the synapse. Campbell and colleagues reported less mitochondria in the pLLn of a truncated Kif5A expressing zebrafish [Campbell et al. 2014]. The *Drosophila* SPG10 model of this study also

showed impaired axonal transport of mitochondria as a very early defect in the SPG10 pathology (Figure 30), resulting in reduced number of mitochondria at the NMJ at later stages. Mitochondrial dysfunction or altered mitochondrial dynamics are a common hallmark of many neurodegenerative disorders like Parkinson's disease, ALS, Huntington's disease, Alzheimer's disease, CMT2A and optic atrophy (for review see [Chang and Reynolds 2006; Chen and Chan 2009; Schon and Przedborski 2011]). Lack of mitochondria at the synapse could serve as a reason for the very early occurring synaptic defects leading to posterior paralysis. As the transport of mitochondria is slowed down, the exchange rate of mitochondria at the synapse could be slowed down, too. Mitochondria in *khc*^{N262S} expressing larvae might be older and consequently less functional than the probably younger ones in control larvae. As damaged mitochondria not only lead to altered ATP production and impaired calcium buffering, but also release apoptotic cell death signals (for review see [Green and Van Houten 2011]), this might be the trigger for later synaptic degeneration.

5.9 The link between mitochondrial calcium homeostasis and Wallerian degeneration

As mentioned before, axonal swellings, accumulations of acetylated tubulin and reduced numbers of mitochondria were discovered in pLLn of zebrafish expressing a Kif5A, which is truncated at the tail domain of the protein [Campbell et al. 2014]. Interestingly, in these swellings an increased calcium signal was detected [Campbell et al. 2014]. The influx of calcium is both, necessary and sufficient to induce axonal degeneration and blocking calcium influx by calcium channel or calpain antagonists inhibited the degeneration [George et al. 1995]. Elevated intracellular calcium concentrations via the influx of extracellular calcium in neurons were shown to occur during Wallerian degeneration [Mishra et al. 2013]. Thus,

calcium is discussed to be the trigger for initiating Wallerian degeneration, which is a special way of degeneration that can be mechanistically distinguished from normal neurodegeneration. Classic neurodegeneration leads to a stepwise retraction of the NMJ to the axon [Eaton et al. 2002]. In contrast, Wallerian degeneration is characterized by the fractionation of the NMJ and was originally found in models of spinal cord injury [Waller 1850]. The term Wallerian-like degeneration describes an NMJ disassembly that shares features of the original Wallerian degeneration, which is caused by nerve injury, but is triggered by different factors. Wallerian degeneration slow (Wld^S) protein can protect axons and NMJs from Wallerian degeneration, but the mechanism behind is not known [Coleman and Freeman 2010]. Studies in *Drosophila* have shown a co-localization of Wld^S protein with mitochondria [Avery et al. 2012]. As already mentioned in the introduction, mitochondria are very important for calcium homeostasis [Ganitkevich 2003] and their mobility can be regulated by intracellular calcium levels [Yi et al. 2004; Wang and Schwarz 2009]. In models of axonal injury, raising calcium concentrations near the side of injury, lead to decreased mitochondrial mobility in controls [Avery et al. 2012]. In the presence of Wld^S mitochondrial mobility remains stable after injury [Avery et al. 2012]. Thereby these mitochondria are able to buffer higher levels of calcium compared to those of wild type larvae [Avery et al. 2012] and further more show increased ATP production [Yahata et al. 2009]. In some models of axonal transport impairments Wld^S also delays neurodegeneration [Coleman 2005]. Although axonal transection (e.g. spinal cord injury) is rare in clinical neuroscience, disruption of axonal transport could also be seen as a form of isolation of axons and synapses from their cell bodies. It is conceivable that impaired axonal transport – especially of mitochondria – can lead to a malfunction of the remaining mitochondria at the NMJ. This then leads to (A) lower levels of ATP that indirectly elevate the intracellular calcium level and

creates an imbalance of cellular homeostasis, (B) activation of the mitochondrial permeability transition pore that leads to mitochondrial damage and (C) the generation of reactive oxygen species [Conforti et al. 2014]. As elevated intracellular calcium levels already can initiate Wallerian degeneration on their own [George et al. 1995], all factors together could result in the initiation of a Wallerian-like degeneration of NMJs in larvae exhibiting impaired axonal transport especially of mitochondria.

5.10 SPG10 pathology in *khc*$^{-/-}$ larvae

Comparison of the pathology of *khc*$^{-/-}$ larvae with overexpression of *khc*^{N262S} has shown a much faster pathological progression in *khc*$^{-/-}$ larvae. Many common features lead to the assumption that the mechanism behind could be the same in all mutants examined in this study (Figure 39).

Axonal swellings with high HRP immunoreactivity in *khc*$^{-/-}$ larvae were already described by Hurd and Saxton [Hurd and Saxton 1996]. The accumulation of Khc in these swellings leads to the suggestion that impaired transport of Khc cargos led to these swellings [Hurd and Saxton 1996]. In the present study it could be shown that cargos indeed accumulate in swellings and might be the trigger for their development (Figure 19). In contrast to larvae expressing *khc*^{N262S}, the examined cargo is consequently reduced at the NMJ. This further supports the traffic jam hypothesis. Thereby, less AZs and PSDs in smaller NMJs could either result from neuronal retraction or from impaired neurodevelopment.

As MTs were partly retracted from terminal boutons and were also fractionated inside NMJs (Figure 23 and Figure 24), the presence of neurodegeneration is clearly shown. Thereby, cargo transport within NMJs could additionally be impaired and promote developmental delay. During normal neuronal retraction materials are transported from the

synapses towards the axon (Figure 14). Without connection to the axon through MTs a coordinated back transport is hardly possible. HRP accumulations at the NMJ, which were also shown by Hurd and Saxton, could thereby also be explained by a kind of traffic jam.

Consequently it might well be that the only possible way of NMJ disassembly is through a Wallerian-like mechanism.

5.11 Pathologic sequence of different *khc* mutants

SPG10 is an autosomal dominant form of HSP [Reid et al. 2002; Schüle et al. 2008]. *In vitro* experiments showed that khc^{N256S} acts in a dominant-negative manner [Ebbing et al. 2008] and in *Drosophila* this mutant acts as an antimorph interfering with endogenous Khc function [Füger et al. 2012]. Both *khc* mutant larvae ($khc^{wt+N262S}$ and khc^{N262S}) used in this study contain presumably different amounts of functional Khc. As Khc is forming dimers, the predicted amount of functional Kinesin-1 depends on the percentage of mutant to wild type Khc in the organism. Following this hypothesis, $khc^{wt+N262S}$ expressing larvae contain more functional Kinesin-1 than larvae expressing only khc^{N262S}. Further on, $khc^{-/-}$ larvae contain less functional Kinesin-1 than khc^{N262S} expressing larvae. In this connection it should be remembered that all larvae develop with maternal Khc from the egg [Hurd and Saxton 1996]. Nevertheless, the amount of functional Khc dimers, present during the whole development, presumably influences the pathological progression.

Summarizing most results of the present study, it could be concluded that all models follow a common pathological pattern, but to a different extent.

In young larvae expressing $khc^{wt+N262S}$ a reduced mitochondrial flux in both directions, the formation of axonal swellings, more axonal Brp and abnormal membrane morphology at

the NMJ were among the first differences to the control of the same larval size (Figure 30). Interestingly, changes at NMJs and axons occurred before considerable behavioral defects were detectable. This could be explained by a compensation of synaptic defects that prevent behavioral defects at this stage. Additionally the reduced mitochondrial flux does not yet lead to reduced number of mitochondria at the NMJ (Figure 30). The larger larvae expressing $khc^{wt+N262S}$ showed, additional to the first pathological features, clear movement defects, increased NMJ size and the beginning of synaptic disassembly.

Small larvae of the more severely affected genotype expressing only khc^{N262S} at 25°C showed slowed locomotion in turning assay and increased Brp intensity, as well as decreased number of mitochondria at the NMJ. In large larvae of this genotype synaptic vesicles are accumulating in the axon and decreased synaptogenesis was detected.

Following the hypothesis that the amount of functional Khc determines the pathologic progression in *Drosophila*, larvae expressing khc^{N262S} at 29°C would be the next model to be integrated into this sequence, because a higher expression rate of mutant Khc protein presumably leads to a lower amount of functional Kinesin-1.

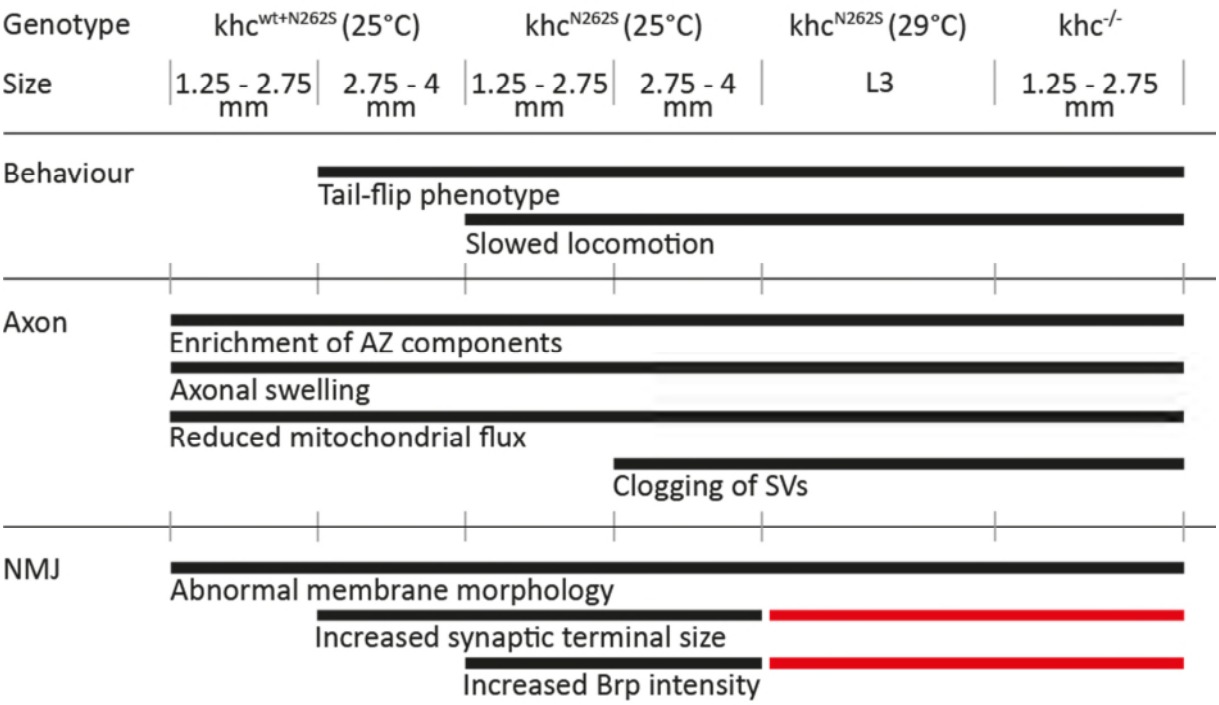

Figure 41: Integration of the previous published SPG10 model in the proposed pathological progression

Illustration of the common pathological features of published *Drosophila* SPG10 models. The least affected larvae are those expressing khc$^{wt+N262S}$ (25°C), the most affected larvae are khc$^{-/-}$ larvae and larvae expressing khc^{N262S} that were kept at 29°C. Red lines indicate the opposite of the black lines (decreased NMJ size instead of increased NMJ size and decreased Brp intensity instead of increased Brp intensity). Data is derived from this study except mitochondrial traffic in axons of khc$^{-/-}$ larvae, which was examined by Hurd and Saxton [Hurd and Saxton 1996] and all data regarding larvae expressing khc^{N262S} kept at 29°C [Füger et al. 2012].

Indeed, *khc^{N262S}* expressing larvae kept at 29°C show most pathological changes observed in *khc^{N262S}* larvae kept at 25°C (Figure 41). Interestingly Füger and colleagues describe in the fast progressive SPG10 model (kept at 29°C) smaller NMJs accompagnied with less VGlut and Brp at the NMJ. These results could also be seen in *khc$^{-/-}$* larvae of this study. One possible explanation is that the likely compensatory increase in NMJ size, bouton size and Brp intensity at NMJs of mutant larvae expressing *khc^{N262S}* and *khc$^{wt+N262S}$* kept at 25°C did not happen in larvae with a faster pathological progression. Possibly because the non-functional Khc dimers build up an early traffic jam and the remaining functional Khc dimers cannot carry enough material to facilitate an over-growing NMJ.

6 CONCLUSION

The slow progressive SPG10 model of this study could link the pathological features of both, neurodevelopmental defects and neurodegeneration. Defects in neurodevelopment like impaired synaptogenesis as well as degenerative changes like altered HRP staining and disrupted MT and FasII organization could be observed in the same animal. As additional signs for degeneration, morphological changes in boutons using 3D convolution and EM were highlighted where SPG10 model larvae exhibited abnormal accumulation of large vesicles and an altered shape of AZs. As the observed developmental defects were only minor, degenerative changes are presumably the primary trigger promoting the pathological changes that cause the pathological hallmarks of mutant Khc in *Drosophila*, the tail-flip phenotype.

These results provide a more detailed view of how SPG10 leads to paralysis of the distal segments in *Drosophila* larvae. A similar advancement in knowledge of the human pathology should provide multiple points for possible interventions that could lead to development of new therapies that cure or halt the progression of SPG10.

7 OUTLOOK

The anterograde axonal transport protein Kinesin-1 is formed out of dimers of Khc. As SPG10 patients are heterozygous for the point mutation N256S in KIF5A, it is assumed that 25% of dimers in patients are wild type dimers and fully functional and according to the dominant negative action of Khc^{N256S} 75% of dimers are non-functional. Therefore, the ratio of wild type Khc to Khc^{N256S} is very important to the progress of the disease. Detailed analysis of the expressed amount of both intrinsic wild type Khc of the larvae and the ectopic overexpression would be extremely helpful for further analysis of the disease progression of SPG10 in *Drosophila*.

As mitochondrial transport is disturbed already in early stages of SPG10 progression in the *Drosophila* model used in this study, whereas the number of mitochondria at the NMJ is not diminished, it would be very interesting to investigate the condition of these mitochondria. If they are really the initiating factor of the behavioral defect seen in this stage of larval disease, the exchange factor would have to be decreased and they would have to be less functional than control mitochondria: either concerning their ability of sequestration of calcium or their production of ATP. As analysis of SPG20 (Spartin) also revealed a diminished ability of mitochondrial calcium uptake [Joshi and Bakowska 2011], parallels in the pathology of SPG10 and SPG20 are conceivable. Further on, mitochondria could release reactive oxygen species that lead to apoptotic cell death signals [Green and Van Houten 2011]. Thereby, reactive oxygen species measuring could also be a possible target for further studies.

To confirm the hypothesis that the behavioral defect in larvae expressing *khc*^{N262S} is originating in defective synapses, electrophysiological analysis of the relevant NMJs could clarify their state of function. Furthermore the examination of the calcium concentrations in axons near axonal swellings (as it was shown in zebrafish [Campbell et al. 2014]) and posterior NMJs would be an interesting point to argue for mitochondrial defects.

Finally, of course a knock-in fly or mouse, rather than knockout or ectopic overexpression of *khc* would be the way in which the pathology of SPG10 could be examined in the most appropriate way.

REFERENCES

Aizawa H, Sekine Y, Takemura R, Zhang Z, Nangaku M, Hirokawa N (1992) Kinesin family in murine central nervous system. J Cell Biol 119:1287-1296.

Alonso MC, Drummond DR, Kain S, Hoeng J, Amos L, Cross RA (2007) An ATP gate controls tubulin binding by the tethered head of kinesin-1. Science 316:120-123.

Asbury CL, Fehr AN, Block SM (2003) Kinesin moves by an asymmetric hand-over-hand mechanism. Science 302:2130-2134.

Ashley J, Packard M, Ataman B, Budnik V (2005) Fasciclin II signals new synapse formation through amyloid precursor protein and the scaffolding protein dX11/Mint. J Neurosci 25:5943-5955.

Ataman B, Ashley J, Gorczyca M, Ramachandran P, Fouquet W, Sigrist SJ, Budnik V (2008) Rapid activity-dependent modifications in synaptic structure and function require bidirectional Wnt signaling. Neuron 57:705-718.

Atherton J, Farabella I, Yu IM, Rosenfeld SS, Houdusse A, Topf M, Moores CA (2014) Conserved mechanisms of microtubule-stimulated ADP release, ATP binding, and force generation in transport kinesins. Elife 3:e03680.

Avery MA, Rooney TM, Pandya JD, Wishart TM, Gillingwater TH, Geddes JW, Sullivan PG, Freeman MR (2012) WldS prevents axon degeneration through increased mitochondrial flux and enhanced mitochondrial Ca2+ buffering. Current biology : CB 22:596-600.

Baas PW, Black MM, Banker GA (1989) Changes in microtubule polarity orientation during the development of hippocampal neurons in culture. J Cell Biol 109:3085-3094.

Baloh RH, Schmidt RE, Pestronk A, Milbrandt J (2007) Altered axonal mitochondrial transport in the pathogenesis of Charcot-Marie-Tooth disease from mitofusin 2 mutations. J Neurosci 27:422-430.

Barkus RV, Klyachko O, Horiuchi D, Dickson BJ, Saxton WM (2008) Identification of an axonal kinesin-3 motor for fast anterograde vesicle transport that facilitates retrograde transport of neuropeptides. Molecular biology of the cell 19:274-283.

Bate M, Broadie K (1995) Wiring by fly: the neuromuscular system of the Drosophila embryo. Neuron 15:513-525.

Bettencourt da Cruz A, Schwarzel M, Schulze S, Niyyati M, Heisenberg M, Kretzschmar D (2005) Disruption of the MAP1B-related protein FUTSCH leads to changes in the neuronal cytoskeleton, axonal transport defects, and progressive neurodegeneration in Drosophila. Molecular biology of the cell 16:2433-2442.

Blackstone C, O'Kane CJ, Reid E (2011) Hereditary spastic paraplegias: membrane traffic and the motor pathway. Nat Rev Neurosci 12:31-42.

Blasius TL, Cai D, Jih GT, Toret CP, Verhey KJ (2007) Two binding partners cooperate to activate the molecular motor Kinesin-1. J Cell Biol 176:11-17.

Bosco DA, Morfini G, Karabacak NM, Song Y, Gros-Louis F, Pasinelli P, Goolsby H, Fontaine BA, Lemay N, McKenna-Yasek D, Frosch MP, Agar JN, Julien JP, Brady ST, Brown RH, Jr. (2010) Wild-type and mutant SOD1 share an aberrant conformation and a common pathogenic pathway in ALS. Nat Neurosci 13:1396-1403.

Bowman AB, Kamal A, Ritchings BW, Philp AV, McGrail M, Gindhart JG, Goldstein LS (2000) Kinesin-dependent axonal transport is mediated by the sunday driver (SYD) protein. Cell 103:583-594.

Brand AH, Perrimon N (1993) Targeted gene expression as a means of altering cell fates and generating dominant phenotypes. Development (Cambridge, England) 118:401-415.

Brendza RP, Serbus LR, Duffy JB, Saxton WM (2000) A function for kinesin I in the posterior transport of oskar mRNA and Staufen protein. Science 289:2120-2122.

Bridgman PC (1999) Myosin Va movements in normal and dilute-lethal axons provide support for a dual filament motor complex. J Cell Biol 146:1045-1060.

Broadie KS, Bate M (1993) Development of the embryonic neuromuscular synapse of Drosophila melanogaster. J Neurosci 13:144-166.

Brough D, Schell MJ, Irvine RF (2005) Agonist-induced regulation of mitochondrial and endoplasmic reticulum motility. The Biochemical journal 392:291-297.

Bryant Z, Stone MD, Gore J, Smith SB, Cozzarelli NR, Bustamante C (2003) Structural transitions and elasticity from torque measurements on DNA. Nature 424:338-341.

Budnik V, Zhong Y, Wu CF (1990) Morphological plasticity of motor axons in Drosophila mutants with altered excitability. J Neurosci 10:3754-3768.

Budnik V, Koh YH, Guan B, Hartmann B, Hough C, Woods D, Gorczyca M (1996) Regulation of synapse structure and function by the Drosophila tumor suppressor gene dlg. Neuron 17:627-640.

Burton PR, Paige JL (1981) Polarity of axoplasmic microtubules in the olfactory nerve of the frog. Proceedings of the National Academy of Sciences of the United States of America 78:3269-3273.

Buszczak M, Paterno S, Lighthouse D, Bachman J, Planck J, Owen S, Skora AD, Nystul TG, Ohlstein B, Allen A, Wilhelm JE, Murphy TD, Levis RW, Matunis E, Srivali N, Hoskins RA, Spradling AC (2007) The carnegie protein trap library: a versatile tool for Drosophila developmental studies. Genetics 175:1505-1531.

Cai D, Hoppe AD, Swanson JA, Verhey KJ (2007) Kinesin-1 structural organization and conformational changes revealed by FRET stoichiometry in live cells. J Cell Biol 176:51-63.

Campbell PD, Shen K, Sapio MR, Glenn TD, Talbot WS, Marlow FL (2014) Unique function of Kinesin Kif5A in localization of mitochondria in axons. J Neurosci 34:14717-14732.

Cao L, Wang W, Jiang Q, Wang C, Knossow M, Gigant B (2014) The structure of apo-kinesin bound to tubulin links the nucleotide cycle to movement. Nature communications 5:5364.

Cartoni R, Arnaud E, Medard JJ, Poirot O, Courvoisier DS, Chrast R, Martinou JC (2010) Expression of mitofusin 2(R94Q) in a transgenic mouse leads to Charcot-Marie-Tooth neuropathy type 2A. Brain : a journal of neurology 133:1460-1469.

Casari G, De Fusco M, Ciarmatori S, Zeviani M, Mora M, Fernandez P, De Michele G, Filla A, Cocozza S, Marconi R, Durr A, Fontaine B, Ballabio A (1998) Spastic paraplegia and OXPHOS impairment caused by mutations in paraplegin, a nuclear-encoded mitochondrial metalloprotease. Cell 93:973-983.

Castiglioni MC (1951) [Distribution of pigments in the eye of alleles of white and their compounds in Drosophila melanogaster]. Scientia genetica; periodico di genetica per i paesi latini 4:57-60.

Chada SR, Hollenbeck PJ (2004) Nerve growth factor signaling regulates motility and docking of axonal mitochondria. Current biology : CB 14:1272-1276.

Chance B, Williams GR (1955) Respiratory enzymes in oxidative phosphorylation. III. The steady state. The Journal of biological chemistry 217:409-427.

Chang DT, Reynolds IJ (2006) Mitochondrial trafficking and morphology in healthy and injured neurons. Progress in neurobiology 80:241-268.

Chang DT, Honick AS, Reynolds IJ (2006) Mitochondrial trafficking to synapses in cultured primary cortical neurons. J Neurosci 26:7035-7045.

Chang J, Lee S, Blackstone C (2014) Spastic paraplegia proteins spastizin and spatacsin mediate autophagic lysosome reformation. J Clin Invest 124:5249-5262.

Chang KT, Niescier RF, Min KT (2011) Mitochondrial matrix Ca2+ as an intrinsic signal regulating mitochondrial motility in axons. Proceedings of the National Academy of Sciences of the United States of America 108:15456-15461.

Chavis P, Westbrook G (2001) Integrins mediate functional pre- and postsynaptic maturation at a hippocampal synapse. Nature 411:317-321.

Chen H, Chan DC (2009) Mitochondrial dynamics--fusion, fission, movement, and mitophagy--in neurodegenerative diseases. Human molecular genetics 18:R169-176.

Chouhan AK, Ivannikov MV, Lu Z, Sugimori M, Llinas RR, Macleod GT (2012) Cytosolic calcium coordinates mitochondrial energy metabolism with presynaptic activity. J Neurosci 32:1233-1243.

Cifuentes-Diaz C, Nicolet M, Goudou D, Rieger F, Mege RM (1994) N-cadherin expression in developing, adult and denervated chicken neuromuscular system: accumulations at both the neuromuscular junction and the node of Ranvier. Development (Cambridge, England) 120:1-11.

Cingolani LA, Goda Y (2008) Actin in action: the interplay between the actin cytoskeleton and synaptic efficacy. Nat Rev Neurosci 9:344-356.

Clark IE, Dodson MW, Jiang C, Cao JH, Huh JR, Seol JH, Yoo SJ, Hay BA, Guo M (2006) Drosophila pink1 is required for mitochondrial function and interacts genetically with parkin. Nature 441:1162-1166.

Coleman M (2005) Axon degeneration mechanisms: commonality amid diversity. Nat Rev Neurosci 6:889-898.

Coleman MP, Freeman MR (2010) Wallerian degeneration, wld(s), and nmnat. Annual review of neuroscience 33:245-267.

Coleman MP, Conforti L, Buckmaster EA, Tarlton A, Ewing RM, Brown MC, Lyon MF, Perry VH (1998) An 85-kb tandem triplication in the slow Wallerian degeneration (Wlds) mouse. Proc Natl Acad Sci U S A 95:9985-9990.

Collins CA, DiAntonio A (2007) Synaptic development: insights from Drosophila. Current opinion in neurobiology 17:35-42.

Conforti L, Gilley J, Coleman MP (2014) Wallerian degeneration: an emerging axon death pathway linking injury and disease. Nat Rev Neurosci 15:394-409.

Conforti L, Wilbrey A, Morreale G, Janeckova L, Beirowski B, Adalbert R, Mazzola F, Di Stefano M, Hartley R, Babetto E, Smith T, Gilley J, Billington RA, Genazzani AA, Ribchester RR, Magni G, Coleman M (2009) Wld S protein requires Nmnat activity and a short N-terminal sequence to protect axons in mice. J Cell Biol 184:491-500.

Corbo M, Hays AP (1992) Peripherin and neurofilament protein coexist in spinal spheroids of motor neuron disease. Journal of neuropathology and experimental neurology 51:531-537.

Couteaux R, Pecot-Dechavassine M (1970) [Synaptic vesicles and pouches at the level of "active zones" of the neuromuscular junction]. Comptes rendus hebdomadaires des seances de l'Academie des sciences Serie D: Sciences naturelles 271:2346-2349.

Coy DL, Hancock WO, Wagenbach M, Howard J (1999) Kinesin's tail domain is an inhibitory regulator of the motor domain. Nature cell biology 1:288-292.

Crimella C, Baschirotto C, Arnoldi A, Tonelli A, Tenderini E, Airoldi G, Martinuzzi A, Trabacca A, Losito L, Scarlato M, Benedetti S, Scarpini E, Spinicci G, Bresolin N, Bassi M (2011) Mutations in the motor and stalk domains of KIF5A in spastic paraplegia type 10 and in axonal Charcot-Marie-Tooth type 2. Clin Genet.

Crosby AH, Proukakis C (2002) Is the transportation highway the right road for hereditary spastic paraplegia? Am J Hum Genet 71:1009-1016.

Daigle JG, Lanson NA, Jr., Smith RB, Casci I, Maltare A, Monaghan J, Nichols CD, Kryndushkin D, Shewmaker F, Pandey UB (2013) RNA-binding ability of FUS regulates neurodegeneration, cytoplasmic mislocalization and incorporation into stress granules associated with FUS carrying ALS-linked mutations. Human molecular genetics 22:1193-1205.

David G, Barrett EF (2003) Mitochondrial Ca2+ uptake prevents desynchronization of quantal release and minimizes depletion during repetitive stimulation of mouse motor nerve terminals. The Journal of physiology 548:425-438.

Davis GW, Bezprozvanny I (2001) Maintaining the stability of neural function: a homeostatic hypothesis. Annual review of physiology 63:847-869.

De Vos KJ, Grierson AJ, Ackerley S, Miller CC (2008) Role of axonal transport in neurodegenerative diseases. Annual review of neuroscience 31:151-173.

De Vos KJ, Chapman AL, Tennant ME, Manser C, Tudor EL, Lau KF, Brownlees J, Ackerley S, Shaw PJ, McLoughlin DM, Shaw CE, Leigh PN, Miller CC, Grierson AJ (2007) Familial amyotrophic lateral sclerosis-linked SOD1 mutants perturb fast axonal transport to reduce axonal mitochondria content. Human molecular genetics 16:2720-2728.

Denker A, Rizzoli SO (2010) Synaptic vesicle pools: an update. Frontiers in synaptic neuroscience 2:135.

Detmer SA, Chan DC (2007) Functions and dysfunctions of mitochondrial dynamics. Nat Rev Mol Cell Biol 8:870-879.

DiAntonio A (2006) Glutamate receptors at the Drosophila neuromuscular junction. International review of neurobiology 75:165-179.

DiAntonio A, Petersen SA, Heckmann M, Goodman CS (1999) Glutamate receptor expression regulates quantal size and quantal content at the Drosophila neuromuscular junction. J Neurosci 19:3023-3032.

Diefenbach RJ, Diefenbach E, Douglas MW, Cunningham AL (2002) The heavy chain of conventional kinesin interacts with the SNARE proteins SNAP25 and SNAP23. Biochemistry 41:14906-14915.

Ding C, Maier E, Roscher AA, Braun A, Cantor CR (2004) Simultaneous quantitative and allele-specific expression analysis with real competitive PCR. BMC genetics 5:8.

Djagaeva I, Rose DJ, Lim A, Venter CE, Brendza KM, Moua P, Saxton WM (2012) Three Routes to Suppression of the Neurodegenerative Phenotypes Caused by Kinesin Heavy Chain Mutations. Genetics.

Dobbins GC, Zhang B, Xiong WC, Mei L (2006) The role of the cytoskeleton in neuromuscular junction formation. Journal of molecular neuroscience : MN 30:115-118.

Dompierre JP, Godin JD, Charrin BC, Cordelieres FP, King SJ, Humbert S, Saudou F (2007) Histone deacetylase 6 inhibition compensates for the transport deficit in Huntington's disease by increasing tubulin acetylation. J Neurosci 27:3571-3583.

Doussau F, Augustine GJ (2000) The actin cytoskeleton and neurotransmitter release: an overview. Biochimie 82:353-363.

Dresbach T, Qualmann B, Kessels MM, Garner CC, Gundelfinger ED (2001) The presynaptic cytomatrix of brain synapses. Cellular and molecular life sciences : CMLS 58:94-116.

Duffy JB (2002) GAL4 system in Drosophila: a fly geneticist's Swiss army knife. Genesis (New York, NY : 2000) 34:1-15.

Eaton BA, Davis GW (2005) LIM Kinase1 controls synaptic stability downstream of the type II BMP receptor. Neuron 47:695-708.

Eaton BA, Fetter RD, Davis GW (2002) Dynactin is necessary for synapse stabilization. Neuron 34:729-741.

Ebbing B, Mann K, Starosta A, Jaud J, Schols L, Schule R, Woehlke G (2008) Effect of spastic paraplegia mutations in KIF5A kinesin on transport activity. Human molecular genetics 17:1245-1252.

El-Husseini AE, Schnell E, Chetkovich DM, Nicoll RA, Bredt DS (2000) PSD-95 involvement in maturation of excitatory synapses. Science 290:1364-1368.

Fannon AM, Colman DR (1996) A model for central synaptic junctional complex formation based on the differential adhesive specificities of the cadherins. Neuron 17:423-434.

Feany MB, Bender WW (2000) A Drosophila model of Parkinson's disease. Nature 404:394-398.

Featherstone DE, Broadie K (2000) Surprises from Drosophila: genetic mechanisms of synaptic development and plasticity. Brain research bulletin 53:501-511.

Ferreira A, Niclas J, Vale RD, Banker G, Kosik KS (1992) Suppression of kinesin expression in cultured hippocampal neurons using antisense oligonucleotides. J Cell Biol 117:595-606.

Fichera M, Lo Giudice M, Falco M, Sturnio M, Amata S, Calabrese O, Bigoni S, Calzolari E, Neri M (2004) Evidence of kinesin heavy chain (KIF5A) involvement in pure hereditary spastic paraplegia. Neurology 63:1108-1110.

Fink JK (2003) Advances in the hereditary spastic paraplegias. Exp Neurol 184:106-110.

Fink JK (2013) Hereditary spastic paraplegia: clinico-pathologic features and emerging molecular mechanisms. Acta neuropathologica.

Finn JT, Weil M, Archer F, Siman R, Srinivasan A, Raff MC (2000) Evidence that Wallerian degeneration and localized axon degeneration induced by local neurotrophin deprivation do not involve caspases. J Neurosci 20:1333-1341.

Finsterer J, Loscher W, Quasthoff S, Wanschitz J, Auer-Grumbach M, Stevanin G (2012) Hereditary spastic paraplegias with autosomal dominant, recessive, X-linked, or maternal trait of inheritance. Journal of the neurological sciences 318:1-18.

Fischer LR, Culver DG, Tennant P, Davis AA, Wang M, Castellano-Sanchez A, Khan J, Polak MA, Glass JD (2004) Amyotrophic lateral sclerosis is a distal axonopathy: evidence in mice and man. Exp Neurol 185:232-240.

Fletcher DA, Mullins RD (2010) Cell mechanics and the cytoskeleton. Nature 463:485-492.

Frank CA (2014) How voltage-gated calcium channels gate forms of homeostatic synaptic plasticity. Front Cell Neurosci 8:40.

Frank CA, Wang X, Collins CA, Rodal AA, Yuan Q, Verstreken P, Dickman DK (2013) New approaches for studying synaptic development, function, and plasticity using Drosophila as a model system. J Neurosci 33:17560-17568.

Frey D, Schneider C, Xu L, Borg J, Spooren W, Caroni P (2000) Early and selective loss of neuromuscular synapse subtypes with low sprouting competence in motoneuron diseases. J Neurosci 20:2534-2542.

Friedman DS, Vale RD (1999) Single-molecule analysis of kinesin motility reveals regulation by the cargo-binding tail domain. Nat Cell Biol 1:293-297.

Fuentes-Medel Y, Ashley J, Barria R, Maloney R, Freeman M, Budnik V (2012) Integration of a retrograde signal during synapse formation by glia-secreted TGF-beta ligand. Current biology : CB 22:1831-1838.

Füger P, Behrends LB, Mertel S, Sigrist SJ, Rasse TM (2007) Live imaging of synapse development and measuring protein dynamics using two-color fluorescence recovery after photo-bleaching at Drosophila synapses. Nat Protocols 2:3285-3298.

Füger P, Sreekumar V, Schüle R, Kern JV, Stanchev DT, Schneider CD, Karle KN, Daub KJ, Siegert VK, Flotenmeyer M, Schwarz H, Schöls L, Rasse TM (2012) Spastic paraplegia mutation N256S in the neuronal microtubule motor KIF5A disrupts axonal transport in a Drosophila HSP model. PLoS genetics 8:e1003066.

Furuta K, Furuta A, Toyoshima YY, Amino M, Oiwa K, Kojima H (2013) Measuring collective transport by defined numbers of processive and nonprocessive kinesin motors. Proc Natl Acad Sci U S A 110:501-506.

Gagliano J, Walb M, Blaker B, Macosko JC, Holzwarth G (2010) Kinesin velocity increases with the number of motors pulling against viscoelastic drag. Eur Biophys J 39:801-813.

Ganitkevich VY (2003) The role of mitochondria in cytoplasmic Ca2+ cycling. Experimental physiology 88:91-97.

Gellerich FN, Gizatullina Z, Arandarcikaite O, Jerzembek D, Vielhaber S, Seppet E, Striggow F (2009) Extramitochondrial Ca2+ in the nanomolar range regulates glutamate-dependent oxidative phosphorylation on demand. PloS one 4:e8181.

Gellerich FN, Gizatullina Z, Trumbeckaite S, Nguyen HP, Pallas T, Arandarcikaite O, Vielhaber S, Seppet E, Striggow F (2010) The regulation of OXPHOS by extramitochondrial calcium. Biochimica et biophysica acta 1797:1018-1027.

Gennerich A, Vale RD (2009) Walking the walk: how kinesin and dynein coordinate their steps. Curr Opin Cell Biol 21:59-67.

George EB, Glass JD, Griffin JW (1995) Axotomy-induced axonal degeneration is mediated by calcium influx through ion-specific channels. J Neurosci 15:6445-6452.

Geva-Dayan K, Domenievitz D, Zahalka R, Fattal-Valevski A (2010) Botulinum toxin injections for pediatric patients with hereditary spastic paraparesis. J Child Neurol 25:969-975.

Gigant B, Wang W, Dreier B, Jiang Q, Pecqueur L, Pluckthun A, Wang C, Knossow M (2013) Structure of a kinesin-tubulin complex and implications for kinesin motility. Nat Struct Mol Biol 20:1001-1007.

Gill SR, Schroer TA, Szilak I, Steuer ER, Sheetz MP, Cleveland DW (1991) Dynactin, a conserved, ubiquitously expressed component of an activator of vesicle motility mediated by cytoplasmic dynein. J Cell Biol 115:1639-1650.

Gindhart JG, Jr., Desai CJ, Beushausen S, Zinn K, Goldstein LS (1998) Kinesin light chains are essential for axonal transport in Drosophila. J Cell Biol 141:443-454.

Glater EE, Megeath LJ, Stowers RS, Schwarz TL (2006) Axonal transport of mitochondria requires milton to recruit kinesin heavy chain and is light chain independent. J Cell Biol 173:545-557.

Goizet C, Boukhris A, Mundwiller E, Tallaksen C, Forlani S, Toutain A, Carriere N, Paquis V, Depienne C, Durr A, Stevanin G, Brice A (2009) Complicated forms of autosomal dominant hereditary spastic paraplegia are frequent in SPG10. Hum Mutat 30:E376-385.

Goldstein LS (2001) Kinesin molecular motors: transport pathways, receptors, and human disease. Proceedings of the National Academy of Sciences of the United States of America 98:6999-7003.

Graf ER, Heerssen HM, Wright CM, Davis GW, DiAntonio A (2011) Stathmin is required for stability of the Drosophila neuromuscular junction. J Neurosci 31:15026-15034.

Green DR, Van Houten B (2011) SnapShot: Mitochondrial quality control. Cell 147:950, 950 e951.

Gunawardena S, Goldstein LS (2001) Disruption of axonal transport and neuronal viability by amyloid precursor protein mutations in Drosophila. Neuron 32:389-401.

Guo HF, Zhong Y (2006) Requirement of Akt to mediate long-term synaptic depression in Drosophila. J Neurosci 26:4004-4014.

Guo X, Macleod GT, Wellington A, Hu F, Panchumarthi S, Schoenfield M, Marin L, Charlton MP, Atwood HL, Zinsmaier KE (2005) The GTPase dMiro is required for axonal transport of mitochondria to Drosophila synapses. Neuron 47:379-393.

Gustafson K, Boulianne GL (1996) Distinct expression patterns detected within individual tissues by the GAL4 enhancer trap technique. Genome / National Research Council Canada = Genome / Conseil national de recherches Canada 39:174-182.

Gutierrez-Medina B, Fehr AN, Block SM (2009) Direct measurements of kinesin torsional properties reveal flexible domains and occasional stalk reversals during stepping. Proc Natl Acad Sci U S A 106:17007-17012.

Guydosh NR, Block SM (2006) Backsteps induced by nucleotide analogs suggest the front head of kinesin is gated by strain. Proc Natl Acad Sci U S A 103:8054-8059.

Gyoeva FK, Sarkisov DV, Khodjakov AL, Minin AA (2004) The tetrameric molecule of conventional kinesin contains identical light chains. Biochemistry 43:13525-13531.

Hackney DD (1988) Kinesin ATPase: rate-limiting ADP release. Proc Natl Acad Sci U S A 85:6314-6318.

Hackney DD (1994) Evidence for alternating head catalysis by kinesin during microtubule-stimulated ATP hydrolysis. Proc Natl Acad Sci U S A 91:6865-6869.

Hackney DD, Stock MF (2000) Kinesin's IAK tail domain inhibits initial microtubule-stimulated ADP release. Nature cell biology 2:257-260.

Hackney DD, Stock MF (2008) Kinesin tail domains and Mg2+ directly inhibit release of ADP from head domains in the absence of microtubules. Biochemistry 47:7770-7778.

Hall CN, Klein-Flugge MC, Howarth C, Attwell D (2012) Oxidative phosphorylation, not glycolysis, powers presynaptic and postsynaptic mechanisms underlying brain information processing. J Neurosci 32:8940-8951.

Hammond JW, Huang CF, Kaech S, Jacobson C, Banker G, Verhey KJ (2010) Posttranslational modifications of tubulin and the polarized transport of kinesin-1 in neurons. Molecular biology of the cell 21:572-583.

Hanein S, Martin E, Boukhris A, Byrne P, Goizet C, Hamri A, Benomar A, Lossos A, Denora P, Fernandez J, Elleuch N, Forlani S, Durr A, Feki I, Hutchinson M, Santorelli FM, Mhiri C, Brice A, Stevanin G (2008) Identification of the SPG15 gene, encoding spastizin, as a frequent cause of complicated autosomal-recessive spastic paraplegia, including Kjellin syndrome. American journal of human genetics 82:992-1002.

Hansen JJ, Durr A, Cournu-Rebeix I, Georgopoulos C, Ang D, Nielsen MN, Davoine CS, Brice A, Fontaine B, Gregersen N, Bross P (2002) Hereditary spastic paraplegia SPG13 is associated with a mutation in the gene encoding the mitochondrial chaperonin Hsp60. American journal of human genetics 70:1328-1332.

Harding AE (1981) Hereditary "pure" spastic paraplegia: a clinical and genetic study of 22 families. Journal of neurology, neurosurgery, and psychiatry 44:871-883.

Harding AE (1983) Classification of the hereditary ataxias and paraplegias. Lancet 1:1151-1155.

Harding AE (1993) Hereditary spastic paraplegias. Seminars in neurology 13:333-336.

Harris JJ, Jolivet R, Attwell D (2012) Synaptic energy use and supply. Neuron 75:762-777.

Hazan J, Fonknechten N, Mavel D, Paternotte C, Samson D, Artiguenave F, Davoine CS, Cruaud C, Durr A, Wincker P, Brottier P, Cattolico L, Barbe V, Burgunder JM, Prud'homme JF, Brice A, Fontaine B, Heilig B, Weissenbach J (1999) Spastin, a new AAA protein, is altered in the most frequent form of autosomal dominant spastic paraplegia. Nature genetics 23:296-303.

Heckscher ES, Lockery SR, Doe CQ (2012) Characterization of Drosophila larval crawling at the level of organism, segment, and somatic body wall musculature. J Neurosci 32:12460-12471.

Hirokawa N, Noda Y (2008) Intracellular transport and kinesin superfamily proteins, KIFs: structure, function, and dynamics. Physiol Rev 88:1089-1118.

Hirokawa N, Niwa S, Tanaka Y (2010) Molecular motors in neurons: transport mechanisms and roles in brain function, development, and disease. Neuron 68:610-638.

Hirokawa N, Pfister KK, Yorifuji H, Wagner MC, Brady ST, Bloom GS (1989) Submolecular domains of bovine brain kinesin identified by electron microscopy and monoclonal antibody decoration. Cell 56:867-878.

Hirose K, Lockhart A, Cross RA, Amos LA (1995) Nucleotide-dependent angular change in kinesin motor domain bound to tubulin. Nature 376:277-279.

Hollenbeck PJ, Saxton WM (2005) The axonal transport of mitochondria. Journal of cell science 118:5411-5419.

Horiuchi D, Barkus RV, Pilling AD, Gassman A, Saxton WM (2005) APLIP1, a kinesin binding JIP-1/JNK scaffold protein, influences the axonal transport of both vesicles and mitochondria in Drosophila. Current biology : CB 15:2137-2141.

Hoyt MA, He L, Totis L, Saunders WS (1993) Loss of function of Saccharomyces cerevisiae kinesin-related CIN8 and KIP1 is suppressed by KAR3 motor domain mutations. Genetics 135:35-44.

Hua W, Young EC, Fleming ML, Gelles J (1997) Coupling of kinesin steps to ATP hydrolysis. Nature 388:390-393.

Hummel T, Krukkert K, Roos J, Davis G, Klambt C (2000) Drosophila Futsch/22C10 is a MAP1B-like protein required for dendritic and axonal development. Neuron 26:357-370.

Hunt AJ, Howard J (1993) Kinesin swivels to permit microtubule movement in any direction. Proc Natl Acad Sci U S A 90:11653-11657.

Hurd DD, Saxton WM (1996) Kinesin Mutations Cause Motor Neuron Disease Phenotypes by Disrupting Fast Axonal Transport in Drosophila. Genetics 144:1075-1085.

Ibanez CF (2007) Message in a bottle: long-range retrograde signaling in the nervous system. Trends in cell biology 17:519-528.

Ikenaka K, Katsuno M, Kawai K, Ishigaki S, Tanaka F, Sobue G (2012) Disruption of axonal transport in motor neuron diseases. International journal of molecular sciences 13:1225-1238.

Johansen J, Halpern ME, Johansen KM, Keshishian H (1989) Stereotypic morphology of glutamatergic synapses on identified muscle cells of Drosophila larvae. J Neurosci 9:710-725.

Jolly AL, Kim H, Srinivasan D, Lakonishok M, Larson AG, Gelfand VI (2010) Kinesin-1 heavy chain mediates microtubule sliding to drive changes in cell shape. Proceedings of the National Academy of Sciences of the United States of America 107:12151-12156.

Joshi DC, Bakowska JC (2011) SPG20 protein spartin associates with cardiolipin via its plant-related senescence domain and regulates mitochondrial Ca2+ homeostasis. PloS one 6:e19290.

Kaan HY, Hackney DD, Kozielski F (2011) The structure of the kinesin-1 motor-tail complex reveals the mechanism of autoinhibition. Science 333:883-885.

Kanai Y, Dohmae N, Hirokawa N (2004) Kinesin transports RNA: isolation and characterization of an RNA-transporting granule. Neuron 43:513-525.

Kanai Y, Okada Y, Tanaka Y, Harada A, Terada S, Hirokawa N (2000) KIF5C, a novel neuronal kinesin enriched in motor neurons. J Neurosci 20:6374-6384.

Karle KN, Mockel D, Reid E, Schols L (2012) Axonal transport deficit in a KIF5A(-/-) mouse model. Neurogenetics 13:169-179.

Kasher PR, De Vos KJ, Wharton SB, Manser C, Bennett EJ, Bingley M, Wood JD, Milner R, McDermott CJ, Miller CC, Shaw PJ, Grierson AJ (2009) Direct evidence for axonal transport defects in a novel mouse model of mutant spastin-induced hereditary spastic paraplegia (HSP) and human HSP patients. Journal of neurochemistry 110:34-44.

Katz B, Miledi R (1970) Further study of the role of calcium in synaptic transmission. J Physiol 207:789-801.

Kawaguchi K (2008) Energetics of kinesin-1 stepping mechanism. FEBS Lett 582:3719-3722.

Kawaguchi K (2013) Role of kinesin-1 in the pathogenesis of SPG10, a rare form of hereditary spastic paraplegia. The Neuroscientist : a review journal bringing neurobiology, neurology and psychiatry 19:336-344.

Kawasaki F, Zou B, Xu X, Ordway RW (2004) Active zone localization of presynaptic calcium channels encoded by the cacophony locus of Drosophila. J Neurosci 24:282-285.

Kelkar N, Gupta S, Dickens M, Davis RJ (2000) Interaction of a mitogen-activated protein kinase signaling module with the neuronal protein JIP3. Molecular and cellular biology 20:1030-1043.

Kern JV, Zhang YV, Kramer S, Brenman JE, Rasse TM (2013) The Kinesin-3, unc-104 regulates dendrite morphogenesis and synaptic development in Drosophila. Genetics 195:59-72.

Keshishian H, Broadie K, Chiba A, Bate M (1996) The drosophila neuromuscular junction: a model system for studying synaptic development and function. Annual review of neuroscience 19:545-575.

Kim CH, Lisman JE (2001) A labile component of AMPA receptor-mediated synaptic transmission is dependent on microtubule motors, actin, and N-ethylmaleimide-sensitive factor. J Neurosci 21:4188-4194.

Kirchner J, Seiler S, Fuchs S, Schliwa M (1999) Functional anatomy of the kinesin molecule in vivo. EMBO J 18:4404-4413.

Kittel RJ, Wichmann C, Rasse TM, Fouquet W, Schmidt M, Schmid A, Wagh DA, Pawlu C, Kellner RR, Willig KI, Hell SW, Buchner E, Heckmann M, Sigrist SJ (2006) Bruchpilot promotes active zone assembly, Ca2+ channel clustering, and vesicle release. Science 312:1051-1054.

Klebe S, Azzedine H, Durr A, Bastien P, Bouslam N, Elleuch N, Forlani S, Charon C, Koenig M, Melki J, Brice A, Stevanin G (2006) Autosomal recessive spastic paraplegia (SPG30) with mild ataxia

and sensory neuropathy maps to chromosome 2q37.3. Brain : a journal of neurology 129:1456-1462.

Kleele T, Marinkovic P, Williams PR, Stern S, Weigand EE, Engerer P, Naumann R, Hartmann J, Karl RM, Bradke F, Bishop D, Herms J, Konnerth A, Kerschensteiner M, Godinho L, Misgeld T (2014) An assay to image neuronal microtubule dynamics in mice. Nature communications 5:4827.

Konishi Y, Setou M (2009) Tubulin tyrosination navigates the kinesin-1 motor domain to axons. Nat Neurosci 12:559-567.

Kull FJ, Endow SA (2013) Force generation by kinesin and myosin cytoskeletal motor proteins. J Cell Sci 126:9-19.

Kull FJ, Sablin EP, Lau R, Fletterick RJ, Vale RD (1996) Crystal structure of the kinesin motor domain reveals a structural similarity to myosin. Nature 380:550-555.

Kwan AC, Dombeck DA, Webb WW (2008) Polarized microtubule arrays in apical dendrites and axons. Proceedings of the National Academy of Sciences of the United States of America 105:11370-11375.

Lahey T, Gorczyca M, Jia XX, Budnik V (1994) The Drosophila tumor suppressor gene dlg is required for normal synaptic bouton structure. Neuron 13:823-835.

Landgraf M, Bossing T, Technau GM, Bate M (1997) The origin, location, and projections of the embryonic abdominal motorneurons of Drosophila. J Neurosci 17:9642-9655.

Lin AL, Fox PT, Hardies J, Duong TQ, Gao JH (2010) Nonlinear coupling between cerebral blood flow, oxygen consumption, and ATP production in human visual cortex. Proceedings of the National Academy of Sciences of the United States of America 107:8446-8451.

Ling SC, Fahrner PS, Greenough WT, Gelfand VI (2004) Transport of Drosophila fragile X mental retardation protein-containing ribonucleoprotein granules by kinesin-1 and cytoplasmic dynein. Proceedings of the National Academy of Sciences of the United States of America 101:17428-17433.

Littleton JT (2000) A genomic analysis of membrane trafficking and neurotransmitter release in Drosophila. J Cell Biol 150:F77-82.

Littleton JT, Ganetzky B (2000) Ion channels and synaptic organization: analysis of the Drosophila genome. Neuron 26:35-43.

Liu KS, Siebert M, Mertel S, Knoche E, Wegener S, Wichmann C, Matkovic T, Muhammad K, Depner H, Mettke C, Buckers J, Hell SW, Muller M, Davis GW, Schmitz D, Sigrist SJ (2011) RIM-binding protein, a central part of the active zone, is essential for neurotransmitter release. Science 334:1565-1569.

Liu YT, Laura M, Hersheson J, Horga A, Jaunmuktane Z, Brandner S, Pittman A, Hughes D, Polke JM, Sweeney MG, Proukakis C, Janssen JC, Auer-Grumbach M, Zuchner S, Shields KG, Reilly MM, Houlden H (2014) Extended phenotypic spectrum of KIF5A mutations: From spastic paraplegia to axonal neuropathy. Neurology 83:612-619.

Liu Z, Chen Y, Wang D, Wang S, Zhang YQ (2010) Distinct presynaptic and postsynaptic dismantling processes of Drosophila neuromuscular junctions during metamorphosis. J Neurosci 30:11624-11634.

Lloyd TE, Verstreken P, Ostrin EJ, Phillippi A, Lichtarge O, Bellen HJ (2000) A genome-wide search for synaptic vesicle cycle proteins in Drosophila. Neuron 26:45-50.

Lloyd TE, Machamer J, O'Hara K, Kim JH, Collins SE, Wong MY, Sahin B, Imlach W, Yang Y, Levitan ES, McCabe BD, Kolodkin AL (2012) The p150(Glued) CAP-Gly domain regulates initiation of retrograde transport at synaptic termini. Neuron 74:344-360.

Lo Giudice M, Neri M, Falco M, Sturnio M, Calzolari E, Di Benedetto D, Fichera M (2006) A missense mutation in the coiled-coil domain of the KIF5A gene and late-onset hereditary spastic paraplegia. Archives of neurology 63:284-287.

Lo Giudice T, Lombardi F, Santorelli FM, Kawarai T, Orlacchio A (2014) Hereditary spastic paraplegia: clinical-genetic characteristics and evolving molecular mechanisms. Exp Neurol 261:518-539.

Lovas JR, Wang X (2013) The meaning of mitochondrial movement to a neuron's life. Biochimica et biophysica acta 1833:184-194.

Ma YZ, Taylor EW (1997) Kinetic mechanism of a monomeric kinesin construct. The Journal of biological chemistry 272:717-723.

Macaskill AF, Rinholm JE, Twelvetrees AE, Arancibia-Carcamo IL, Muir J, Fransson A, Aspenstrom P, Attwell D, Kittler JT (2009) Miro1 is a calcium sensor for glutamate receptor-dependent localization of mitochondria at synapses. Neuron 61:541-555.

Mackler JM, Drummond JA, Loewen CA, Robinson IM, Reist NE (2002) The C(2)B Ca(2+)-binding motif of synaptotagmin is required for synaptic transmission in vivo. Nature 418:340-344.

Maday S, Twelvetrees AE, Moughamian AJ, Holzbaur EL (2014) Axonal transport: cargo-specific mechanisms of motility and regulation. Neuron 84:292-309.

Magrane J, Sahawneh MA, Przedborski S, Estevez AG, Manfredi G (2012) Mitochondrial dynamics and bioenergetic dysfunction is associated with synaptic alterations in mutant SOD1 motor neurons. J Neurosci 32:229-242.

Mahr A, Aberle H (2006) The expression pattern of the Drosophila vesicular glutamate transporter: a marker protein for motoneurons and glutamatergic centers in the brain. Gene Expr Patterns 6:299-309.

Mandelkow EM, Thies E, Trinczek B, Biernat J, Mandelkow E (2004) MARK/PAR1 kinase is a regulator of microtubule-dependent transport in axons. J Cell Biol 167:99-110.

Marques G, Zhang B (2006) Retrograde signaling that regulates synaptic development and function at the Drosophila neuromuscular junction. International review of neurobiology 75:267-285.

Martin E, Yanicostas C, Rastetter A, Naini SM, Maouedj A, Kabashi E, Rivaud-Pechoux S, Brice A, Stevanin G, Soussi-Yanicostas N (2012) Spatacsin and spastizin act in the same pathway required for proper spinal motor neuron axon outgrowth in zebrafish. Neurobiology of disease 48:299-308.

Martin M, Iyadurai SJ, Gassman A, Gindhart JG, Jr., Hays TS, Saxton WM (1999) Cytoplasmic dynein, the dynactin complex, and kinesin are interdependent and essential for fast axonal transport. Molecular biology of the cell 10:3717-3728.

Marx A, Muller J, Mandelkow EM, Hoenger A, Mandelkow E (2006) Interaction of kinesin motors, microtubules, and MAPs. J Muscle Res Cell Motil 27:125-137.

Massaro CM, Pielage J, Davis GW (2009) Molecular mechanisms that enhance synapse stability despite persistent disruption of the spectrin/ankyrin/microtubule cytoskeleton. J Cell Biol 187:101-117.

Matkovic T, Siebert M, Knoche E, Depner H, Mertel S, Owald D, Schmidt M, Thomas U, Sickmann A, Kamin D, Hell SW, Burger J, Hollmann C, Mielke T, Wichmann C, Sigrist SJ (2013) The Bruchpilot cytomatrix determines the size of the readily releasable pool of synaptic vesicles. J Cell Biol 202:667-683.

Menon KP, Carrillo RA, Zinn K (2013) Development and plasticity of the Drosophila larval neuromuscular junction. Wiley interdisciplinary reviews Developmental biology 2:647-670.

Miki H, Okada Y, Hirokawa N (2005) Analysis of the kinesin superfamily: insights into structure and function. Trends Cell Biol 15:467-476.

Miki H, Setou M, Kaneshiro K, Hirokawa N (2001) All kinesin superfamily protein, KIF, genes in mouse and human. Proceedings of the National Academy of Sciences of the United States of America 98:7004-7011.

Miller KE, Sheetz MP (2004) Axonal mitochondrial transport and potential are correlated. Journal of cell science 117:2791-2804.

Mink JW, Blumenschine RJ, Adams DB (1981) Ratio of central nervous system to body metabolism in vertebrates: its constancy and functional basis. The American journal of physiology 241:R203-212.

Mironov SL (2007) ADP regulates movements of mitochondria in neurons. Biophysical journal 92:2944-2952.

Mishra B, Carson R, Hume RI, Collins CA (2013) Sodium and potassium currents influence Wallerian degeneration of injured Drosophila axons. J Neurosci 33:18728-18739.

Misko A, Jiang S, Wegorzewska I, Milbrandt J, Baloh RH (2010) Mitofusin 2 is necessary for transport of axonal mitochondria and interacts with the Miro/Milton complex. J Neurosci 30:4232-4240.

Morfini G, Pigino G, Opalach K, Serulle Y, Moreira JE, Sugimori M, Llinas RR, Brady ST (2007) 1-Methyl-4-phenylpyridinium affects fast axonal transport by activation of caspase and protein kinase C. Proceedings of the National Academy of Sciences of the United States of America 104:2442-2447.

Mori T, Vale RD, Tomishige M (2007) How kinesin waits between steps. Nature 450:750-754.

Mosca TJ, Carrillo RA, White BH, Keshishian H (2005) Dissection of synaptic excitability phenotypes by using a dominant-negative Shaker K+ channel subunit. Proceedings of the National Academy of Sciences of the United States of America 102:3477-3482.

Motta F, Antonello CE (2014) Analysis of complications in 430 consecutive pediatric patients treated with intrathecal baclofen therapy: 14-year experience. J Neurosurg Pediatr 13:301-306.

Moughamian AJ, Holzbaur EL (2012) Dynactin is required for transport initiation from the distal axon. Neuron 74:331-343.

Musumeci O, Bassi MT, Mazzeo A, Grandis M, Crimella C, Martinuzzi A, Toscano A (2011) A novel mutation in KIF5A gene causing hereditary spastic paraplegia with axonal neuropathy. Neurol Sci 32:665-668.

Nakajima K, Yin X, Takei Y, Seog DH, Homma N, Hirokawa N (2012) Molecular motor KIF5A is essential for GABA(A) receptor transport, and KIF5A deletion causes epilepsy. Neuron 76:945-961.

Nakata T, Hirokawa N (1995) Point mutation of adenosine triphosphate-binding motif generated rigor kinesin that selectively blocks anterograde lysosome membrane transport. J Cell Biol 131:1039-1053.

Nangaku M, Sato-Yoshitake R, Okada Y, Noda Y, Takemura R, Yamazaki H, Hirokawa N (1994) KIF1B, a novel microtubule plus end-directed monomeric motor protein for transport of mitochondria. Cell 79:1209-1220.

Nicholls DG, Budd SL (2000) Mitochondria and neuronal survival. Physiological reviews 80:315-360.

Novarino G et al. (2014) Exome sequencing links corticospinal motor neuron disease to common neurodegenerative disorders. Science 343:506-511.

Ohashi S, Koike K, Omori A, Ichinose S, Ohara S, Kobayashi S, Sato TA, Anzai K (2002) Identification of mRNA/protein (mRNP) complexes containing Puralpha, mStaufen, fragile X protein, and

myosin Va and their association with rough endoplasmic reticulum equipped with a kinesin motor. J Biol Chem 277:37804-37810.

Ohtsuka T, Takao-Rikitsu E, Inoue E, Inoue M, Takeuchi M, Matsubara K, Deguchi-Tawarada M, Satoh K, Morimoto K, Nakanishi H, Takai Y (2002) Cast: a novel protein of the cytomatrix at the active zone of synapses that forms a ternary complex with RIM1 and munc13-1. J Cell Biol 158:577-590.

Okada Y, Yamazaki H, Sekine-Aizawa Y, Hirokawa N (1995) The neuron-specific kinesin superfamily protein KIF1A is a unique monomeric motor for anterograde axonal transport of synaptic vesicle precursors. Cell 81:769-780.

Olichon A, Guillou E, Delettre C, Landes T, Arnaune-Pelloquin L, Emorine LJ, Mils V, Daloyau M, Hamel C, Amati-Bonneau P, Bonneau D, Reynier P, Lenaers G, Belenguer P (2006) Mitochondrial dynamics and disease, OPA1. Biochim Biophys Acta 1763:500-509.

Osterloh JM et al. (2012) dSarm/Sarm1 is required for activation of an injury-induced axon death pathway. Science 337:481-484.

Pack-Chung E, Kurshan PT, Dickman DK, Schwarz TL (2007) A Drosophila kinesin required for synaptic bouton formation and synaptic vesicle transport. Nat Neurosci 10:980-989.

Packard M, Koo ES, Gorczyca M, Sharpe J, Cumberledge S, Budnik V (2002) The Drosophila Wnt, wingless, provides an essential signal for pre- and postsynaptic differentiation. Cell 111:319-330.

Palacios IM, St Johnston D (2002) Kinesin light chain-independent function of the Kinesin heavy chain in cytoplasmic streaming and posterior localisation in the Drosophila oocyte. Development (Cambridge, England) 129:5473-5485.

Parent CA (2004) Making all the right moves: chemotaxis in neutrophils and Dictyostelium. Current opinion in cell biology 16:4-13.

Park J, Lee SB, Lee S, Kim Y, Song S, Kim S, Bae E, Kim J, Shong M, Kim JM, Chung J (2006) Mitochondrial dysfunction in Drosophila PINK1 mutants is complemented by parkin. Nature 441:1157-1161.

Paschal BM, Vallee RB (1987) Retrograde transport by the microtubule-associated protein MAP 1C. Nature 330:181-183.

Paschinger K, Rendic D, Wilson IB (2009) Revealing the anti-HRP epitope in Drosophila and Caenorhabditis. Glycoconjugate journal 26:385-395.

Patel H, Cross H, Proukakis C, Hershberger R, Bork P, Ciccarelli FD, Patton MA, McKusick VA, Crosby AH (2002) SPG20 is mutated in Troyer syndrome, an hereditary spastic paraplegia. Nature genetics 31:347-348.

Paul MM, Pauli M, Ehmann N, Hallermann S, Sauer M, Kittel RJ, Heckmann M (2015) Bruchpilot and Synaptotagmin collaborate to drive rapid glutamate release and active zone differentiation. Front Cell Neurosci 9:29.

Perlson E, Hanz S, Ben-Yaakov K, Segal-Ruder Y, Seger R, Fainzilber M (2005) Vimentin-dependent spatial translocation of an activated MAP kinase in injured nerve. Neuron 45:715-726.

Petersen SA, Fetter RD, Noordermeer JN, Goodman CS, DiAntonio A (1997) Genetic analysis of glutamate receptors in Drosophila reveals a retrograde signal regulating presynaptic transmitter release. Neuron 19:1237-1248.

Phelps CB, Brand AH (1998) Ectopic gene expression in Drosophila using GAL4 system. Methods (San Diego, Calif) 14:367-379.

Pielage J, Fetter RD, Davis GW (2005) Presynaptic spectrin is essential for synapse stabilization. Current biology : CB 15:918-928.

Pielage J, Fetter RD, Davis GW (2006) A postsynaptic spectrin scaffold defines active zone size, spacing, and efficacy at the Drosophila neuromuscular junction. J Cell Biol 175:491-503.

Pielage J, Cheng L, Fetter RD, Carlton PM, Sedat JW, Davis GW (2008) A presynaptic giant ankyrin stabilizes the NMJ through regulation of presynaptic microtubules and transsynaptic cell adhesion. Neuron 58:195-209.

Pilling AD, Horiuchi D, Lively CM, Saxton WM (2006) Kinesin-1 and Dynein are the primary motors for fast transport of mitochondria in Drosophila motor axons. Molecular biology of the cell 17:2057-2068.

Pollard TD, Earnshaw WC, Lippincott-Schwartz J (2007) Cell Biology. Spektrum Akademischer Verlag 2nd Edition:920.

Prüßing K, Voigt A, Schulz JB (2013) Drosophila melanogaster as a model organism for Alzheimer's disease. Mol Neurodegener 8:35.

Qin G, Schwarz T, Kittel RJ, Schmid A, Rasse TM, Kappei D, Ponimaskin E, Heckmann M, Sigrist SJ (2005) Four different subunits are essential for expressing the synaptic glutamate receptor at neuromuscular junctions of Drosophila. J Neurosci 25:3209-3218.

Rainier S, Chai JH, Tokarz D, Nicholls RD, Fink JK (2003) NIPA1 gene mutations cause autosomal dominant hereditary spastic paraplegia (SPG6). American journal of human genetics 73:967-971.

Rasse TM, Fouquet W, Schmid A, Kittel RJ, Mertel S, Sigrist CB, Schmidt M, Guzman A, Merino C, Qin G, Quentin C, Madeo FF, Heckmann M, Sigrist SJ (2005) Glutamate receptor dynamics organizing synapse formation in vivo. Nat Neurosci 8:898-905.

Reed NA, Cai D, Blasius TL, Jih GT, Meyhofer E, Gaertig J, Verhey KJ (2006) Microtubule acetylation promotes kinesin-1 binding and transport. Current biology : CB 16:2166-2172.

Reid E, Dearlove AM, Rhodes M, Rubinsztein DC (1999) A new locus for autosomal dominant "pure" hereditary spastic paraplegia mapping to chromosome 12q13, and evidence for further genetic heterogeneity. Am J Hum Genet 65:757-763.

Reid E, Kloos M, Ashley-Koch A, Hughes L, Bevan S, Svenson I, Graham F, Gaskell P, Dearlove A, Pericak-Vance M, Rubinsztein D, Marchuk D (2002) A Kinesin Heavy Chain (KIF5A) Mutation in Hereditary Spastic Paraplegia (SPG10). The American Journal of Human Genetics 71:1189-1194.

Rice S, Lin AW, Safer D, Hart CL, Naber N, Carragher BO, Cain SM, Pechatnikova E, Wilson-Kubalek EM, Whittaker M, Pate E, Cooke R, Taylor EW, Milligan RA, Vale RD (1999) A structural change in the kinesin motor protein that drives motility. Nature 402:778-784.

Riedl J, Crevenna AH, Kessenbrock K, Yu JH, Neukirchen D, Bista M, Bradke F, Jenne D, Holak TA, Werb Z, Sixt M, Wedlich-Soldner R (2008) Lifeact: a versatile marker to visualize F-actin. Nature methods 5:605-607.

Rizzoli SO, Betz WJ (2005) Synaptic vesicle pools. Nat Rev Neurosci 6:57-69.

Roos J, Hummel T, Ng N, Klambt C, Davis GW (2000) Drosophila Futsch regulates synaptic microtubule organization and is necessary for synaptic growth. Neuron 26:371-382.

Ruiz-Canada C, Ashley J, Moeckel-Cole S, Drier E, Yin J, Budnik V (2004) New synaptic bouton formation is disrupted by misregulation of microtubule stability in aPKC mutants. Neuron 42:567-580.

Sablin EP, Kull FJ, Cooke R, Vale RD, Fletterick RJ (1996) Crystal structure of the motor domain of the kinesin-related motor ncd. Nature 380:555-559.

Salinas S, Proukakis C, Crosby A, Warner TT (2008) Hereditary spastic paraplegia: clinical features and pathogenetic mechanisms. The Lancet Neurology 7:1127-1138.

Sambrook J, Fritsch E, Maniatis T (1989) Molecular Cloning: A Laboratory Manual, 2nd Edition. Cold Spring Harbour Press, New York, USA.

Sanyal S (2009) Genomic mapping and expression patterns of C380, OK6 and D42 enhancer trap lines in the larval nervous system of Drosophila. Gene Expr Patterns 9:371-380.

Sasaki S, Maruyama S, Yamane K, Sakuma H, Takeishi M (1990) Ultrastructure of swollen proximal axons of anterior horn neurons in motor neuron disease. Journal of the neurological sciences 97:233-240.

Saxton WM, Hollenbeck PJ (2012) The axonal transport of mitochondria. Journal of cell science 125:2095-2104.

Saxton WM, Hicks J, Goldstein LS, Raff EC (1991) Kinesin heavy chain is essential for viability and neuromuscular functions in Drosophila, but mutants show no defects in mitosis. Cell 64:1093-1102.

Schmid A, Hallermann S, Kittel RJ, Khorramshahi O, Frolich AM, Quentin C, Rasse TM, Mertel S, Heckmann M, Sigrist SJ (2008) Activity-dependent site-specific changes of glutamate receptor composition in vivo. Nat Neurosci 11:659-666.

Schnitzer MJ, Block SM (1997) Kinesin hydrolyses one ATP per 8-nm step. Nature 388:386-390.

Scholey JM, Heuser J, Yang JT, Goldstein LS (1989) Identification of globular mechanochemical heads of kinesin. Nature 338:355-357.

Schon EA, Przedborski S (2011) Mitochondria: the next (neurode)generation. Neuron 70:1033-1053.

Schüle R, Kremer BP, Kassubek J, Auer-Grumbach M, Kostic V, Klopstock T, Klimpe S, Otto S, Boesch S, van de Warrenburg BP, Schols L (2008) SPG10 is a rare cause of spastic paraplegia in European families. Journal of neurology, neurosurgery, and psychiatry 79:584-587.

Schuster CM, Davis GW, Fetter RD, Goodman CS (1996) Genetic dissection of structural and functional components of synaptic plasticity. I. Fasciclin II controls synaptic stabilization and growth. Neuron 17:641-654.

Seitz A, Kojima H, Oiwa K, Mandelkow EM, Song YH, Mandelkow E (2002) Single-molecule investigation of the interference between kinesin, tau and MAP2c. EMBO J 21:4896-4905.

Setou M, Seog DH, Tanaka Y, Kanai Y, Takei Y, Kawagishi M, Hirokawa N (2002) Glutamate-receptor-interacting protein GRIP1 directly steers kinesin to dendrites. Nature 417:83-87.

Severt WL, Biber TU, Wu X, Hecht NB, DeLorenzo RJ, Jakoi ER (1999) The suppression of testis-brain RNA binding protein and kinesin heavy chain disrupts mRNA sorting in dendrites. J Cell Sci 112 (Pt 21):3691-3702.

Shang Z, Zhou K, Xu C, Csencsits R, Cochran JC, Sindelar CV (2014) High-resolution structures of kinesin on microtubules provide a basis for nucleotide-gated force-generation. Elife 3:e04686.

Shapira M, Zhai RG, Dresbach T, Bresler T, Torres VI, Gundelfinger ED, Ziv NE, Garner CC (2003) Unitary assembly of presynaptic active zones from Piccolo-Bassoon transport vesicles. Neuron 38:237-252.

Sheng ZH, Cai Q (2012) Mitochondrial transport in neurons: impact on synaptic homeostasis and neurodegeneration. Nat Rev Neurosci 13:77-93.

Shimazaki H, Takiyama Y, Ishiura H, Sakai C, Matsushima Y, Hatakeyama H, Honda J, Sakoe K, Naoi T, Namekawa M, Fukuda Y, Takahashi Y, Goto J, Tsuji S, Goto Y, Nakano I (2012) A homozygous mutation of C12orf65 causes spastic paraplegia with optic atrophy and neuropathy (SPG55). Journal of medical genetics 49:777-784.

Shubeita GT, Tran SL, Xu J, Vershinin M, Cermelli S, Cotton SL, Welte MA, Gross SP (2008) Consequences of motor copy number on the intracellular transport of kinesin-1-driven lipid droplets. Cell 135:1098-1107.

Silverman MA, Kaech S, Ramser EM, Lu X, Lasarev MR, Nagalla S, Banker G (2010) Expression of kinesin superfamily genes in cultured hippocampal neurons. Cytoskeleton (Hoboken, NJ) 67:784-795.

Simpson MA, Cross H, Proukakis C, Pryde A, Hershberger R, Chatonnet A, Patton MA, Crosby AH (2003) Maspardin is mutated in mast syndrome, a complicated form of hereditary spastic paraplegia associated with dementia. American journal of human genetics 73:1147-1156.

Smith R, Taylor JP (2011) Dissection and imaging of active zones in the Drosophila neuromuscular junction. J Vis Exp.

Smith RB, Machamer JB, Kim NC, Hays TS, Marques G (2012) Relay of retrograde synaptogenic signals through axonal transport of BMP receptors. Journal of cell science 125:3752-3764.

Snow PM, Patel NH, Harrelson AL, Goodman CS (1987) Neural-specific carbohydrate moiety shared by many surface glycoproteins in Drosophila and grasshopper embryos. J Neurosci 7:4137-4144.

Soderblom C, Blackstone C (2006) Traffic accidents: molecular genetic insights into the pathogenesis of the hereditary spastic paraplegias. Pharmacol Ther 109:42-56.

Sollner T, Whiteheart SW, Brunner M, Erdjument-Bromage H, Geromanos S, Tempst P, Rothman JE (1993) SNAP receptors implicated in vesicle targeting and fusion. Nature 362:318-324.

Song H, Endow SA (1998) Decoupling of nucleotide- and microtubule-binding sites in a kinesin mutant. Nature 396:587-590.

Spradling AC, Stern D, Beaton A, Rhem EJ, Laverty T, Mozden N, Misra S, Rubin GM (1999) The Berkeley Drosophila Genome Project gene disruption project: Single P-element insertions mutating 25% of vital Drosophila genes. Genetics 153:135-177.

Stepanova T, Slemmer J, Hoogenraad CC, Lansbergen G, Dortland B, De Zeeuw CI, Grosveld F, van Cappellen G, Akhmanova A, Galjart N (2003) Visualization of microtubule growth in cultured neurons via the use of EB3-GFP (end-binding protein 3-green fluorescent protein). J Neurosci 23:2655-2664.

Stevanin G et al. (2007) Mutations in SPG11, encoding spatacsin, are a major cause of spastic paraplegia with thin corpus callosum. Nature genetics 39:366-372.

Stewart BA, McLean JR (2004) Population density regulates Drosophila synaptic morphology in a Fasciclin-II-dependent manner. Journal of neurobiology 61:392-399.

Stewart BA, Atwood HL, Renger JJ, Wang J, Wu CF (1994) Improved stability of Drosophila larval neuromuscular preparations in haemolymph-like physiological solutions. Journal of comparative physiology A, Sensory, neural, and behavioral physiology 175:179-191.

Straube A, Hause G, Fink G, Steinberg G (2006) Conventional kinesin mediates microtubule-microtubule interactions in vivo. Molecular biology of the cell 17:907-916.

Su Q, Cai Q, Gerwin C, Smith CL, Sheng ZH (2004) Syntabulin is a microtubule-associated protein implicated in syntaxin transport in neurons. Nature cell biology 6:941-953.

Sudhof TC (2004) The synaptic vesicle cycle. Annual review of neuroscience 27:509-547.

Svoboda K, Schmidt CF, Schnapp BJ, Block SM (1993) Direct observation of kinesin stepping by optical trapping interferometry. Nature 365:721-727.

Tang Y, Zucker RS (1997) Mitochondrial involvement in post-tetanic potentiation of synaptic transmission. Neuron 18:483-491.

Taya S, Shinoda T, Tsuboi D, Asaki J, Nagai K, Hikita T, Kuroda S, Kuroda K, Shimizu M, Hirotsune S, Iwamatsu A, Kaibuchi K (2007) DISC1 regulates the transport of the NUDEL/LIS1/14-3-3epsilon complex through kinesin-1. J Neurosci 27:15-26.

Tejedor FJ, Bokhari A, Rogero O, Gorczyca M, Zhang J, Kim E, Sheng M, Budnik V (1997) Essential role for dlg in synaptic clustering of Shaker K+ channels in vivo. J Neurosci 17:152-159.

Tessa A, Silvestri G, de Leva MF, Modoni A, Denora PS, Masciullo M, Dotti MT, Casali C, Melone MA, Federico A, Filla A, Santorelli FM (2008) A novel KIF5A/SPG10 mutation in spastic paraplegia associated with axonal neuropathy. Journal of neurology 255:1090-1092.

Thomas U, Kim E, Kuhlendahl S, Koh YH, Gundelfinger ED, Sheng M, Garner CC, Budnik V (1997) Synaptic clustering of the cell adhesion molecule fasciclin II by discs-large and its role in the regulation of presynaptic structure. Neuron 19:787-799.

Trichas G, Begbie J, Srinivas S (2008) Use of the viral 2A peptide for bicistronic expression in transgenic mice. BMC biology 6:40.

Tsai PI, Kao HH, Grabbe C, Lee YT, Ghose A, Lai TT, Peng KP, Van Vactor D, Palmer RH, Chen RH, Yeh SR, Chien CT (2008) Fak56 functions downstream of integrin alphaPS3betanu and suppresses MAPK activation in neuromuscular junction growth. Neural development 3:26.

Uchida A, Alami NH, Brown A (2009) Tight functional coupling of kinesin-1A and dynein motors in the bidirectional transport of neurofilaments. Molecular biology of the cell 20:4997-5006.

Uchimura S, Oguchi Y, Hachikubo Y, Ishiwata S, Muto E (2010) Key residues on microtubule responsible for activation of kinesin ATPase. The EMBO journal 29:1167-1175.

Uemura S, Ishiwata S (2003) Loading direction regulates the affinity of ADP for kinesin. Nat Struct Biol 10:308-311.

Uemura S, Kawaguchi K, Yajima J, Edamatsu M, Toyoshima YY, Ishiwata S (2002) Kinesin-microtubule binding depends on both nucleotide state and loading direction. Proc Natl Acad Sci U S A 99:5977-5981.

Vale RD, Reese TS, Sheetz MP (1985) Identification of a novel force-generating protein, kinesin, involved in microtubule-based motility. Cell 42:39-50.

Valentine MT, Gilbert SP (2007) To step or not to step? How biochemistry and mechanics influence processivity in Kinesin and Eg5. Curr Opin Cell Biol 19:75-81.

van der Bliek AM, Shen Q, Kawajiri S (2013) Mechanisms of mitochondrial fission and fusion. Cold Spring Harb Perspect Biol 5.

van Niekerk EA, Willis DE, Chang JH, Reumann K, Heise T, Twiss JL (2007) Sumoylation in axons triggers retrograde transport of the RNA-binding protein La. Proceedings of the National Academy of Sciences of the United States of America 104:12913-12918.

Verhey KJ, Hammond JW (2009) Traffic control: regulation of kinesin motors. Nature reviews Molecular cell biology 10:765-777.

Verhey KJ, Kaul N, Soppina V (2011) Kinesin assembly and movement in cells. Annual review of biophysics 40:267-288.

Verhey KJ, Lizotte DL, Abramson T, Barenboim L, Schnapp BJ, Rapoport TA (1998) Light chain-dependent regulation of Kinesin's interaction with microtubules. J Cell Biol 143:1053-1066.

Verhey KJ, Meyer D, Deehan R, Blenis J, Schnapp BJ, Rapoport TA, Margolis B (2001) Cargo of kinesin identified as JIP scaffolding proteins and associated signaling molecules. J Cell Biol 152:959-970.

Verstreken P, Ly CV, Venken KJ, Koh TW, Zhou Y, Bellen HJ (2005) Synaptic mitochondria are critical for mobilization of reserve pool vesicles at Drosophila neuromuscular junctions. Neuron 47:365-378.

Wagh DA, Rasse TM, Asan E, Hofbauer A, Schwenkert I, Durrbeck H, Buchner S, Dabauvalle MC, Schmidt M, Qin G, Wichmann C, Kittel R, Sigrist SJ, Buchner E (2006) Bruchpilot, a protein with homology to ELKS/CAST, is required for structural integrity and function of synaptic active zones in Drosophila. Neuron 49:833-844.

Waller A (1850) Experiments on the section of glossopharyngeal and hypoglossal nerves of the frog and observations of the alternatives produced thereby in the structure of their primitive fibres. Philos Trans R Soc Lond B Biol Sci 140:423–429.

Wang L, Brown A (2010) A hereditary spastic paraplegia mutation in kinesin-1A/KIF5A disrupts neurofilament transport. Molecular neurodegeneration 5:52.

Wang L, Ho CL, Sun D, Liem RK, Brown A (2000) Rapid movement of axonal neurofilaments interrupted by prolonged pauses. Nature cell biology 2:137-141.

Wang X, Schwarz TL (2009) The mechanism of Ca2+ -dependent regulation of kinesin-mediated mitochondrial motility. Cell 136:163-174.

Werth JL, Thayer SA (1994) Mitochondria buffer physiological calcium loads in cultured rat dorsal root ganglion neurons. J Neurosci 14:348-356.

Westermann B (2012) Bioenergetic role of mitochondrial fusion and fission. Biochim Biophys Acta 1817:1833-1838.

Weyhersmuller A, Hallermann S, Wagner N, Eilers J (2011) Rapid active zone remodeling during synaptic plasticity. J Neurosci 31:6041-6052.

Whitmore AV, Lindsten T, Raff MC, Thompson CB (2003) The proapoptotic proteins Bax and Bak are not involved in Wallerian degeneration. Cell death and differentiation 10:260-261.

Woehlke G, Ruby AK, Hart CL, Ly B, Hom-Booher N, Vale RD (1997) Microtubule interaction site of the kinesin motor. Cell 90:207-216.

Wong YL, Dietrich KA, Naber N, Cooke R, Rice SE (2009) The Kinesin-1 tail conformationally restricts the nucleotide pocket. Biophysical journal 96:2799-2807.

Wyatt RM, Balice-Gordon RJ (2003) Activity-dependent elimination of neuromuscular synapses. Journal of neurocytology 32:777-794.

Xia CH, Roberts EA, Her LS, Liu X, Williams DS, Cleveland DW, Goldstein LS (2003) Abnormal neurofilament transport caused by targeted disruption of neuronal kinesin heavy chain KIF5A. J Cell Biol 161:55-66.

Xiong X, Collins CA (2012) A conditioning lesion protects axons from degeneration via the Wallenda/DLK MAP kinase signaling cascade. J Neurosci 32:610-615.

Yahata N, Yuasa S, Araki T (2009) Nicotinamide mononucleotide adenylyltransferase expression in mitochondrial matrix delays Wallerian degeneration. J Neurosci 29:6276-6284.

Yamada M, Toba S, Takitoh T, Yoshida Y, Mori D, Nakamura T, Iwane AH, Yanagida T, Imai H, Yu-Lee LY, Schroer T, Wynshaw-Boris A, Hirotsune S (2010) mNUDC is required for plus-end-directed transport of cytoplasmic dynein and dynactins by kinesin-1. The EMBO journal 29:517-531.

Yang Y, Gehrke S, Imai Y, Huang Z, Ouyang Y, Wang JW, Yang L, Beal MF, Vogel H, Lu B (2006) Mitochondrial pathology and muscle and dopaminergic neuron degeneration caused by

inactivation of Drosophila Pink1 is rescued by Parkin. Proc Natl Acad Sci U S A 103:10793-10798.

Yao A, Jin S, Li X, Liu Z, Ma X, Tang J, Zhang YQ (2011) Drosophila FMRP regulates microtubule network formation and axonal transport of mitochondria. Human molecular genetics 20:51-63.

Yi M, Weaver D, Hajnoczky G (2004) Control of mitochondrial motility and distribution by the calcium signal: a homeostatic circuit. J Cell Biol 167:661-672.

Yildiz A, Tomishige M, Vale RD, Selvin PR (2004) Kinesin walks hand-over-hand. Science 303:676-678.

Yun M, Zhang X, Park CG, Park HW, Endow SA (2001) A structural pathway for activation of the kinesin motor ATPase. The EMBO journal 20:2611-2618.

Zala D, Hinckelmann MV, Yu H, Lyra da Cunha MM, Liot G, Cordelieres FP, Marco S, Saudou F (2013) Vesicular glycolysis provides on-board energy for fast axonal transport. Cell 152:479-491.

Zhai Q, Wang J, Kim A, Liu Q, Watts R, Hoopfer E, Mitchison T, Luo L, He Z (2003) Involvement of the ubiquitin-proteasome system in the early stages of wallerian degeneration. Neuron 39:217-225.

Zhang LI, Poo MM (2001) Electrical activity and development of neural circuits. Nat Neurosci 4 Suppl:1207-1214.

Zhang Y, Roxburgh R, Huang L, Parsons J, Davies TC (2014) The effect of hydrotherapy treatment on gait characteristics of hereditary spastic paraparesis patients. Gait Posture 39:1074-1079.

Zhao L, Wang D, Wang Q, Rodal AA, Zhang YQ (2013) Drosophila cyfip regulates synaptic development and endocytosis by suppressing filamentous actin assembly. PLoS Genet 9:e1003450.

Zhao X, Alvarado D, Rainier S, Lemons R, Hedera P, Weber CH, Tukel T, Apak M, Heiman-Patterson T, Ming L, Bui M, Fink JK (2001) Mutations in a newly identified GTPase gene cause autosomal dominant hereditary spastic paraplegia. Nature genetics 29:326-331.

Zito K, Parnas D, Fetter RD, Isacoff EY, Goodman CS (1999) Watching a synapse grow: noninvasive confocal imaging of synaptic growth in Drosophila. Neuron 22:719-729.

Zuchner S, Wang G, Tran-Viet KN, Nance MA, Gaskell PC, Vance JM, Ashley-Koch AE, Pericak-Vance MA (2006) Mutations in the novel mitochondrial protein REEP1 cause hereditary spastic paraplegia type 31. American journal of human genetics 79:365-369.

Zuchner S et al. (2004) Mutations in the mitochondrial GTPase mitofusin 2 cause Charcot-Marie-Tooth neuropathy type 2A. Nature genetics 36:449-451.

Zucker RS (1989) Short-term synaptic plasticity. Annual review of neuroscience 12:13-31.